One Earth

Article

# Socio-demographic factors shape mortality risk linked to compound drought-heatwave events under climate change in China

## Graphical abstract

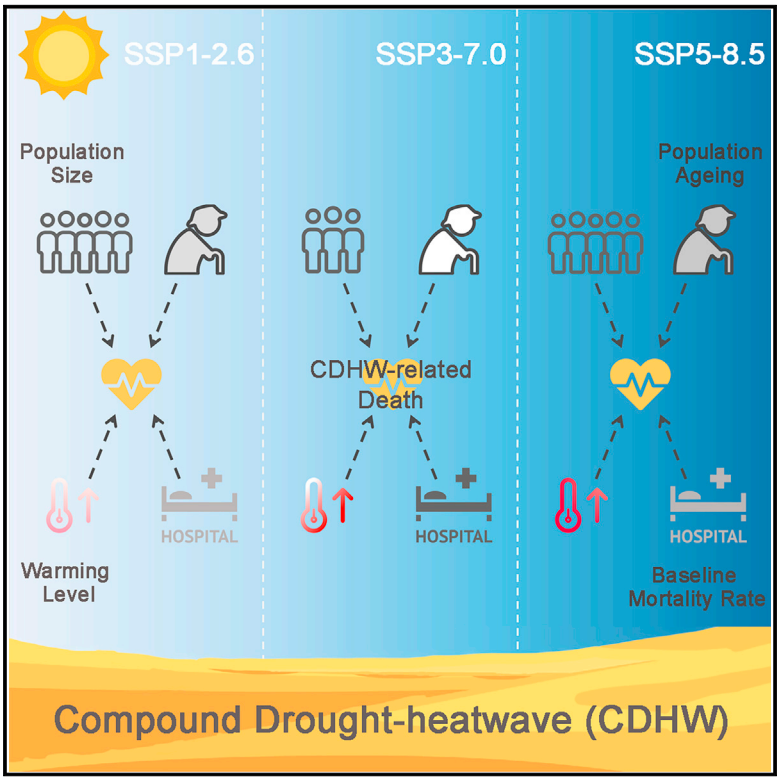


## Highlights

- CDHWs are projected to continue an increasing trend under warming scenarios in China
- Exposures to CDHWs elevate mortality risk, with women facing a higher risk
- Socio-demographic factors will significantly influence future CDHW-related deaths
- Remarkable regional inequalities in health impacts of CDHWs exist in China

## Authors

Xin Yao, Ying Qu, Liqiang Zhang, ..., Suhong Liu, Qihao Wang, Chenghu Zhou

## Correspondence

zhanglq@bnu.edu.cn (L.Z.), baichen-slhr@ruc.edu.cn (C.B.), zhouch@lreis.ac.cn (C.Z.)

## In brief

Anthropogenic warming has increased the frequency of simultaneous drought and heatwave occurrences, further intensifying CDHW events globally. However, the CDHW-mortality relationship and the effects of socio-demographic factors remain poorly understood. We find that the increasing frequency, duration, and severity of CDHWs all elevate the mortality risk. Notably, population aging and changes in baseline mortality rates have a greater impact on the CDHW-related mortality burden than the level of warming under climate change.

Yao et al., 2024, One Earth 7, 1–15
November 15, 2024 
https://doi.org/10.1016/j.oneear.2024.09.016

CellPress

One Earth

CellPress

Article

# Socio-demographic factors shape mortality risk linked to compound drought-heatwave events under climate change in China

Xin Yao,[1] Ying Qu,[1] Liqiang Zhang,[1,7,*] Ashok K. Mishra,[2] Jiabo Yin,[3] Ruiqiang Ding,[1] Jing Yang,[1] Chen Bai,[4,*] Lei Zhang,[1] Mengting Li,[4] Pan Liu,[3] Jintai Lin,[5] Qiwei Yu,[1] Suhong Liu,[1] Qihao Wang,[1] and Chenghu Zhou[6,*]

[1]Faculty of Geographical Science, Beijing Normal University, Beijing 100875, China
[2]Zachry Department of Civil & Environmental Engineering, Texas A&M University, College Station 77843, TX, USA
[3]State Key Laboratory of Water Resources Engineering and Management, Wuhan University, Wuhan, Hubei 430072, China
[4]School of Labor and Human Resources, Renmin University of China, Beijing 100872, China
[5]Laboratory for Climate and Ocean-Atmosphere Studies, Department of Atmospheric and Oceanic Sciences, School of Physics, Peking University, Beijing 100871, China
[6]Institute of Geographical Science and Natural Resources, Chinese Academy of Sciences, Beijing 100101, China
[7]Lead contact
*Correspondence: zhanglq@bnu.edu.cn (L.Z.), baichen-slhr@ruc.edu.cn (C.B.), zhouch@lreis.ac.cn (C.Z.)
https://doi.org/10.1016/j.oneear.2024.09.016

**SCIENCE FOR SOCIETY** Droughts and heatwaves are becoming increasingly common. As their frequency grows, so too do the chances of these events co-occurring (i.e., compound drought-heatwave [CDHW] events), which exacerbates societal and environmental risk. Despite this growing concern and projections indicating more severe events in the future, the likelihood that CDHWs will lead to loss of life and the factors that heighten vulnerability remain poorly understood, compromising mitigation and adaptation strategies. Our results demonstrate that increasing CDHW frequency, duration, and severity substantially elevate mortality risk, but the primary causes of elevated risk are socio-demographic factors associated with population aging. This work emphasizes the need for mitigation and adaptation actions that reduce the adverse impacts of CDHWs on population health, particularly for the elderly.

## SUMMARY

Droughts and heatwaves have far-reaching impacts on human health, and their compound effects are more severe. However, our understanding of the impact of compound drought-heatwave (CDHW) on mortality risk, which is a key input for policy prioritization to protect vulnerable populations, remains limited, particularly considering socio-demographic factors such as baseline mortality reductions, population size changes, and aging. Here, we project future changes in CDHW and associated mortality in China under three Shared Socioeconomic Pathways (SSPs). Under the highest emission scenario (SSP5-8.5), CDHW exposures led to 11.88 (95% confidence interval [95%CI], 8.77–14.80) million premature deaths among Chinese individuals aged 65 years and older by 2100. Notably, even under the least warming pathway (SSP1-2.6), deaths increase due to the expanding size of vulnerable populations. Population aging and baseline mortality changes are more influential in shaping future mortality risks than CDHW exposure levels. Our findings provide valuable insights into understanding and planning for future risk.

## INTRODUCTION

Droughts and heatwaves are two of the costliest climate-related hazards, exerting profound effects on both human society and ecosystems.[1–3] These extreme events are driven by complex interactions among physical processes and initiated by similar synoptic circulation anomalies,[4,5] and they often co-occur.[6,7] As droughts occur more frequently and temperature warming triggers stronger land-atmosphere feedbacks,[8] compound drought-heatwave (CDHW) events have increased globally,[9,10] including in Asia,[11,12] Europe,[13,14] North America,[15] South America,[16] and Oceania,[17,18] amplifying adverse impacts on socio-ecosystem sustainability and human health.[19,20]

Please cite this article in press as: Yao et al., Socio-demographic factors shape mortality risk linked to compound drought-heatwave events under climate change in China, One Earth (2024), https://doi.org/10.1016/j.oneear.2024.09.016



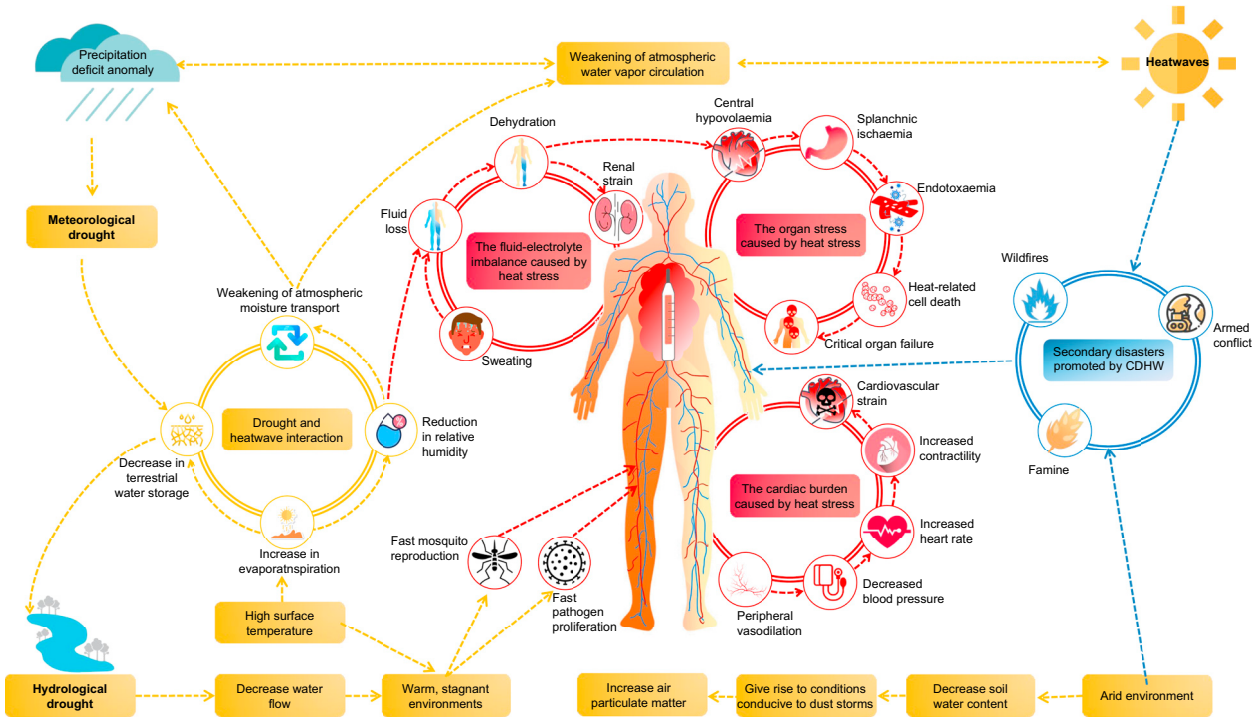


**Figure 1. CDHW influence on human health**

Summary of the processes generating CDHWs and their human health impacts, including human physiological responses to CDHWs, drought-heatwave interactions, and secondary disasters caused by CDHWs.

The impacts of droughts or heatwaves on human health have been widely reported. For example, droughts increase morbidity and mortality,[21–23] including mental illness due to economic losses,[24] heart and respiratory system diseases caused by dust and wildfires,[25] and waterborne infectious diseases.[26,27] Heatwaves also pose a major threat globally to human health by substantially contributing to increased morbidity and mortality,[28–30] especially for older populations with cardiopulmonary and other chronic diseases.[30–32] Concerningly, CDHWs may intensify health hazards through intricate interactions, leading to greater impacts than individual extremes. First, CDHWs amplify the human physiological responses to heatwaves or droughts (Figure 1, red boxes). For instance, in drought conditions, the human heat-regulation physiologies increase cardiac workloads and perspiration, resulting in greater strains on the heart and electrolyte imbalances,[30] elevating the heat-related mortality rate.[30,33] Second, drought-heatwave interactions can generate or amplify compound extreme (Figure 1, yellow boxes), such as elevated temperatures leading to increased evapotranspiration, thereby intensifying drought. Third, CDHWs are more likely to trigger various secondary disasters such as wildfires and famines (Figure 1, blue boxes), posing a severe threat to human health.[34–36] Understanding CDHW dynamics is thus essential for implementing the UN Sustainable Development Goals (SDGs), in particular SDG3 and SDG13, which aim to improve healthy lives and combat climate change. Previous studies have investigated the CDHW characteristics using data from recent observational periods and simulations of future climate change scenarios.[10,37,38] However, there is a lack of systematic assessment of the CDHW impacts on human health, which is crucial for informing adaptation and mitigation strategies.

Further, a range of factors can modulate the impact of CDHWs on human health, such as emission policies, energy transition, and socio-demographic trends.[39–41] For example, socio-demographic patterns can change the size and vulnerability of the exposed populations, thereby exerting complex effects on the health burdens of CDHWs. Meanwhile, improvements in the healthcare system can reduce the baseline mortality rate,[42] mitigating the health consequences of risk factors, including those arising from CDHWs. However, less is known about the roles of CDHWs and socio-demographic factors on human health in the projected climate scenarios.

Given China's complex natural and geographical conditions, as well as its dynamic socio-demographic characteristics, it serves as an ideal case for studying future changes in CDHWs and their impact on mortality risk. During recent decades, there has been a substantial increase in drought frequency, severity, duration, and spatial extent across China,[43,44] accompanied by a significant rise in heatwaves.[45,46] The inherent interplay of climate and diverse geographical conditions makes China prone to more frequent CDHWs.[12,47,48] Meanwhile, it is now home to the largest population of adults aged 60 years and older, accounting for 25.6% of the entire global old population in 2020.[49–51] Between 2006 and 2050, the number of Chinese citizens older than 65 years is projected to triple due to declining birth rates and longer life expectancies, reaching about 25% of the total national population,[52] which will aggravate the health impacts of CDHWs.

Please cite this article in press as: Yao et al., Socio-demographic factors shape mortality risk linked to compound drought-heatwave events under climate change in China, One Earth (2024), https://doi.org/10.1016/j.oneear.2024.09.016



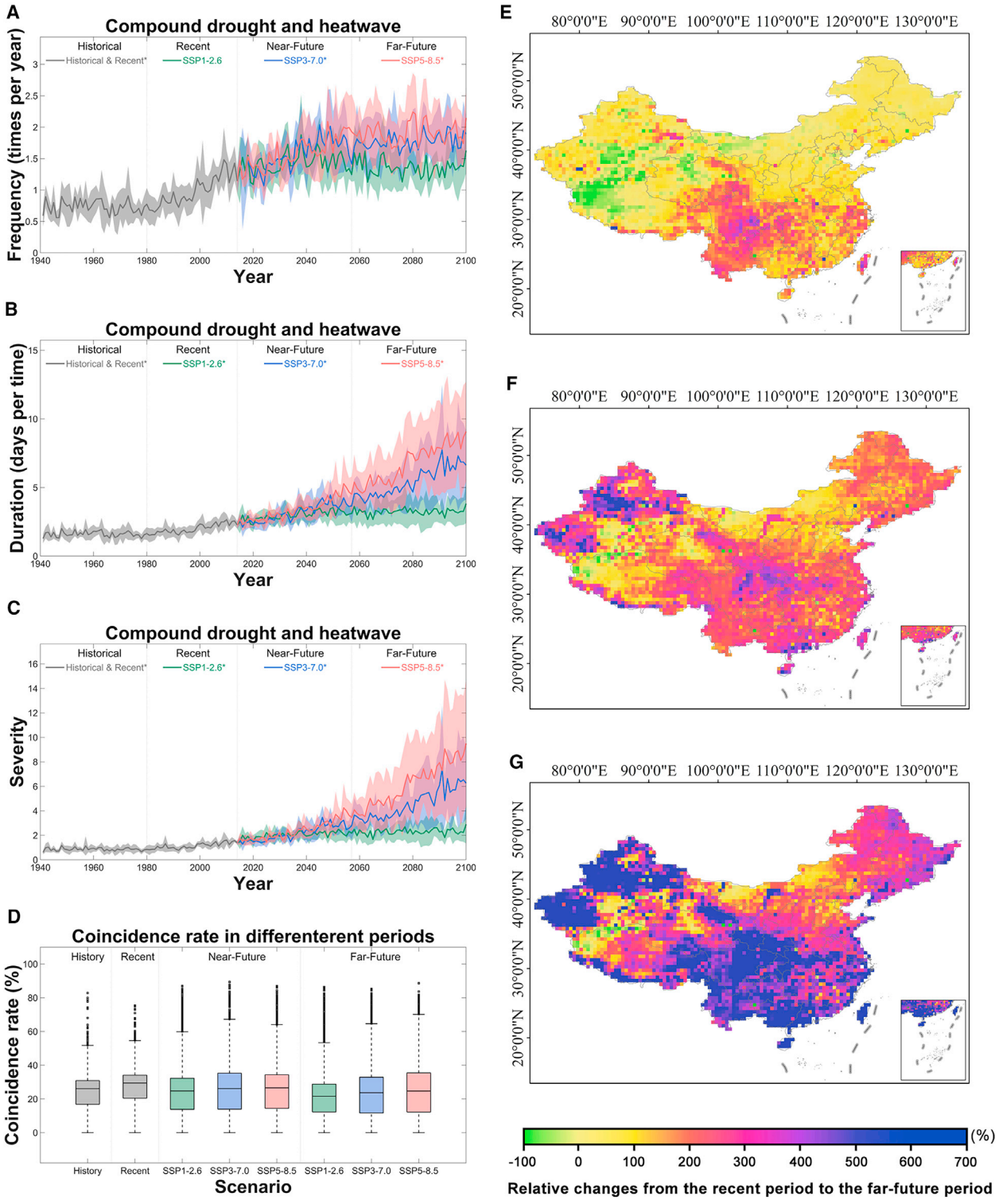


**Figure 2. Historical and projected changes in CDHW characteristics**

(A–C) Variations in GCM-GHM-based MME mean projections of CDHW characteristics—(A) frequency, (B) duration, and (C) severity—spatially averaged over China for historical (1941–1980), recent (1981–2014), and future periods (2015–2100) based on the selected future climate scenarios (SSP1-2.6, SSP3-7.0, and SSP5-8.5). The asterisks indicate that the change is significant (*$p < 0.05$) as detected by Mann-Kendall trend tests. The shading represents the 95%CIs.

*(legend continued on next page)*

Please cite this article in press as: Yao et al., Socio-demographic factors shape mortality risk linked to compound drought-heatwave events under climate change in China, One Earth (2024), https://doi.org/10.1016/j.oneear.2024.09.016



Here, we employ an integrated framework to simulate future human activities and emissions for each province in China, which enables us to systematically evaluate changes in CDHW characteristics under the historical (1941–1980), recent (1981–2014), near-future (2015–2057), and far-future (2058–2100) climate scenarios and assess their impacts on mortality (Figure S1). We further decompose the total mortality effects by examining the contributions of four individual factors to identify primary drivers that may vary across provinces and over time. By exploring the spatiotemporal patterns and mortality impacts of CDHWs in China, the presented modeling framework reveals the underlying processes and dynamics that shape CDHW patterns and their associated health burdens. Our research offers valuable information on the relationship between anthropogenic warming, climate extremes, and human health. This information is crucial for advancing sustainable science to address the escalating threat of climate change on human health in a warming world. In the long-term future, the impacts of socio-demographic factors on the mortality risk of older adults are expected to become increasingly significant.

## RESULTS

### Methods summary

Leveraging bias-corrected simulation outputs from five global climate models (GCMs) and two global hydrological models (GHMs) under the Coupled Model Intercomparison Project 6 (CMIP6), we calculate CDHW metrics for quantifying the projected changes in CDHW characteristics in China under various future scenarios (2015–2100) relative to the historical (1941–1980) and recent observed (1981–2014) periods. We utilize an integrated SSP-RCP scenario framework by combining Shared Socioeconomic Pathways (SSPs) with Representative Concentration Pathways (RCPs). RCPs provide climate projections without linking to societal pathways, while SSPs outline societal futures without considering climate impacts. By combining them, we can better assess climate risks and devise adaptation or mitigation strategies.[53] Further, socio-demographic factors and extreme climate events are interconnected, and SSPs represent changes in factors such as economic growth and urbanization that influence future greenhouse gas emissions and heat-related events. We select three commonly used scenarios[54,55]—SSP1-2.6 (sustainability), SSP3-7.0 (regional rivalry), and SSP5-8.5 (fossil-fueled development)—to explore how socio-demographic factors impact compound extremes under climate change. It is worth mentioning that the likelihood of the SSP5-8.5 scenario may decrease in the future due to global climate efforts, technological advancements, policy changes, increased public awareness about global warming, and more sustainable practices. However, examining this scenario provides valuable insights into how varying levels of global warming can affect mortality risk. Based on a cohort of older adults aged 65 years and older from the Chinese Longitudinal Healthy Longevity Survey (CLHLS) during 2002–2014, we employ the Cox proportional hazards model to estimate the hazard ratio (HR) of the all-cause mortality of Chinese older adults' exposures to different CDHWs and explore variations in their impacts across age and sex subgroups. Finally, we quantify the impacts on human health, measured by CDHW-related deaths, using socio-demographic projections consistent with SSPs[56–58] and the CDHW-mortality relationships.

### Historical, recent, and projected changes in CDHWs

We investigate the trends in the three types of climatic extreme events (heatwave, drought, and CDHW) under different definitions and their spatial patterns during 1941–2100 based on the multi-model ensemble (MME) mean of 10 GCM-GHM coupling models from the CMIP6 (see section "experimental procedures"). Note S2 presents the validations of the daily maximum 2-m air temperature ($T_{max}$), daily mean 2-m air temperature ($T_{mean}$), and daily precipitation (P) simulations from five GCMs and the terrestrial water storage (TWS) simulations from 10 GCM-GHM coupling models as well as the results from the MME mean.

Using the Mann-Kendall test, we identify statistically significant trends in the CDHW time series (Figures S3–S5). Except for some CDHW frequencies derived from TWS-based drought severity index (TWS-DSI), which show no significant changes under the SSP1-2.6 (Figure S3), all other CDHWs exhibit significant increases in frequencies, duration, and severity across the three SSP-RCP scenarios (Figures S3–S5). The frequency of CDHWs identified using TWS-DSI is higher than those identified using standardized precipitation index (SPI) and standardized precipitation-evapotranspiration index (SPEI) (Figure S3). This difference may be attributed to the fact that TWS represents vertically integrated water storage, whereas these conventional indices can only capture partial water storages or fluxes,[59,60] thereby rendering TWS-DSI more sensitive in identifying droughts.[37] Notably, as the definitions of heatwaves for identifying CDHWs become more stringent (with increased temperature and duration thresholds), the disparities in CDHW characteristics across the three distinct scenarios become more pronounced (Figures S3–S5). This underscores the importance of climate actions such as controlling greenhouse gas emissions in mitigating more severe heatwaves.

For the optimal CDHW definition (with a 92.5th percentile temperature threshold, 3-day duration threshold, and TWS-DSI as the drought index; see section "experimental procedures") identified to capture the impact on mortality risk, all characteristics of CDHWs increased during the period 1941–2014 (Figures 2A–2C). CDHW frequency, duration, and severity substantially increase in the future scenarios (Figures 2A–2C), except the CDHW frequency under the SSP1-2.6 scenario (Figure 2A). Under the SSP3-7.0 scenario, models project that the frequency of CDHWs is likely to increase by 0.69 or 0.61 (95% confidence interval [95%CI], 0.58–0.80, or 0.46–0.77) times/year, with a rise in the CDHW duration by 4.20 or 1.50 (95%CI, 1.99–6.41, or 1.01–1.99) days/time and severity of each CDHW event by

(D) Boxplots of coincidence rates in various scenario-period combinations. The center line indicates the median value, the box bounds indicate the 25th/75th percentile values, the whiskers indicate the minimum/maximum values, and the circles indicate the outliers.
(E–G) Spatial patterns of relative changes in (E) frequency, (F) duration, and (G) severity of CDHWs between two periods (recent, 1981–2014, and far-future, 2058–2100). The CDHWs in (A)–(G) are all identified based on the 92.5th percentile temperature threshold, 3-day duration threshold, and TWS-DSI as the drought index.

Please cite this article in press as: Yao et al., Socio-demographic factors shape mortality risk linked to compound drought-heatwave events under climate change in China, One Earth (2024), https://doi.org/10.1016/j.oneear.2024.09.016





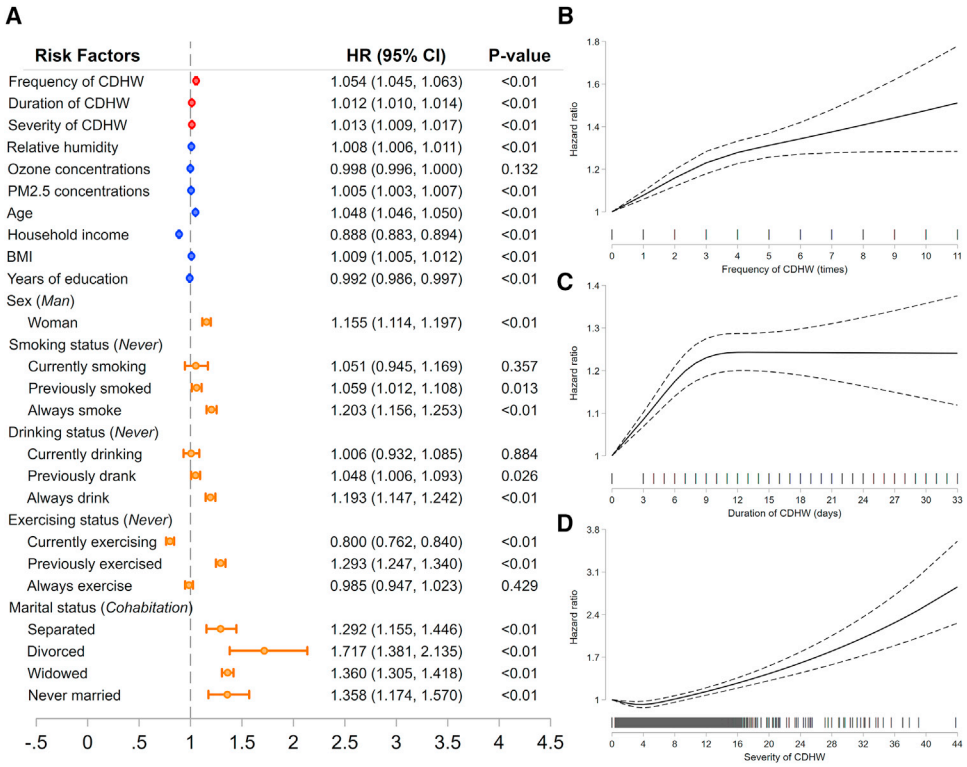


**Figure 3. The results of Cox proportional hazards models**

(A) HRs and 95%CIs for the association between all-cause mortality and CDHW exposures for the baseline model. Points and lines represent HR estimates and their corresponding 95%CIs, respectively. Red indicates the primary explanatory variables, blue represents continuous control variables, and orange denotes categorical control variables, with the reference group specified in parentheses after the variable name.

(B–D) Curve associations between all-cause mortality and 1-unit increase in (B) frequency, (C) duration, and (D) severity of CDHWs. The dashed lines indicate 95%CIs. The reference of frequency, duration, and severity is 0 (curve results from model 2).

4.41 or 1.42 (95%CI, 1.91–6.91, or 0.96–1.89) by the end of far future or near future compared to the year 2014. Compared to the sustainability scenarios (SSP1-2.6), a statistically significant increase in CDHW characteristics is projected for the fossil-fueled development scenario (SSP5-8.5) followed by the regional rivalry scenario (SSP3-7.0), which is consistent with recent literature.[38,61]

The promotion in the CDHW frequency can be driven by two main factors: (1) increases in the frequency of droughts or heatwaves independently, and (2) increases in the likelihood of droughts and heatwaves co-occurring. Almost of the characteristics of heatwaves in China exhibit a substantial promotion in all scenario-period combinations (Figures S9D–S9F), while the drought characteristics remain relatively stable, except for an increase under the SSP5-8.5 scenario (Figures S9A–S9C). We also calculate the coincidence rate to represent the likelihood of droughts and heatwaves co-occurring as the ratio of the total number of CDHWs to the heatwave events per year at any given location (section "experimental procedures"). The coincidence rate in different scenario-period combinations shows slight variations (Figures 2D and S10), suggesting that the intensified CDHWs in China are primarily driven by the intensification of heatwaves.

We quantify the spatial risk of climatic extremes under climate change, which is valuable for developing adaptation strategies.[38] Compared to the historical period, 8.71%–18.79% of the regions in China have experienced over double frequency, duration, and severity of CDHWs in recent decades (Figures S11A–S11C). Under the SSP5-8.5 scenario, by the end of this century, we project that 35.22%, 85.52%, and 92.99% of the regions in China will witness over double increases in CDHW frequency, duration, and severity compared to the recent period (Figures 2E–2G). Although there are variations in the spatial patterns of CDHW characteristics under different definitions (Figures S6–S8), the most significant increases in CDHW characteristics are observed in southwestern China and northern Xinjiang (Figures 2E–2G and S6–S8), underscoring the regional inequalities of potential health impacts. The promotions in other scenario-period combinations are slightly lower but are still larger compared to the recent CDHW characteristics (Figures S11–S13).

## Exposure-mortality associations

We use the Cox proportional hazards model[62,63] to quantify the association between exposures to CDHW characteristics and all-cause mortality of older adults (Equation 4 in section "experimental procedures"). As shown in Figure 3A and Table S7, we note that exposures to CDHWs significantly elevate mortality risk of older adults. For older adults exposed to each additional CDHW in the year preceding their survey dates, mortality risk increases by 5.4% (95%CI, 4.5%–6.3%). Similarly, for each

Please cite this article in press as: Yao et al., Socio-demographic factors shape mortality risk linked to compound drought-heatwave events under climate change in China, One Earth (2024), https://doi.org/10.1016/j.oneear.2024.09.016



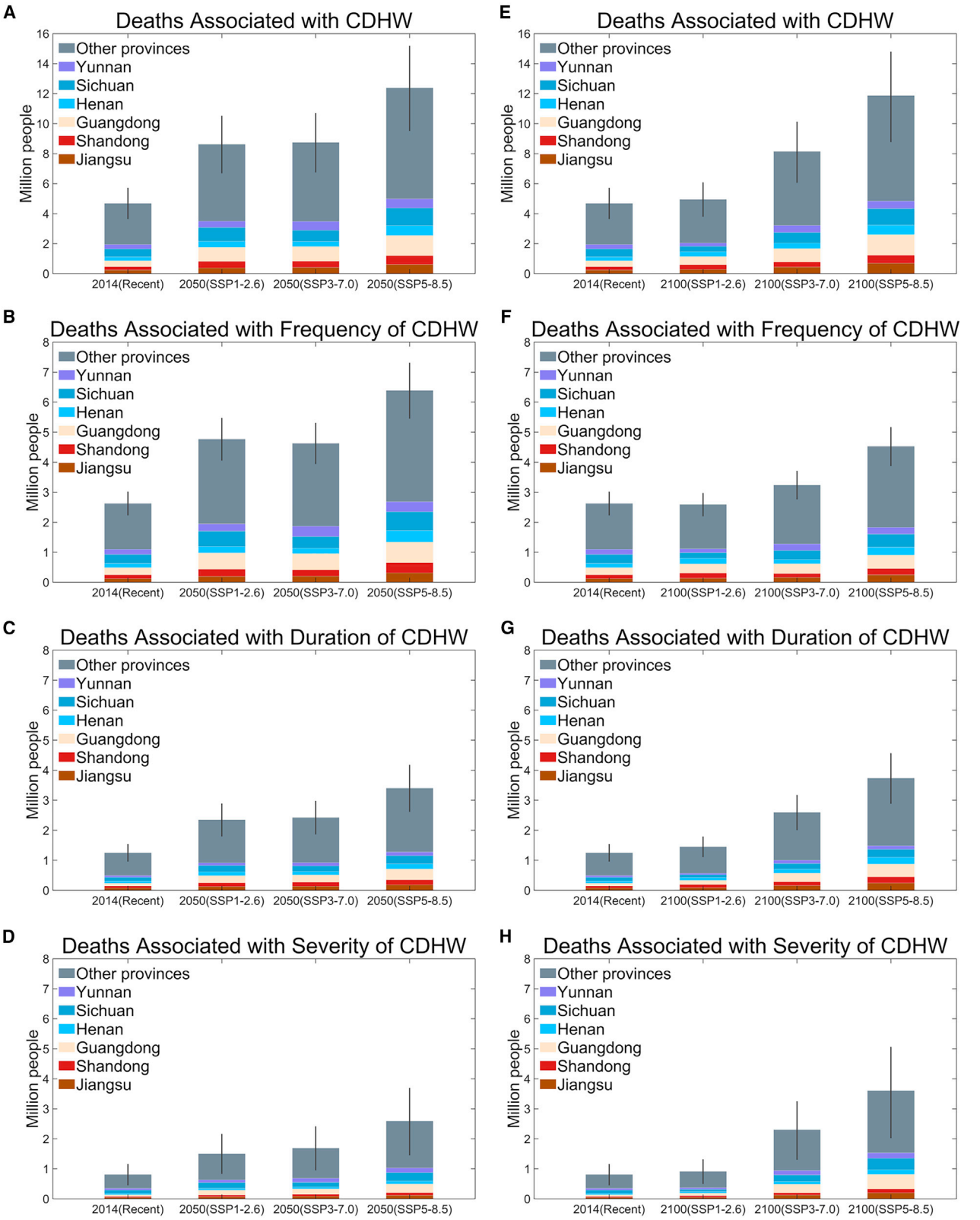


*(legend on next page)*

Please cite this article in press as: Yao et al., Socio-demographic factors shape mortality risk linked to compound drought-heatwave events under climate change in China, One Earth (2024), https://doi.org/10.1016/j.oneear.2024.09.016



additional day of the CDHW duration in the year before their survey date, there is a 1.2% increase (95%CI, 1.0%–1.4%) in mortality risk of older adults. Furthermore, for every unit increase in the CDHW severity experienced by older adults in the year before their survey date, there is a 1.3% increase (95%CI, 0.9%–1.3%) in mortality risk.

Figure S14 and Table S9 show the robustness tests using seven models (section "experimental procedures"). These tests highlight that the effects of the three CDHW characteristics remain significant and remarkably stable. To assess the potential nonlinear relationship between different CDHW characteristics and all-cause mortality risk, we individually fitted penalized splines with three knots for CDHW frequency, duration, and severity (model 2). The HR curves for CDHW frequency and duration both exhibit a saturation phenomenon (Figures 3B and 3C), wherein the slope of the curve decreases when the frequency exceeds three occurrences (Figure 3B). The saturation phenomenon is more pronounced for CDHW duration, as the effects level off when the duration exceeds 11 days (Figure 3C). We observe steeper slopes in the HR curve when the CDHW severity exceeds 12 (Figure 3D). We also conduct analyses stratified by age (strata variable by 5 years) and sex. In these analyses, except for the effects of CDHW duration and severity, which are modulated by sex (Figure S15; column 2–3 in Table S11), the impacts of a 1-unit increase in the three CDHW characteristics experienced by older adults in the year before the survey does not differ by age and sex (Tables S10 and S11). Specifically, when CDHW duration (severity) increases by 1 unit, the HR for females is 1.016 (1.018), slightly higher than that for males (1.009; Figures S9A and S9C).

## CDHW-related deaths

Using the exposure-mortality function in model 2 and socio-demographic projections consistent with SSPs,[56–58] we estimated the total burden of all-cause mortality of the exposed older adults in China under different scenarios. The CDHW-related all-cause deaths are projected to be higher in 2050 and 2100 compared to 2014 across all scenarios (Figure 4). In 2050, CDHW-related deaths in the scenario with highest mortality burden are 1.4 times that of the lowest scenario (Figure 4A), while, in 2100, CDHW-related deaths in the highest scenario are 2.4 times those of the lowest scenario (Figure 4E). The lowest burden is found in SSP1-2.6 (the most sustainable scenario) and the central estimate based on the exposure-mortality function is 8.62 (95%CI, 6.68–10.53) million in 2050, while it is 4.95 (95%CI, 3.80–6.08) million by the year 2100. The highest burden is found in the SSP5-8.5 scenario where fossil fuels continue to be used; that is, 12.39 (95%CI, 9.50–15.19) million in the year 2050 and 11.88 (95%CI, 8.77–14.80) million in the year 2100. Therefore, the health damage from CDHWs is expected to be substantial in the coming decades and can exacerbate rapidly under some plausible future scenarios.

Interestingly, the CDHW-related health burden does not increase monotonically with warming levels. For instance, the scenario with the lowest warming level (SSP1-2.6) is associated with higher deaths related to the frequency of CDHWs than that with the higher warming level (SSP3-7.0, Figure 4B). This suggests that other factors may moderate the CDHW-related health burden.

We observe from Figures 4A–4H that the future spatial distributions of CDHW-related health burdens remain unequal. The three SSP-RCP scenarios reveal that approximately 40% of national CDHW-related deaths only occur in six provinces: Yunnan, Sichuan, Henan, Guangdong, Shandong, and Jiangsu. Although the increases in CDHW characteristics in Jiangsu and Shandong (the eastern provinces of China) do not stand out prominently across all scenarios (Figures 2E, 2F, and S11–S13), the large size of the population exposures to CDHWs and the increasing population vulnerability due to population aging make the future health burden considerable. Thus, inequalities in CDHW-related health might persist in the future as the nation grapples with interconnected challenges associated with economic, demographic, and energy-demand growth.

## The determining role of socio-demographic factors

To explain the variations in health burdens across regions and scenarios, we decompose the aggregate changes in CDHW-related deaths in 2050 and 2100 relative to 2014 into the effects of four individual factors. The first factor is the change in the exposure level as a result of energy, air pollution, and climate efforts. We then consider three socio-demographic factors that affect the size of the exposed population and their vulnerability: population size, population aging, and changes in the baseline mortality rate.

We find that the socio-demographic factors play a dominant role in shaping the future health burden related to CDHWs (Figures 5A–5H). The impact of CDHW exposures is relatively low in most regions and scenarios. In particular, population aging would substantially exacerbate the future health burden. In all three scenarios, it is projected that, by 2050, aging alone will lead to an increase in national CDHW-related deaths by 221%, 132%, and 265%, respectively (Figure 5A). This is because the older adult groups have a higher baseline mortality rate compared to the younger population groups and the former is more vulnerable to mortality risk.[64] On the other hand, for the scenarios that assume rapid economic growth and improved healthcare (such as SSP1-2.6 and SSP5-8.5), the baseline mortality rate is projected to decline for each specific age group (Table S13), which lowers all-cause deaths from CDHW exposures. For instance, in 2050, the declining baseline mortality rate is expected to reduce the national CDHW-related deaths by 134% and 169% under both SSP1-2.6 and SSP5-8.5 (Figure 5A).

Comparing the decomposition results between the mid-century (2050) and the end of the century (2100), we find that the contribution of changes in CDHW exposures becomes more prominent and varies considerably across different scenarios. In the sustainable-development scenario (SSP1-2.6), the changes in CDHW exposures lead to a 10% increase in national CDHW-related deaths by 2100, while there are 100% and 314%

**Figure 4. CDHW-related all-cause deaths in China across different scenarios**

(A–H) All-cause deaths related to CDHWs and their characteristics in three SSP-RCP scenarios in (A–D) 2050 and (E–H) 2100 are projected. The bars represent the results using the central estimates of the HR functions from model 2, and the error bars represent the deaths estimated on the basis of the 95%CI of the HR functions. Different colors represent different provinces.

Please cite this article in press as: Yao et al., Socio-demographic factors shape mortality risk linked to compound drought-heatwave events under climate change in China, One Earth (2024), https://doi.org/10.1016/j.oneear.2024.09.016



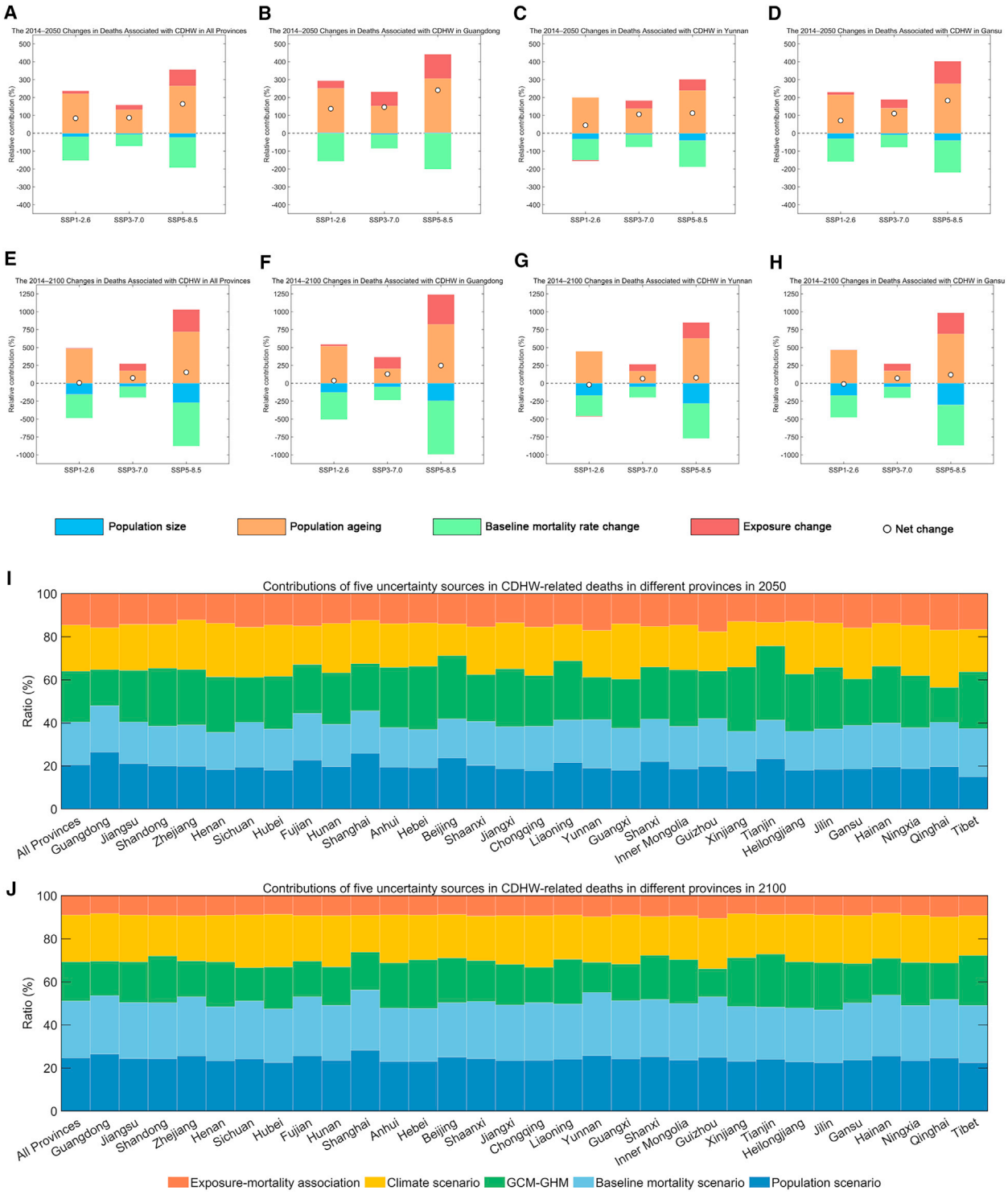


**Figure 5. Factors driving changes and uncertainty sources in CDHW-related deaths**

(A–H) Combining the effects of these four factors (i.e., CDHW characteristics, baseline mortality, population aging, and population size), the white dots represent the net changes in CDHW-related deaths for selected provinces at different gross domestic product (GDP) levels in 2050 and 2100.

(I and J) The sources of uncertainties in CDHW-related deaths in 2050 and 2100. Different provinces are arranged in descending order of GDP.

Please cite this article in press as: Yao et al., Socio-demographic factors shape mortality risk linked to compound drought-heatwave events under climate change in China, One Earth (2024), https://doi.org/10.1016/j.oneear.2024.09.016





increases (Figure 5E) in the other two scenarios, underscoring the importance of climate-mitigation efforts.

The contributions of the socio-demographic factors to mortality risk vary with the levels of gross domestic product (GDP) (Figures 5B–5D and 5F–5H). In the provinces with higher GDP, such as Guangdong, population aging is more severe. The increasing elderly population in these provinces leads to a substantial rise in CDHW-related deaths (Figures 5B and 5F). However, in the provinces with medium and lower GDP, such as Yunnan and Gansu, where the size of the populations is smaller, the impact of CDHW exposure changes is proportionately higher (Figures 5C, 5D, 5G, and 5H). These disparities further exacerbate regional inequalities in CDHW-related deaths.

Last, we decompose the overall uncertainty of projections based on CMIP6, exposure-mortality associations, and SSPs into five different sources (Figures 5I and 5J). In 2050, the largest source of uncertainty in CDHW-related death projections nationwide is the variability between different GCM-GHM coupling models, accounting for 23.68% (Figure 5I). By 2100, the uncertainty in socio-demographic projections consistent with SSPs increases, with population and baseline mortality rate projections contributing 26.51% and 27.09% of the uncertainty in CDHW-related deaths, respectively (Figure 5J). Moreover, the uncertainty contribution ratios vary across different provinces, due to the different SSPs and GCM-GHM coupling models (Figures 5I and 5J).

## DISCUSSION

Anthropogenic warming has led to more frequent simultaneous occurrences of droughts and heatwaves, resulting in a rise in CDHW events. These events have a significant impact on human health and socioeconomic development. Previous studies have primarily focused on the spatiotemporal changes in CDHW characteristics under different SSP-RCP scenarios.[10,37,38] However, our understanding of the relationship between CDHW events and mortality is still limited, especially when considering additional socio-demographic factors alongside CDHW events. Leveraging the GCM-GHM coupling models and CLHLS data from 2002 to 2014, we reveal that the increasing frequency, duration, and severity of CDHWs are associated with an increased all-cause mortality risk of older adults. Under the three climate warming scenarios, we project increasing trends in CDHWs in China, underscoring the profound threat posed by more frequent and intense CDHWs in the coming decades.

The mortality risk from CDHWs depends not only on the degree of climate warming but also on the vulnerability of populations.[65] We show that older women experienced a higher HR compared to older men due to increased duration and severity of CDHWs. The surveyed older adults were born in the socioeconomically challenging times of 1920s–1940s (Table S3). Their infancy, childhood, and adolescence experienced food shortages that might worsen their late-life health. Women's nutrition was usually worse than that of their male counterparts during the periods of food scarcity.[66] This might induce a higher CDHW-related mortality risk for older women than older men.

By comparing the three future scenarios with different socioeconomic pathways, greenhouse gas emission-control efforts, or climate mitigation, we observe CDHW-related deaths nationwide in the scenario with the highest mortality burden are 2.4 times those of the lowest scenario in the year 2100. This difference is mainly attributed to the varying levels of population aging and baseline mortality rates across different regions, periods, and scenarios. The net impacts of these socio-demographic factors often lead to an increase in future CDHW-related deaths. From the mid-century to the end of this century, CDHW-related deaths will continue to rise. This implies that great efforts to control greenhouse gas emissions are crucial to counteract the effects of socio-demographic trends, such as aging that may make future populations more vulnerable to CDHWs.

In addition to changes in population size, population aging, and baseline mortality rates, other socio-demographic factors, such as marital status, household income, and education, might also affect the mortality risk, thereby further influencing the death burden associated with CDHWs. For instance, increased income and extended years of education can effectively reduce the mortality risk among older adults (Figure 3A). This is likely because affluent or well-educated households have better living conditions, such as access to air conditioning; staying hydrated; cool roof materials; and cleaner, safer drinking water.[67–69] These insights provide new directions for the formulation of policies to minimize the impact of climate extremes on human health.

Notably, the regional inequalities in CDHW-related health burdens will be widened in the future. Slower economic growth may delay the efforts to strengthen greenhouse gas control policies, leading to higher warming levels.[70,71] It may also result in a slower improvement in the baseline mortality rates,[41] exacerbating the health burden of the population exposure to CDHWs. Therefore, the development of underdeveloped regions should remain a priority to reduce inequalities in health, sanitation, and the economy.

This study has several limitations. First, our results may underestimate the potential for the enhanced durations of CDHWs, because the current generation climate models fail to accurately reproduce the planetary wave resonance conditions that have been implicated in the increase of persistent summer weather extremes.[72–74] Second, due to the lack of age-structured projection data at the grid scale, we downscale the IIASA SSP population data[56] to the grid level[41] using the NASA SEDAC gridded global population projections,[57] which may weaken the representation of the regional health burden inequalities. Third, SSP2-4.5 is considered a more plausible trajectory for China. However, due to the lack of TWS projection from GCM-GHM under the SSP2.4-5 in the current ISIMIP2b/3b framework, future work can be devoted to exploring the CDHW evolution under this scenario. Nevertheless, our findings provide evidence that the risks associated with future CDHWs are expected to significantly intensify, posing a severe threat to human health under the influence of socio-demographic factors. We call for stark adaptation actions to mitigate the adverse impacts of climate warming on health and alleviate the growing pressures on global sustainability, particularly in underdeveloped regions.

## EXPERIMENTAL PROCEDURES

### SSP-RCP scenarios

Based on the projections on energy use, land use, and emissions of air pollutants and greenhouse gases, the SSP-RCP scenario framework pioneers

Please cite this article in press as: Yao et al., Socio-demographic factors shape mortality risk linked to compound drought-heatwave events under climate change in China, One Earth (2024), https://doi.org/10.1016/j.oneear.2024.09.016



a process for developing scenarios with various socioeconomic narratives and global warming levels. The SSPs include different narratives of future trends in socioeconomic drivers and environmental actions. The RCPs consider different targets for end-of-century climate-forcing levels to represent varying levels of climate-mitigation efforts. As such, the SSP-RCP integrated-scenario architecture captures the central features of global socioeconomic trends, greenhouse gas emission-control efforts, and climate policies through the end of the century. This study selects three scenarios that cover a range of SSPs and RCPs: the sustainability scenario (SSP1-2.6), the regional rivalry scenario (SSP3-7.0), and the fossil-fueled development scenario (SSP5-8.5) (please see Note S1 for more details).

### Models, simulation settings, and forcing data

The large ensemble simulations include 30 scenario-model combinations from CMIP6. The CMIP6-based projections contain three SSP-RCP scenarios (i.e., SSP1-2.6, SSP3-7.0, and SSP5-8.5), five GCMs, and two GHMs. The five GCMs include Geophysical Fluid Dynamics Laboratory earth system model version 4 (GFDL-ESM4), Institut Pierre-Simon Laplace climate model version 6A-low resolution (IPSL-CM6A-LR), Max Planck Institute earth system model version 1.2-high resolution (MPI-ESM1-2-HR), Meteorological Research Institute earth system model version 2.0 (MRI-ESM2-0), and United Kingdom earth system model version 1.0-low vertical resolution-low horizontal resolution (UKESM1-0-LL). The two GHMs include Community Water Model (CWatM) and global hydrological model H08. All models simulate the key terrestrial hydrological (e.g., soil, vegetation and river) processes (please see the details in Table S2), which are forced by the Inter-Sectoral Impact Model Intercomparison Project 3b (ISIMIP3b) daily meteorological forcing data[61] from five GCMs under CMIP6 (Table S1). For each GCM, we utilize bias-corrected outputs of daily maximum 2-m air temperature ($T_{max}$) to identify and calculate heatwave characteristics, daily mean 2-m air temperature ($T_{mean}$), and daily precipitation (P) to compute the SPI and the SPEI. Additionally, we use TWS from 10 GCM-GHM coupling models to obtain TWS-DSI. All simulations cover both the historical period (1941–2014) and future projections (2015–2100), which are conducted at a spatial resolution of 0.5° × 0.5°. We derive the MME mean using two ways. The first way involves taking the simple arithmetic average of the results from the 10 GCM-GHM coupling models. The second way involves using Pearson correlation coefficients between each GCM-GHM coupling model and the validation data as weights to calculate a weighted average. All subsequent statistical analyses in our study are based on the weighted average MME.

### Validation of the GCM-GHM simulations

TWS anomalies from Gravity Recovery and Climate Experiment (GRACE) satellite measurements are employed to validate TWS simulations from GCM-GHM coupling models for the 2002–2014 period. We use the latest monthly land-mass grids products from the Jet Propulsion Laboratory of the California Institute of Technology.[75] The monthly land-mass grids contain water-mass anomalies given as equivalent water thickness derived from GRACE time-variable gravity observations during the specified time span and relative to the specified time-mean reference period (2004–2009). The TWS anomalies data have a spatial resolution of 1° × 1°, and the TWS simulation results from GCM-GHM coupling models are bilinearly interpolated to a spatial resolution of 1° × 1° for matching the TWS anomalies data during the validation.

To validate the simulated $T_{max}$, $T_{mean}$, and P simulations from GCMs, we collected climate station data from the National Climatic Data Center (NCDC) for the years 1942–2014. The NCDC is a division of the National Oceanic and Atmospheric Administration (NOAA) in the United States, responsible for collecting, storing, analyzing, and disseminating global meteorological, climatic, and environmental data. The NCDC meteorological data include information such as temperature, precipitation, wind speed, and wind direction from various locations worldwide. We utilized 3-h temperature and precipitation data for Chinese regions and calculated $T_{max}$, $T_{mean}$, and P. These data were then used to validate the simulations by matching them with GCM outputs at the grid cells corresponding to the station locations.

### Relative humidity and air pollutant data

To strengthen the precise identification of the association between CDHW and mortality risk, we calculate atmospheric relative humidity and collect air pollutant data as additional control variables. The relative humidity is estimated based on daily maximum temperature and daily mean dew point temperature by using the Magnus approximation.[76]

$$RH = \frac{\exp\left(\frac{17.625 \times T_d}{243.04+T_d}\right)}{\exp\left(\frac{17.625 \times T_{max}}{243.04+T_{max}}\right)} \times 100 \quad \text{(Equation 1)}$$

where $T_d$ and $T_{max}$ represent daily mean dew point temperature and daily maximum temperature in °C. These temperature data are from the European Centre for Medium-Range Weather Forecasts Reanalysis v5 (ERA5).[77] The ERA5 combines satellite and *in situ* observations with state-of-the-art assimilation and modeling techniques to provide estimates of climate variables with global coverage and one-hourly and 0.25° × 0.25° resolution. In addition, we collect $PM_1$, $PM_{2.5}$, $PM_{10}$, and ozone data from the ChinaHighAirPollutants (CHAP) dataset,[78] with a spatial resolution of 1 km and a temporal resolution of 1 day.

### Older population data

Our survey samples are obtained from the CLHLS, which is a prospective, longitudinal and population-based study of older adults in China. The survey began in 1998 and has been conducted every 2–3 years. It covers half of the cities and counties across 23 provinces (including provincial-level municipalities and autonomous regions) in China. These counties account for approximately 85% of the national total population. The CLHLS in 1998 and 2000 primarily focused on elderly individuals aged 80 years and above, while the surveys included the population aged 65 years and above from 2002 to 2020 in China. The CLHLS was approved by the Biomedical Ethics Committee, Peking University, Beijing, China (IRB00001052-13074). Written informed consent was obtained from all participants.

From the CLHLS for the years 2002–2014, we select 35,085 respondents from 944 county-level administrative units. Among these respondents, 20,536 (58.53%) are male and 14,549 (41.47%) are female, 1,659 older adults participated in five waves (471 of whom died), 1,948 older adults participated in four waves (984 of whom died), 4,595 participated in three waves (2,407 of whom died), 8,212 participated in two waves (5,243 of whom died), and 18,671 participated in one wave (12,233 of whom died).

Each older adult is matched with CDHW characteristics, atmospheric relative humidity, and air pollutant data in the county where he/she lives from 1 year before the survey date. This involves separately recording the number of CDHWs, duration and average severity of each CDHW, average relative humidity, average $PM_1$ concentration, average $PM_{2.5}$ concentration, average $PM_{10}$ concentration, and average ozone concentration experienced by each older adult in the year prior to the survey date. These data at the county level are obtained by aggregating the grid-scale data into counties and weighted according to the areas of their boundaries. When the county's area is smaller than that of a single grid, the data in it are derived from the grid where it is located. For some older adults, we reassign their counties due to factors such as the county boundaries change (Note S3), and also collect their socioeconomic status, health, education, diseases, and their families (Note S4 and Table S3). Finally, we construct a panel dataset of 35,085 respondents with a follow-up period of 13 years, resulting in 64,967 follow-up records and 21,338 death records.

### Drought identification and characteristics

We use three different drought indices in this study: (1) TWS-DSI to identify terrestrial water storage deficits,[59] (2) SPI to identify precipitation deficits,[79] and (3) SPEI to capture the combined effects of precipitation and evaporative demand on regional water availability.[80] Our analysis uses SPI and SPEI values calculated at 6-month timescales, given their ability to capture seasonal to medium-term trends in drought conditions.[81,82] Similar to previous study, we define drought as any period characterized by contiguous periods where TWS-DSI is less than −0.8[37] or SPI/SPEI is less than −1.64 (i.e., fifth percentile).[81] If a given month is under drought, all days during that month are

considered to be under drought. The severity of drought is taken as the average absolute value of TWS-DSI/SPI/SPEI indices during the days under drought. Further details on calculating drought indices are provided in the Note S5.

Droughts are characterized by the following three metrics: (1) frequency, defined as the total number of drought events in a given year; (2) duration, defined as the average number of days for each drought event in a given year; and (3) severity, defined as the average absolute value of the TWS-DSI/SPI/SPEI of each drought event in a given year.

### CDHW identification and characteristics

Heatwave definitions in the literature vary globally.[15,32,37,83] Generally, a heatwave is defined as consecutive days with daily temperature measures exceeding specific thresholds, including absolute and relative thresholds. To determine which heatwave definition is the best to capture the health impact of CDHWs, we generate 15 heatwave definitions by combining five relative thresholds ($T_{max}$ exceeded 90.0th, 92.5th, 95th, 97.5$^{th}$, and 99th percentiles of the reference period 1941–2014) with three durations of $\geq$2, $\geq$3, and $\geq$4 days. Considering the possible epidemiological significance,[37,84] two successive heatwave events are independent if they are at least 2 days apart. Otherwise, they are clustered into a single event. We also assess the heatwave characteristics using the following three metrics: (1) frequency, defined as the total number of heatwave events in a given year; (2) duration, defined as the average days of each heatwave event in a given year; and (3) severity (*HWs*), where *HWs* is estimated by summing the daily $T_{max}$ anomalies:

$$HW_s = \sum_{d=1}^{d=D}\left(\frac{T_{max,d} - T_{25p}}{T_{75p} - T_{25p}}\right); D \geq 2/3/4 \quad \text{(Equation 2)}$$

where *D* denotes the duration of a heatwave event, $T_{max,d}$ is the daily maximum temperature at day *d* in this event, and $T_{25p}$ and $T_{75p}$ are the 25th and 75th percentiles of $T_{max}$ over the study period.

A CDHW event is identified as a heatwave and a drought event occurring simultaneously.[10,37,38] By combining 15 heatwave definitions with three drought indices, we obtain 45 CDHW definitions. CDHW characteristics are also assessed using the following three metrics: (1) frequency, defined as the total number of CDHWs in a given year; (2) duration, defined as the average days of each CDHW event in a given year; and (3) severity (*CDHWs*), where *CDHWs* is estimated as the product of the daily standardized values of $T_{max}$ and the absolute value of daily TWS-DSI/SPI/SPEI (the value is determined to be the same as the monthly TWS-DSI/SPI/SPEI for each month) in the CDHW event. The severity for a CDHW (*CDHWs*) is thus given as:

$$CDHW_s = \sum_{d=1}^{d=CDHW_D}\left[(-1 \times \mathrm{TWS} - \mathrm{DSI_d}/\mathrm{SPI_d}/\mathrm{SPEI_d}) \times \left(\frac{T_{max,d} - T_{25p}}{T_{75p} - T_{25p}}\right)\right]; CDHW_D \geq 2/3/4 \quad \text{(Equation 3)}$$

where $CDHW_D$ represents the duration of the coinciding days, and $\mathrm{TWS-DSI_d/SPI_d/SPEI_d}$ is the TWS-DSI/SPI/SPEI value at day *d*, which is consistent at a monthly scale. Then, the *CDHWs* for a given year is the average severity of all CDHWs within the year. We also calculate the coincidence rate to represent the likelihood of droughts and heatwaves co-occurring as the ratio of the total number of CDHWs and heatwave events for a given year at any given location.

### Cox proportional hazards model

Participants were followed from study enrollment until the first occurrence of the following events: lost contact, death, or the last date at which follow-up was considered complete (December 31, 2014). The deaths of older adults are considered censoring events. The Cox proportional hazards model is employed to estimate HRs and 95%CIs for the associations between CDHW exposures and mortality risk of older adults. To check for the co-linearity, we calculate the variance inflation factor (VIF) for each variable using the 45 CDHW definitions (Table S4) and select the optimal definition for capturing the impact of CDHW on mortality risk by computing the Akaike information criterion (AIC) and Bayesian information criterion (BIC) for different models (Table S5). We find that the optimal CDHW definition, consistent with previous research,[37,83] involves defining heatwave as a consecutive period of at least 3 days with $T_{max}$ exceeding the 92.5th percentile of the reference period, along with using TWS-DSI as the drought index (Table S5). We further find that the variations in the three characteristics of CDHWs have largely independent and varying effects on the mortality risk of older adults (Tables S6 and S7). Therefore, we incorporate the three characteristics into the model to investigate how variations in these CDHW characteristics, experienced by elderly individuals, affect mortality risk:

$$ln(M_t) = \alpha_1 CDHW_f + \alpha_2 CDHW_d + \alpha_3 CDHW_s + \beta X + ln(\gamma_0(t)) + \varepsilon_t \quad \text{(Equation 4)}$$

where $M_t$ represents the mortality risk of older adults at time *t*; $\gamma_0(t)$ represents the baseline mortality risk of older adults at time *t*; $CDHW_{f/d/s}$ is CDHW frequency, duration, and severity, respectively; *X* represents the control variable;, $\alpha$ and $\beta$ are regression coefficients; and $\varepsilon$ is the error term.

We use age (strata variable by 1 year), sex, smoking status, drinking status, physical activity, body-mass index, household income, marital status, education, relative humidity, and air pollutant as the control variables in the baseline model. Due to the high co-linearity among the concentrations of $PM_1$, $PM_{2.5}$, and $PM_{10}$ (Table S4), we opt to include $PM_{2.5}$ in the baseline model. We test the proportional hazards assumption using the Schoenfeld residual test and do not find evidence of a violation (Table S8).

All statistical tests are two-sided with $p < 0.05$ considered to be statistically significant. Analyses are conducted using the Stata statistical software, version 16.0.

### Robustness tests

We conduct seven robustness tests regarding the effects of frequency, duration, and severity of CDHWs by adjusting the regression samples (models 3–4) and incorporating various variables into the baseline model (models 5–9). These tests include (1) excluding the samples of older adults in Guangxi province, where the highest number of deaths occurs (model 3); (2) excluding older adults from the year with the highest mortality rate in 2006 (model 4); (3) including urban-rural residence as an additional control variable (model 5); (4) including the counties where the older adults are located as the additional control variable (model 6); (5) including urban-rural residence and counties of the older adults as the additional control variables (model 7); (6) including diseases of the older adults as the additional control variable (model 8); and (7) only controlling for age and sex (model 9). A detailed description of the control variables is found in Note S4.

### CDHW-related health burdens

For each 5-year age group from age 65 to 99 years, we calculate the number of deaths attributable (AN) to CDHWs in 34 provinces of China. We consider three characteristics that have been found to be associated with mortality risk: frequency, duration, and severity. Our analyses are all conducted at the grid scale and then aggregated to the provincial scale.

For each 0.5° × 0.5° grid cell, age group and CDHW characteristics as well as the all-cause deaths associated with CDHW exposure are calculated through Equation 5.

$$AN_{i,t} = \sum_{a=65}^{99} P_{i,t} \times Age_{i,t,a} \times y^0_{i,t,a} \times AF_{i,t} \quad \text{(Equation 5)}$$

where $y^0_{i,t,a}$ is the age-specific baseline mortality rate for the exposed population in the grid cell *i* at time *t*, *a* is the age group at 5-year intervals from 65 to 99 years (that is, 65–69, 70–74, …, 95–99 years), and *AF* is the attributable fraction and is the size of the exposed population in the grid cell *i* at time *t*. In particular, *AF* is calculated by $AF = (HR - 1)/HR$. *HR* is the HR attributable to CDHW exposures. Below we describe the data source and methods for each parameter.

#### *Population and age*

Based on the population and economic projections from the integrated assessment models, we obtain the age-specific population projections from two datasets. For total population and age structures, we use the projections from the International Institute for Applied Systems Analysis (IIASA) SSP population dataset,[56] which include projections from 2010 to 2100 (with 5-year intervals)

for each 5-year age group. Similar to the previous study,[41] to match the spatial resolution of the CDHW characteristics simulation, we downscale population to the grid level using the NASA Socioeconomic Data and Applications Center (SEDAC) gridded global population projections from 2010 to 2100 with 10-year intervals and a 0.5° resolution.[57]

$y^0$

For the year of 2014 and future periods for each SSP, we use the age-specific baseline mortality rates projected by the International Futures (IFs) model v7.89.[59] The baseline mortality rates from IFs are projected on the basis of primary drivers such as income, education, and technological advancement, combined with a range of other social and behavioral factors. To cross-check the validity of the projected baseline mortality rates, we check the 2017–2019 baseline mortality rates from IFs against the rates reported by the Global Burden of Disease (GBD) studies,[85] and find that they are comparable (Table S12).

*AF*

We use the exposure-mortality functions obtained from model 2 and the MME mean of the GCM-GHM coupling models to estimate HR and AF for each grid cell in a given year under different scenarios. There are differences in response to CDHW duration and severity by sex, while other HRs do not show differences based on sex and 5-year age groups.

### Decomposition analysis

For each 0.5° × 0.5° grid cell, we compute the percentage contribution of the following four individual factors to future changes in CDHW-related deaths using the decomposition method[86]: (1) effect of the population size, (2) effect of the change in age structure (i.e., population aging), (3) effect of the changes in CDHW exposures, and (4) effect of the mortality rates independent of exposure to CDHWs (i.e., the change in the baseline mortality rate due to the changes in access to healthcare, treatment, and other risk factors). We estimate the contribution of different factors by sequentially introducing each factor into the AN equation. The differences between each consecutive step provide an estimate of the relative contribution of each factor. We then estimate the results under all sequence permutations of the four factors (i.e., 24 combinations). The final estimation of the contributions from different factors is the average of the results for all sequences. Further details are provided in Note S6.

### Uncertainty assessment

Estimation of the mortality burden under climate change involves numerous uncertainties deriving from the complex interactions among SSP-RCP scenarios, climate models and scenarios, projection of the baseline mortality rate, and uncertainty in estimated future CDHW-mortality associations. We consider the differences in population and baseline mortality rates under the three SSP scenarios. Other sources of uncertainties in attributable deaths are related to CIs for CHDW-mortality relationships, differences in climate model predictions under the three SSP-RCP scenarios, and variabilities in CDHW predictions of 10 GCM-GHM coupling models in specific SSP-RCP scenarios. The sources of uncertainties at different time points are analyzed using a method similar to the decomposition of the driving factors.

## RESOURCE AVAILABILITY

### Lead contact

Requests for further information and resources should be directed to and will be fulfilled by the lead contact, Prof. Liqiang Zhang (zhanglq@bnu.edu.cn).

### Materials availability

This study did not generate new unique materials.

### Data and code availability

The CMIP6-based simulations are freely available from the ISIMIP project portal (https://data.isimip.org/search/tree/ISIMIP3b). The GRACE products are available from https://grace.jpl.nasa.gov/data/get-data/. The ERA5 reanalysis data are from https://www.ecmwf.int/en/forecasts/datasets/reanalysis-datasets/era5. The climate station data are from https://www.ncei.noaa.gov/. The ChinaHighAirPollutants data are from https://weijing-rs.github.io/product.html. The CLHLS data are available upon reasonable request through the public website dedicated to the CLHLS dataset. The following link provides the application process to help get access to the data: https://opendata.pku.edu.cn/dataverse/CHADS. All code for this study has been deposited at https://doi.org/10.5281/zenodo.12731062.

## ACKNOWLEDGMENTS

This work was supported by the National Natural Science Foundation of China under grants 41925006, 42293272, and 72104240. We sincerely thank Prof. Cascade Tuholske for his suggestions.

## AUTHOR CONTRIBUTIONS

Conceptualization, X.Y. and Liqiang Zhang; methodology, X.Y., Y.Q., J. Yin, Lei Zhang, J.L., and Q.Y.; investigation, C.B., M.L., Lei Zhang, and P.L.; visualization, X.Y.; supervision, Liqiang Zhang, A.K.M., R.D., J. Yang, S.L., C.Z., and P.L.; writing – original draft, X.Y., Liqiang Zhang, and Q.W.; writing – review and editing, X.Y., Liqiang Zhang, A.K.M., J. Yin, and Y.Q.

## DECLARATION OF INTERESTS

The authors declare no competing interests.

## SUPPLEMENTAL INFORMATION

Supplemental information can be found online at https://doi.org/10.1016/j.oneear.2024.09.016.

Received: January 14, 2024
Revised: May 27, 2024
Accepted: September 25, 2024
Published: October 17, 2024

## REFERENCES

1. Easterling, D.R., Meehl, G.A., Parmesan, C., Changnon, S.A., Karl, T.R., and Mearns, L.O. (2000). Climate extremes: observations, modeling, and impacts. Science *289*, 2068–2074. https://doi.org/10.1126/science.289.5487.2068.
2. Meehl, G.A., and Tebaldi, C. (2004). More intense, more frequent, and longer lasting heat waves in the 21st century. Science *305*, 994–997. https://doi.org/10.1126/science.1098704.
3. Ciais, P., Reichstein, M., Viovy, N., Granier, A., Ogée, J., Allard, V., Aubinet, M., Buchmann, N., Bernhofer, C., Carrara, A., et al. (2005). Europe-wide reduction in primary productivity caused by the heat and drought in 2003. Nature *437*, 529–533. https://doi.org/10.1038/nature03972.
4. Jaeger, W.K., Amos, A., Conklin, D.R., Langpap, C., Moore, K., and Plantinga, A.J. (2019). Scope and limitations of drought management within complex human–natural systems. Nat. Sustain. *2*, 710–717. https://doi.org/10.1038/s41893-019-0326-y.
5. Zhang, P., Jeong, J.H., Yoon, J.H., Kim, H., Wang, S.Y.S., Linderholm, H.W., Fang, K., Wu, X., Chen, D., and Chen, D. (2020). Abrupt shift to hotter and drier climate over inner East Asia beyond the tipping point. Science *370*, 1095–1099. https://doi.org/10.1126/science.abb3368.
6. Lim, E.P., Hendon, H.H., Boschat, G., Hudson, D., Thompson, D.W.J., Dowdy, A.J., and Arblaster, J.M. (2019). Australian hot and dry extremes induced by weakenings of the stratospheric polar vortex. Nat. Geosci. *12*, 896–901. https://doi.org/10.1038/s41561-019-0456-x.
7. Bevacqua, E., Zappa, G., Lehner, F., and Zscheischler, J. (2022). Precipitation trends determine future occurrences of compound hot–dry events. Nat. Clim. Change *12*, 350–355. https://doi.org/10.1038/s41558-022-01309-5.
8. Dirmeyer, P.A., Jin, Y., Singh, B., and Yan, X. (2013). Evolving land–atmosphere interactions over North America from CMIP5 simulations. J. Clim. *26*, 7313–7327. https://doi.org/10.1175/JCLI-D-12-00454.1.
9. Alizadeh, M.R., Adamowski, J., Nikoo, M.R., AghaKouchak, A., Dennison, P., and Sadegh, M. (2020). A century of observations reveals increasing

likelihood of continental-scale compound dry-hot extremes. Sci. Adv. *6*, eaaz4571. https://doi.org/10.1126/sciadv.aaz4571.

10. Mukherjee, S., and Mishra, A.K. (2021). Increase in compound drought and heatwaves in a warming world. Geophys. Res. Lett. *48*, e2020GL090617. https://doi.org/10.1029/2020GL090617.
11. Sharma, S., and Mujumdar, P. (2017). Increasing frequency and spatial extent of concurrent meteorological droughts and heatwaves in India. Sci. Rep. *7*, 15582. https://doi.org/10.1038/s41598-017-15896-3.
12. Yu, R., and Zhai, P. (2020). More frequent and widespread persistent compound drought and heat event observed in China. Sci. Rep. *10*, 14576. https://doi.org/10.1038/s41598-020-71312-3.
13. Manning, C., Widmann, M., Bevacqua, E., Van Loon, A.F., Maraun, D., and Vrac, M. (2019). Increased probability of compound long-duration dry and hot events in Europe during summer (1950–2013). Environ. Res. Lett. *14*, 094006. https://doi.org/10.1088/1748-9326/ab23bf.
14. Markonis, Y., Kumar, R., Hanel, M., Rakovec, O., Máca, P., and AghaKouchak, A. (2021). The rise of compound warm-season droughts in Europe. Sci. Adv. *7*, eabb9668. https://doi.org/10.1126/sciadv.abb9668.
15. Mazdiyasni, O., and AghaKouchak, A. (2015). Substantial increase in concurrent droughts and heatwaves in the United States. Proc. Natl. Acad. Sci. USA *112*, 11484–11489. https://doi.org/10.1073/pnas.1422945112.
16. Geirinhas, J.L., Russo, A., Libonati, R., Sousa, P.M., Miralles, D.G., and Trigo, R.M. (2021). Recent increasing frequency of compound summer drought and heatwaves in Southeast Brazil. Environ. Res. Lett. *16*, 034036. https://doi.org/10.1088/1748-9326/abe0eb.
17. Lewis, S.C., and Karoly, D.J. (2013). Anthropogenic contributions to Australia's record summer temperatures of 2013. Geophys. Res. Lett. *40*, 3705–3709. https://doi.org/10.1002/grl.50673.
18. Cowan, T., Purich, A., Perkins, S., Pezza, A., Boschat, G., and Sadler, K. (2014). More frequent, longer, and hotter heat waves for Australia in the twenty-first century. J. Clim. *27*, 5851–5871. https://doi.org/10.1175/JCLI-D-14-00092.1.
19. Reichstein, M., Bahn, M., Ciais, P., Frank, D., Mahecha, M.D., Seneviratne, S.I., Zscheischler, J., Beer, C., Buchmann, N., Frank, D.C., et al. (2013). Climate extremes and the carbon cycle. Nature *500*, 287–295. https://doi.org/10.1038/nature12350.
20. Gampe, D., Zscheischler, J., Reichstein, M., O'Sullivan, M., Smith, W.K., Sitch, S., and Buermann, W. (2021). Increasing impact of warm droughts on northern ecosystem productivity over recent decades. Nat. Clim. Change *11*, 772–779. https://doi.org/10.1038/s41558-021-01112-8.
21. CDC, U.S., EPA, U.S., NOAA, AWA (2010). When Every Drop Counts: Protecting Public Health during Drought Conditions—A Guide for Public Health Professionals (U.S. Department of Health and Human Services).
22. English, P.B., Sinclair, A.H., Ross, Z., Anderson, H., Boothe, V., Davis, C., Ebi, K., Kagey, B., Malecki, K., Shultz, R., et al. (2009). Environmental health indicators of climate change for the United States: findings from the State Environmental Health Indicator Collaborative. Environ. Health Perspect. *117*, 1673–1681. https://doi.org/10.1289/ehp.0900708.
23. Kalis, M.A., Miller, M.D., and Wilson, R.J. (2009). Public health and drought. J. Environ. Health *72*, 10–11.
24. Peterson, T.C., Karl, T.R., Kossin, J.P., Kunkel, K.E., Lawrimore, J.H., McMahon, J.R., Vose, R.S., Yin, X., and Yin, X. (2014). Changes in weather and climate extremes: State of knowledge relevant to air and water quality in the United States. J. Air Waste Manag. Assoc. *64*, 184–197. https://doi.org/10.1080/10962247.2013.851044.
25. Tong, D.Q., Wang, J.X.L., Gill, T.E., Lei, H., and Wang, B. (2017). Intensified dust storm activity and Valley fever infection in the southwestern United States. Geophys. Res. Lett. *44*, 4304–4312. https://doi.org/10.1002/2017GL073524.
26. Delpla, I., Jung, A.V., Baures, E., Clement, M., and Thomas, O. (2009). Impacts of climate change on surface water quality in relation to drinking water production. Environ. Int. *35*, 1225–1233. https://doi.org/10.1016/j.envint.2009.07.001.
27. Trtanj, J., Jantarasami, L., Brunkard, J., Collier, T., Jacobs, J., Lipp, E., McLellan, S., Moore, S., Paerl, H., Ravenscroft, J., et al. (2016). Ch. 6: Climate impacts on water-related illness. In The impacts of climate change on human health in the United States: a scientific assessment, pp. 157–188.
28. Haines, A., Kovats, R.S., Campbell-Lendrum, D., and Corvalán, C. (2006). Climate change and human health: impacts, vulnerability, and mitigation. Lancet *367*, 2101–2109. https://doi.org/10.1016/S0140-6736(06)68933-2.
29. Zeng, Q., Li, G., Cui, Y., Jiang, G., and Pan, X. (2016). Estimating temperature-mortality exposure-response relationships and optimum ambient temperature at the multi-city level of China. Int. J. Environ. Res. Publ. Health *13*, 279. https://doi.org/10.3390/ijerph13030279.
30. Ebi, K.L., Capon, A., Berry, P., Broderick, C., de Dear, R., Havenith, G., Honda, Y., Kovats, R.S., Ma, W., Malik, A., et al. (2021). Hot weather and heat extremes: health risks. Lancet *398*, 698–708. https://doi.org/10.1016/S0140-6736(21)01208-3.
31. Oudin Åström, D., Schifano, P., Asta, F., Lallo, A., Michelozzi, P., Rocklöv, J., and Forsberg, B. (2015). The effect of heat waves on mortality in susceptible groups: a cohort study of a mediterranean and a northern European City. Environ. Health *14*, 1–8. https://doi.org/10.1186/s12940-015-0012-0.
32. Xu, Z., FitzGerald, G., Guo, Y., Jalaludin, B., and Tong, S. (2016). Impact of heatwave on mortality under different heatwave definitions: a systematic review and meta-analysis. Environ. Int. *89–90*, 193–203. https://doi.org/10.1016/j.envint.2016.02.007.
33. Mitchell, D., Heaviside, C., Vardoulakis, S., Huntingford, C., Masato, G., P Guillod, B., Frumhoff, P., Bowery, A., Wallom, D., Allen, M., and Allen, M. (2016). Attributing human mortality during extreme heat waves to anthropogenic climate change. Environ. Res. Lett. *11*, 074006. https://doi.org/10.1088/1748-9326/11/7/074006.
34. Park Williams, A., Allen, C.D., Macalady, A.K., Griffin, D., Woodhouse, C.A., Meko, D.M., Swetnam, T.W., Rauscher, S.A., Seager, R., Grissino-Mayer, H.D., et al. (2013). Temperature as a potent driver of regional forest drought stress and tree mortality. Nat. Clim. Change *3*, 292–297. https://doi.org/10.1038/nclimate1693.
35. Anderegg, W.R.L., Schwalm, C., Biondi, F., Camarero, J.J., Koch, G., Litvak, M., Ogle, K., Shaw, J.D., Shevliakova, E., Williams, A.P., et al. (2015). Pervasive drought legacies in forest ecosystems and their implications for carbon cycle models. Science *349*, 528–532. https://doi.org/10.1126/science.aab1833.
36. Zampieri, M., Ceglar, A., Dentener, F., and Toreti, A. (2017). Wheat yield loss attributable to heat waves, drought and water excess at the global, national and subnational scales. Environ. Res. Lett. *12*, 064008. https://doi.org/10.1088/1748-9326/aa723b.
37. Yin, J., Gentine, P., Slater, L., Gu, L., Pokhrel, Y., Hanasaki, N., Guo, S., Xiong, L., Schlenker, W., and Schlenker, W. (2023). Future socio-ecosystem productivity threatened by compound drought–heatwave events. Nat. Sustain. *6*, 259–272. https://doi.org/10.1038/s41893-022-01024-1.
38. Tripathy, K.P., Mukherjee, S., Mishra, A.K., Mann, M.E., and Williams, A.P. (2023). Climate change will accelerate the high-end risk of compound drought and heatwave events. Proc. Natl. Acad. Sci. USA *120*, e2219825120. https://doi.org/10.1073/pnas.2219825120.
39. Buonocore, J.J., Luckow, P., Norris, G., Spengler, J.D., Biewald, B., Fisher, J., and Levy, J.I. (2016). Health and climate benefits of different energy-efficiency and renewable energy choices. Nat. Clim. Change *6*, 100–105. https://doi.org/10.1038/nclimate2771.
40. Scovronick, N., Budolfson, M., Dennig, F., Errickson, F., Fleurbaey, M., Peng, W., Socolow, R.H., Spears, D., Wagner, F., and Wagner, F. (2019). The impact of human health co-benefits on evaluations of global climate policy. Nat. Commun. *10*, 2095. https://doi.org/10.1038/s41467-019-09499-x.
41. Yang, H., Huang, X., Westervelt, D.M., Horowitz, L., and Peng, W. (2022). Socio-demographic factors shaping the future global health burden from

air pollution. Nat. Sustain. *6*, 58–68. https://doi.org/10.1038/s41893-022-00976-8.

42. Kruk, M.E., Gage, A.D., Arsenault, C., Jordan, K., Leslie, H.H., Roder-DeWan, S., Adeyi, O., Barker, P., Daelmans, B., Doubova, S.V., et al. (2018). High-quality health systems in the Sustainable Development Goals era: time for a revolution. Lancet Global Health *6*, e1196–e1252.
43. Chen, H., and Sun, J. (2015). Changes in drought characteristics over China using the standardized precipitation evapotranspiration index. J. Clim. *28*, 5430–5447. https://doi.org/10.1175/JCLI-D-14-00707.1.
44. Shao, D., Chen, S., Tan, X., and Gu, W. (2018). Drought characteristics over China during 1980–2015. Int. J. Climatol. *38*, 3532–3545. https://doi.org/10.1002/joc.5515.
45. Wei, K., and Chen, W. (2011). An abrupt increase in the summer high temperature extreme days across China in the mid-1990s. Adv. Atmos. Sci. *28*, 1023–1029. https://doi.org/10.1007/s00376-010-0080-6.
46. Guo, X., Huang, J., Luo, Y., Zhao, Z., and Xu, Y. (2017). Projection of heat waves over China for eight different global warming targets using 12 CMIP5 models. Theor. Appl. Climatol. *128*, 507–522. https://doi.org/10.1007/s00704-015-1718-1.
47. Hao, Z., Hao, F., Singh, V.P., and Zhang, X. (2018). Changes in the severity of compound drought and hot extremes over global land areas. Environ. Res. Lett. *13*, 124022. https://doi.org/10.1088/1748-9326/aaee96.
48. Kong, Q., Guerreiro, S.B., Blenkinsop, S., Li, X.F., and Fowler, H.J. (2020). Increases in summertime concurrent drought and heatwave in Eastern China. Weather Clim. Extrem. *28*, 100242. https://doi.org/10.1016/j.wace.2019.100242.
49. Ren, Z. (2022). China aging research report 2022. http://www.caoss.org.cn/UploadFile/pic/20229281791192316.pdf.
50. Tatum, M. (2022). China's population peak. Lancet *399*, 509. https://doi.org/10.1016/S0140-6736(22)00227-6.
51. Cai, W., Zhang, C., Zhang, S., Bai, Y., Callaghan, M., Chang, N., Chen, B., Chen, H., Cheng, L., Cui, X., et al. (2022). The 2022 China report of the Lancet Countdown on health and climate change: leveraging climate actions for healthy ageing. Lancet Public Health *7*, e1073–e1090. https://doi.org/10.1016/S2468-2667(22)00224-9.
52. O'Meara, S. (2020). How health research will support China's ageing population. Nature *578*, 1–3. https://doi.org/10.1038/d41586-020-00279-y.
53. O'Neill, B.C., Carter, T.R., Ebi, K., Harrison, P.A., Kemp-Benedict, E., Kok, K., Kriegler, E., Preston, B.L., Riahi, K., Sillmann, J., et al. (2020). Achievements and needs for the climate change scenario framework. Nat. Clim. Change *10*, 1074–1084. https://doi.org/10.1038/s41558-020-00952-0.
54. Eyring, V., Bony, S., Meehl, G.A., Senior, C.A., Stevens, B., Stouffer, R.J., and Taylor, K.E. (2016). Overview of the Coupled Model Intercomparison Project Phase 6 (CMIP6) experimental design and organization. Geosci. Model Dev. (GMD) *9*, 1937–1958. https://doi.org/10.5194/gmd-9-1937-2016.
55. IPCC Climate Change 2021 (2021). The Physical Science Basis. In Contribution of Working Group I to the Sixth Assessment Report of the Intergovernmental Panel on Climate Change, V. Masson-Delmotte, P. Zhai, A. Pirani, S.L. Connors, C. Péan, S. Berger, N. Caud, Y. Chen, L. Goldfarb, and M.I. Gomis, eds. (Cambridge Univ. Press).
56. Riahi, K., Van Vuuren, D.P., Kriegler, E., Edmonds, J., O'Neill, B.C., Fujimori, S., Bauer, N., Calvin, K., Dellink, R., Fricko, O., et al. (2017). The Shared Socioeconomic Pathways and their energy, land use, and greenhouse gas emissions implications: An overview. Global Environ. Change *42*, 153–168. https://doi.org/10.1016/j.gloenvcha.2016.05.009.
57. Jones, B., and O'Neill, B.C. (2017). Global Population Projection Grids Based on Shared Socioeconomic Pathways (SSPs), 2010-2100 (NASA Socioeconomic Data and Applications Center (SEDAC)).
58. International Futures, F.S.P.C. (2022). International Futures (IFs) Modeling System*7.89* (Josef Korbel School of International Studies, University of Denver). https://pardee.du.edu/access-ifs.
59. Zhao, M., Zhang, J., Zhang, J., Velicogna, I., Liang, C., and Li, Z. (2020). Ecological restoration impact on total terrestrial water storage. Nat. Sustain. *4*, 56–62. https://doi.org/10.1038/s41893-020-00600-7.
60. Pokhrel, Y., Felfelani, F., Satoh, Y., Boulange, J., Burek, P., Gädeke, A., Gerten, D., Gosling, S.N., Grillakis, M., Gudmundsson, L., et al. (2021). Global terrestrial water storage and drought severity under climate change. Nat. Clim. Change *11*, 226–233. https://doi.org/10.1038/s41558-020-00972-w.
61. Wu, X., Hao, Z., Zhang, Y., Zhang, X., and Hao, F. (2022). Anthropogenic influence on compound dry and hot events in China based on Coupled Model Intercomparison Project Phase 6 models. Int. J. Climatol. *42*, 4379–4390. https://doi.org/10.1002/joc.7473.
62. Lien, E.C., Westermark, A.M., Zhang, Y., Yuan, C., Li, Z., Lau, A.N., Sapp, K.M., Wolpin, B.M., Vander Heiden, M.G., and Vander Heiden, M.G. (2021). Low glycaemic diets alter lipid metabolism to influence tumour growth. Nature *599*, 302–307. https://doi.org/10.1038/s41586-021-04049-2.
63. Hill, W., Lim, E.L., Weeden, C.E., Lee, C., Augustine, M., Chen, K., Kuan, F.C., Marongiu, F., Evans, E.J., Jr., Moore, D.A., et al. (2023). Lung adenocarcinoma promotion by air pollutants. Nature *616*, 159–167. https://doi.org/10.1038/s41586-023-05874-3.
64. US Burden of Disease Collaborators, Mokdad, A.H., Ballestros, K., Echko, M., Glenn, S., Olsen, H.E., Mullany, E., Lee, A., Khan, A.R., Ahmadi, A., et al. (2018). The state of US health, 1990-2016: Burden of diseases, injuries, and risk factors among US states. JAMA, J. Am. Med. Assoc. *319*, 1444–1472. https://doi.org/10.1001/jama.2018.0158.
65. Field, C.B., and Barros, V.R. (2014). Climate Change 2014–Impacts, Adaptation and Vulnerability: Regional Aspects (Cambridge University Press).
66. Watts, N., Adger, W.N., Agnolucci, P., Blackstock, J., Byass, P., Cai, W., Chaytor, S., Colbourn, T., Collins, M., Cooper, A., et al. (2015). Health and climate change: policy responses to protect public health. Lancet *386*, 1861–1914. https://doi.org/10.1016/S0140-6736(15)60854-6.
67. Green, H., Bailey, J., Schwarz, L., Vanos, J., Ebi, K., and Benmarhnia, T. (2019). Impact of heat on mortality and morbidity in low and middle income countries: a review of the epidemiological evidence and considerations for future research. Environ. Res. *171*, 80–91. https://doi.org/10.1016/j.envres.2019.01.010.
68. Scheelbeek, P.F.D., Dangour, A.D., Jarmul, S., Turner, G., Sietsma, A.J., Minx, J.C., Callaghan, M., Ajibade, I., Austin, S.E., Biesbroek, R., et al. (2021). The effects on public health of climate change adaptation responses: a systematic review of evidence from low-and middle-income countries. Environ. Res. Lett. *16*, 073001. https://doi.org/10.1088/1748-9326/ac092c.
69. Jay, O., Capon, A., Berry, P., Broderick, C., de Dear, R., Havenith, G., Honda, Y., Kovats, R.S., Ma, W., Malik, A., et al. (2021). Reducing the health effects of hot weather and heat extremes: from personal cooling strategies to green cities. Lancet *398*, 709–724. https://doi.org/10.1016/S0140-6736(21)01209-5.
70. Marjanović, V., Milovančević, M., and Mladenović, I. (2016). Prediction of GDP growth rate based on carbon dioxide (CO2) emissions. J. CO2 Util. *16*, 212–217. https://doi.org/10.1016/j.jcou.2016.07.009.
71. Sterpu, M., Soava, G., and Mehedintu, A. (2018). Impact of economic growth and energy consumption on greenhouse gas emissions: Testing environmental curves hypotheses on EU countries. Sustainability *10*, 3327. https://doi.org/10.3390/su10093327.
72. Petoukhov, V., Petri, S., Rahmstorf, S., Coumou, D., Kornhuber, K., and Schellnhuber, H.J. (2016). Role of quasiresonant planetary wave dynamics in recent boreal spring-to-autumn extreme events. Proc. Natl. Acad. Sci. USA *113*, 6862–6867. https://doi.org/10.1073/pnas.1606300113.
73. Mann, M.E., Rahmstorf, S., Kornhuber, K., Steinman, B.A., Miller, S.K., and Coumou, D. (2017). Influence of anthropogenic climate change on planetary wave resonance and extreme weather events. Sci. Rep. *7*, 45242. https://doi.org/10.1038/srep45242.

74. Mann, M.E., Rahmstorf, S., Kornhuber, K., Steinman, B.A., Miller, S.K., Petri, S., and Coumou, D. (2018). Projected changes in persistent extreme summer weather events: The role of quasi-resonant amplification. Sci. Adv. *4*, eaat3272. https://doi.org/10.1126/sciadv.aat3272.

75. Landerer, F.W., and Swenson, S.C. (2012). Accuracy of scaled GRACE terrestrial water storage estimates. Water Resour. Res. *48*, W04531. https://doi.org/10.1029/2011WR011453.

76. Alduchov, O.A., and Eskridge, R.E. (1996). Improved Magnus form approximation of saturation vapor pressure. J. Appl. Meteorol. *35*, 601–609. https://doi.org/10.1175/1520-0450(1996)035<0601:IMFAOS>2.0.CO;2.

77. Copernicus Climate Change Service: ECMWF Reanalysis v5 (ERA5). https://www.ecmwf.int/en/forecasts/datasets/reanalysis-datasets/era5.

78. Wei, J., Li, Z., Lyapustin, A., Sun, L., Peng, Y., Xue, W., Su, T., Cribb, M., and Cribb, M. (2021). Reconstructing 1-km-resolution high-quality PM2. 5 data records from 2000 to 2018 in China: spatiotemporal variations and policy implications. Remote Sens. Environ. *252*, 112136. https://doi.org/10.1016/j.rse.2020.112136.

79. McKee, T.B., Doesken, N.J., and Kleist, J. (1993). The relationship of drought frequency and duration to time scales. In Proceedings of the 8th Conference on Applied Climatology, *17*, pp. 179–183.

80. Vicente-Serrano, S.M., Beguería, S., and López-Moreno, J.I. (2010). A multiscalar drought index sensitive to global warming: the standardized precipitation evapotranspiration index. J. Clim. *23*, 1696–1718. https://doi.org/10.1175/2009JCLI2909.1.

81. Generoso, R., Couharde, C., Damette, O., and Mohaddes, K. (2020). The growth effects of El Nino and La Nina: Local weather conditions matter. Ann. Econ. Stat. *140*, 83–126. https://doi.org/10.15609/annaeconstat2009.140.0083.

82. Rastogi, D., Trok, J., Depsky, N., Monier, E., and Jones, A. (2023). Historical evaluation and future projections of compound heatwave and drought extremes over the conterminous United States in CMIP6. Environ. Res. Lett. *19*, 014039. https://doi.org/10.1088/1748-9326/ad0efe.

83. Chen, H., Zhao, L., Cheng, L., Zhang, Y., Wang, H., Gu, K., Bao, J., Yang, J., Liu, Z., Huang, J., et al. (2022). Projections of heatwave-attributable mortality under climate change and future population scenarios in China. Lancet Reg. Health. West. Pac. *28*, 100582. https://doi.org/10.1016/j.lanwpc.2022.100582.

84. Keellings, D., and Waylen, P. (2014). Increased risk of heat waves in Florida: Characterizing changes in bivariate heat wave risk using extreme value analysis. Appl. Geogr. *46*, 90–97. https://doi.org/10.1016/j.apgeog.2013.11.008.

85. GBD 2019 Demographics Collaborators (2020). Global age-sex-specific fertility, mortality, healthy life expectancy (HALE), and population estimates in 204 countries and territories, 1950–2019: a comprehensive demographic analysis for the Global Burden of Disease Study 2019. Lancet *396*, 1160–1203. https://doi.org/10.1016/S0140-6736(20)30977-6.

86. GBD 2017 Risk Factor Collaborators (2018). Global, regional, and national comparative risk assessment of 84 behavioural, environmental and occupational, and metabolic risks or clusters of risks for 195 countries and territories, 1990–2017: a systematic analysis for the Global Burden of Disease Study 2017. Lancet *392*, 1923–1994. https://doi.org/10.1016/S0140-6736(18)32225-6.

**One Earth, Volume *7***

## Supplemental information

# Socio-demographic factors shape mortality risk linked to compound drought-heatwave events under climate change in China

**Xin Yao, Ying Qu, Liqiang Zhang, Ashok K. Mishra, Jiabo Yin, Ruiqiang Ding, Jing Yang, Chen Bai, Lei Zhang, Mengting Li, Pan Liu, Jintai Lin, Qiwei Yu, Suhong Liu, Qihao Wang, and Chenghu Zhou**

## Supplemental Figures

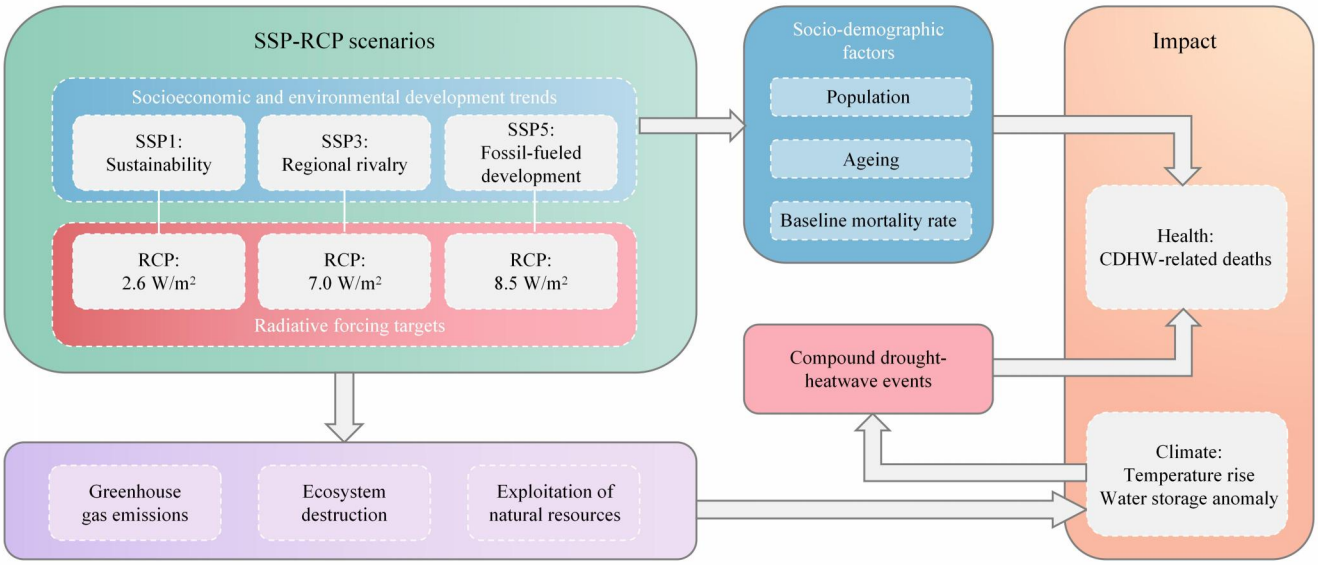


**Fig. S1.** | **The integrated modeling framework to assess future temperature rise, terrestrial water storage anomaly, and CDHW-related health burden.** We consider three scenarios that vary in socioeconomic trends, greenhouse gas emission control efforts and climate targets, i.e. SSP1-2.6, SSP3-7.0 and SSP5-8.5. For each scenario, we simulate the daily maximum 2 m air temperature ($T_{max}$) and terrestrial water storage (TWS) at 0.5°×0.5° spatial resolution using ten GCM-GHM coupling models from CMIP6. More detailed descriptions of the scenarios are available in Methods and in Supplementary Note 1.

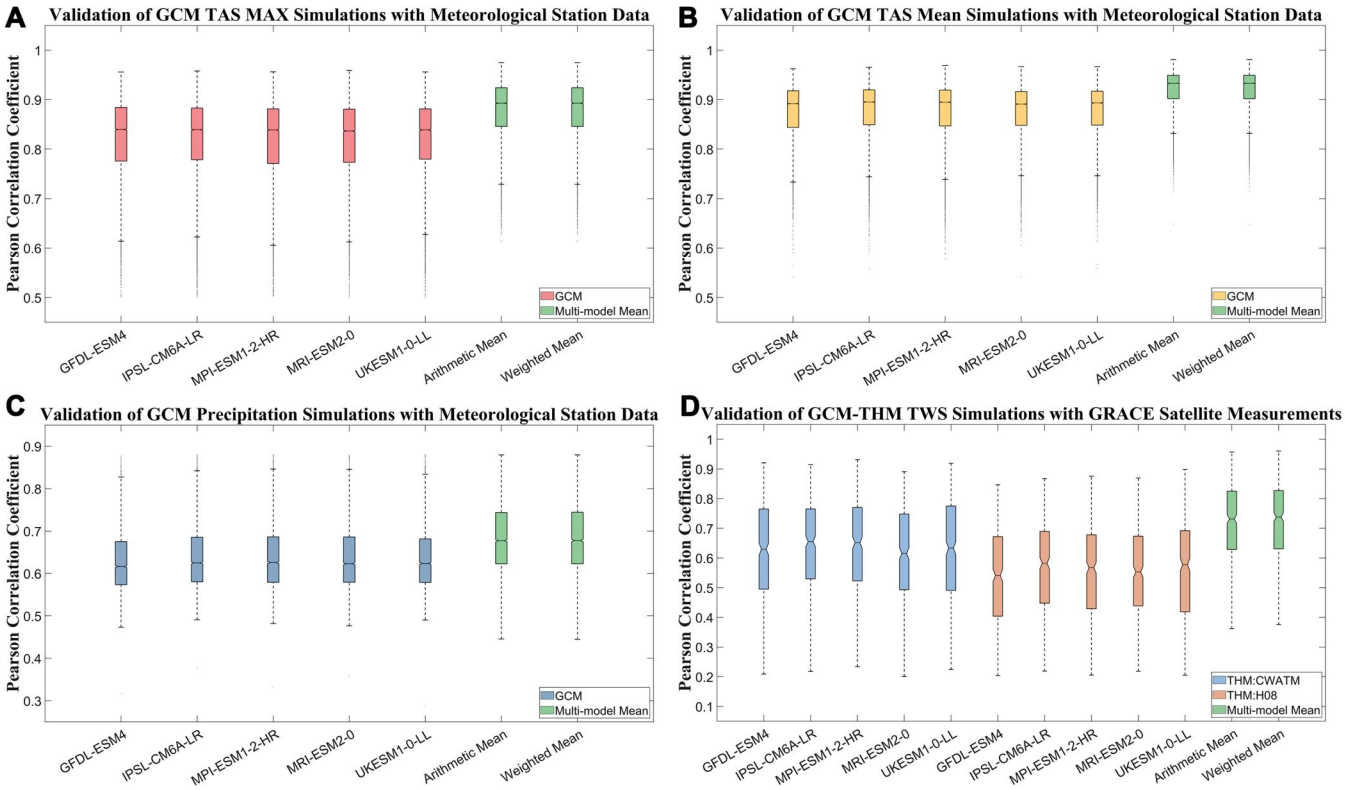


**Fig. S2.** | **Validation of the GCM-GHM coupling model simulations. A**, validation of GCM $T_{max}$ simulations with meteorological station data. **B**, validation of GCM daily mean temperature simulations with meteorological station data. **C**, validation of GCM daily precipitation simulations with meteorological station data. **D**, validation of GCM-GHM TWS simulations with GRACE satellite measurements. The centre line indicates the median value, the box bounds indicate the 25th/75th percentile values, the whiskers indicate the minimum/maximum values and the points indicate the outliers.


**Fig. S3.** | **Historical and projected changes in the frequency of CDHWs under different definitions.** Variations in the spatially averaged frequency of CDHWs under different definitions across China for historical (1941 to 1980), recent (1981 to 2014), and future periods (2015 to 2100) based on selected future climate scenarios (SSP1-2.6, SSP3-7.0, and SSP5-8.5). The asterisks indicate that the change is significant ($p<0.05$), which is detected by Mann-Kendall trend test. The shading represents the 95% confidence intervals (CIs).

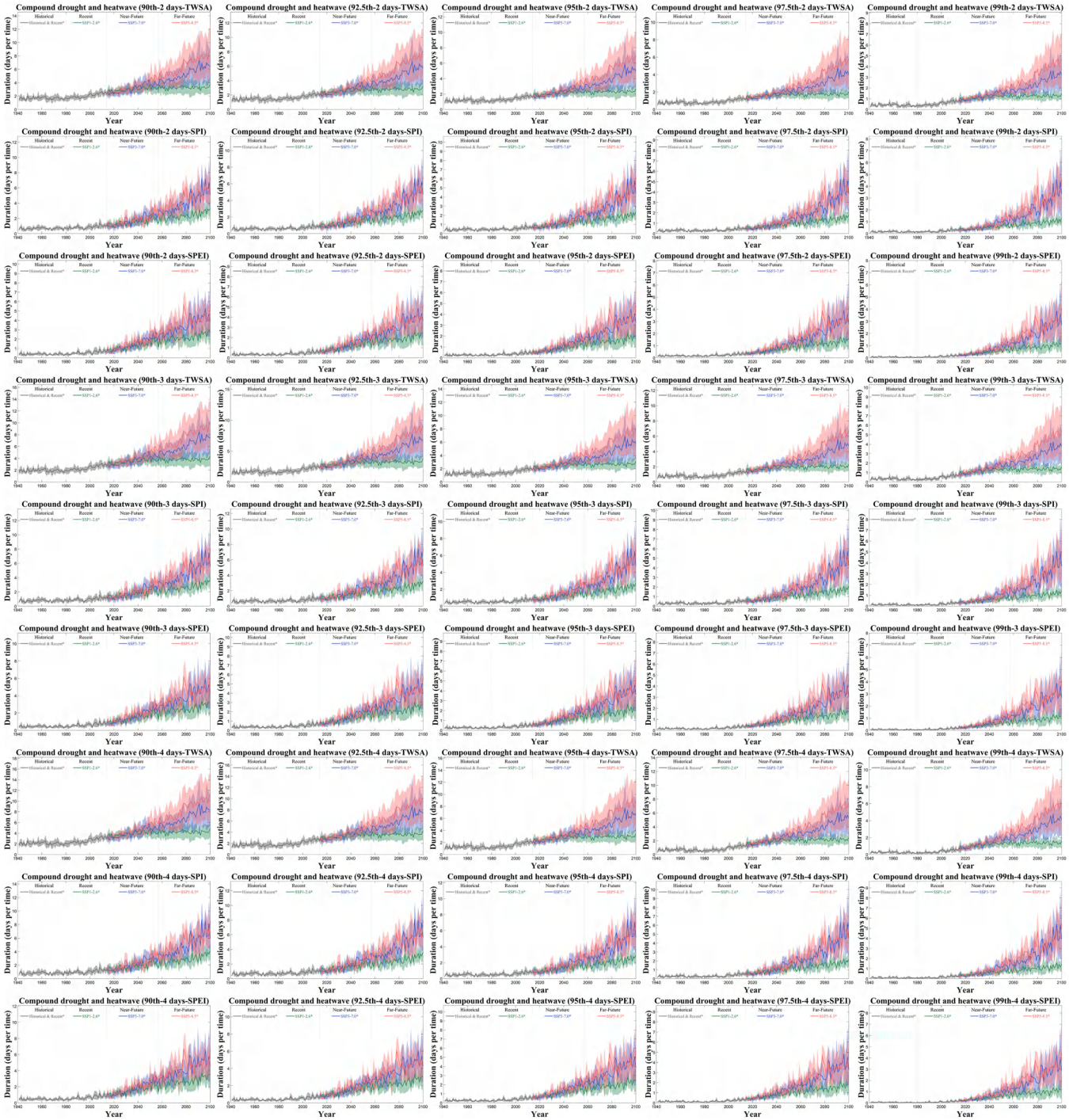


**Fig. S4.** | **Historical and projected changes in the duration of CDHWs under different definitions.** Variations in the spatially averaged duration of CDHWs under different definitions across China for historical (1941 to 1980), recent (1981 to 2014), and future periods (2015 to 2100) based on selected future climate scenarios (SSP1-2.6, SSP3-7.0, and SSP5-8.5). The asterisks indicate that the change is significant ($p<0.05$), which is detected by Mann-Kendall trend test. The shading represents the 95% CIs.

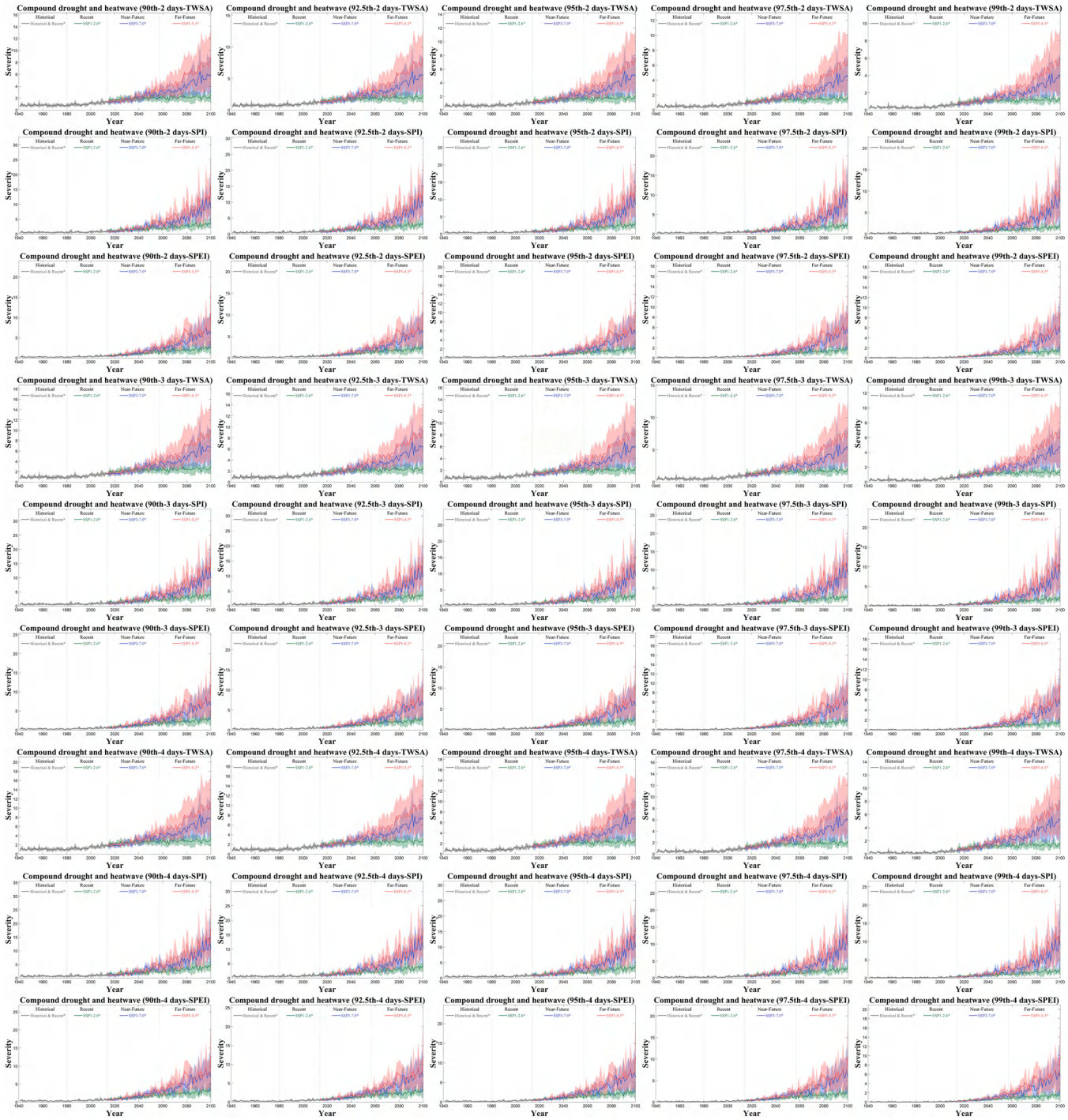


**Fig. S5.** | **Historical and projected changes in the severity of CDHWs under different definitions.** Variations in the spatially averaged severity of CDHWs under different definitions across China for historical (1941 to 1980), recent (1981 to 2014), and future periods (2015 to 2100) based on selected future climate scenarios (SSP1-2.6, SSP3-7.0, and SSP5-8.5). The asterisks indicate that the change is significant ($p<0.05$), which is detected by Mann-Kendall trend test. The shading represents the 95% CIs.

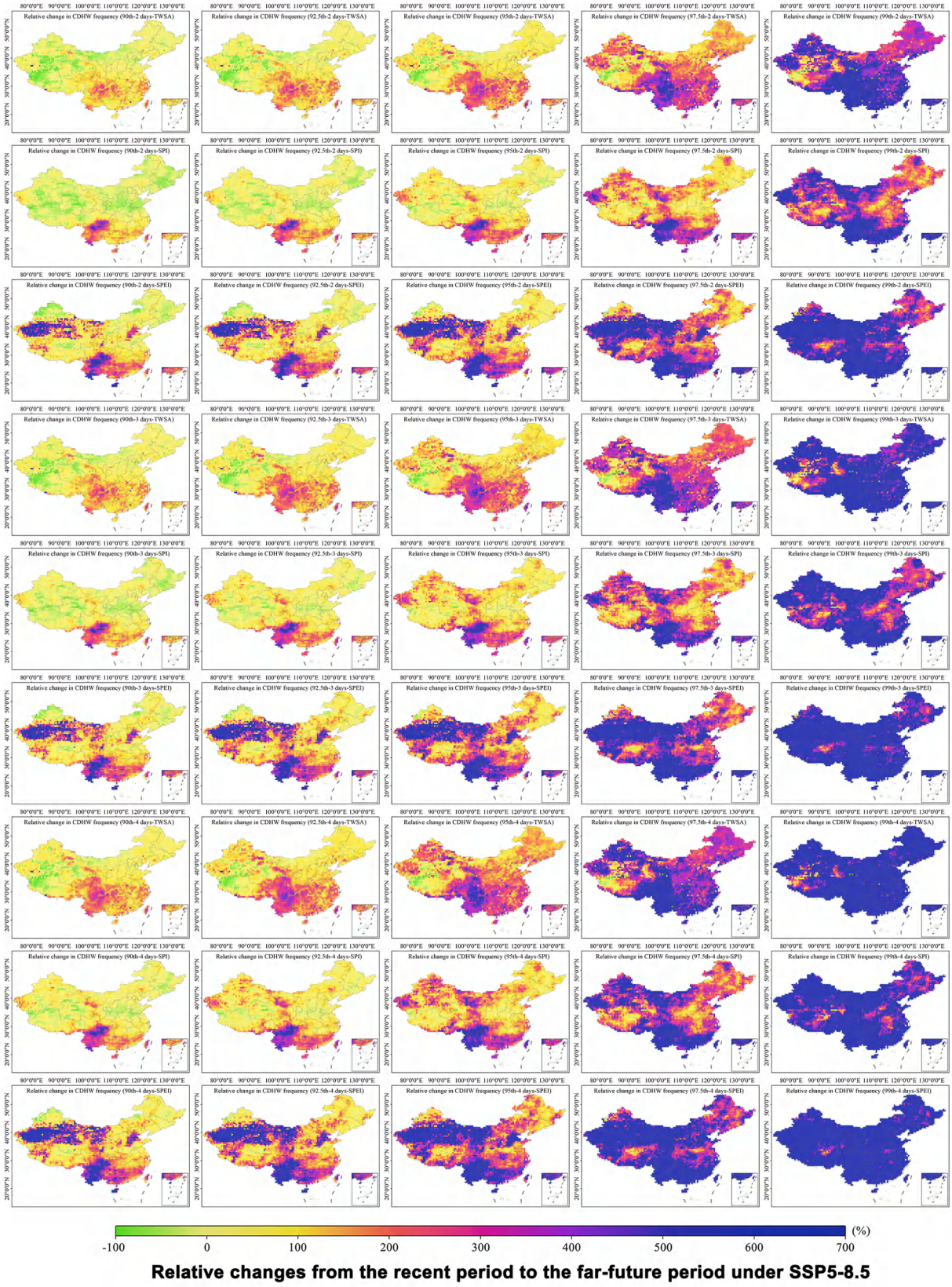


**Fig. S6.** | **The changes in the frequency of CDHWs under different definitions.** Spatial patterns of relative changes in frequency of CDHWs under different definitions between recent (1981 to 2014) and far-future (2058 to 2100) periods under SSP-5.85 scenarios.

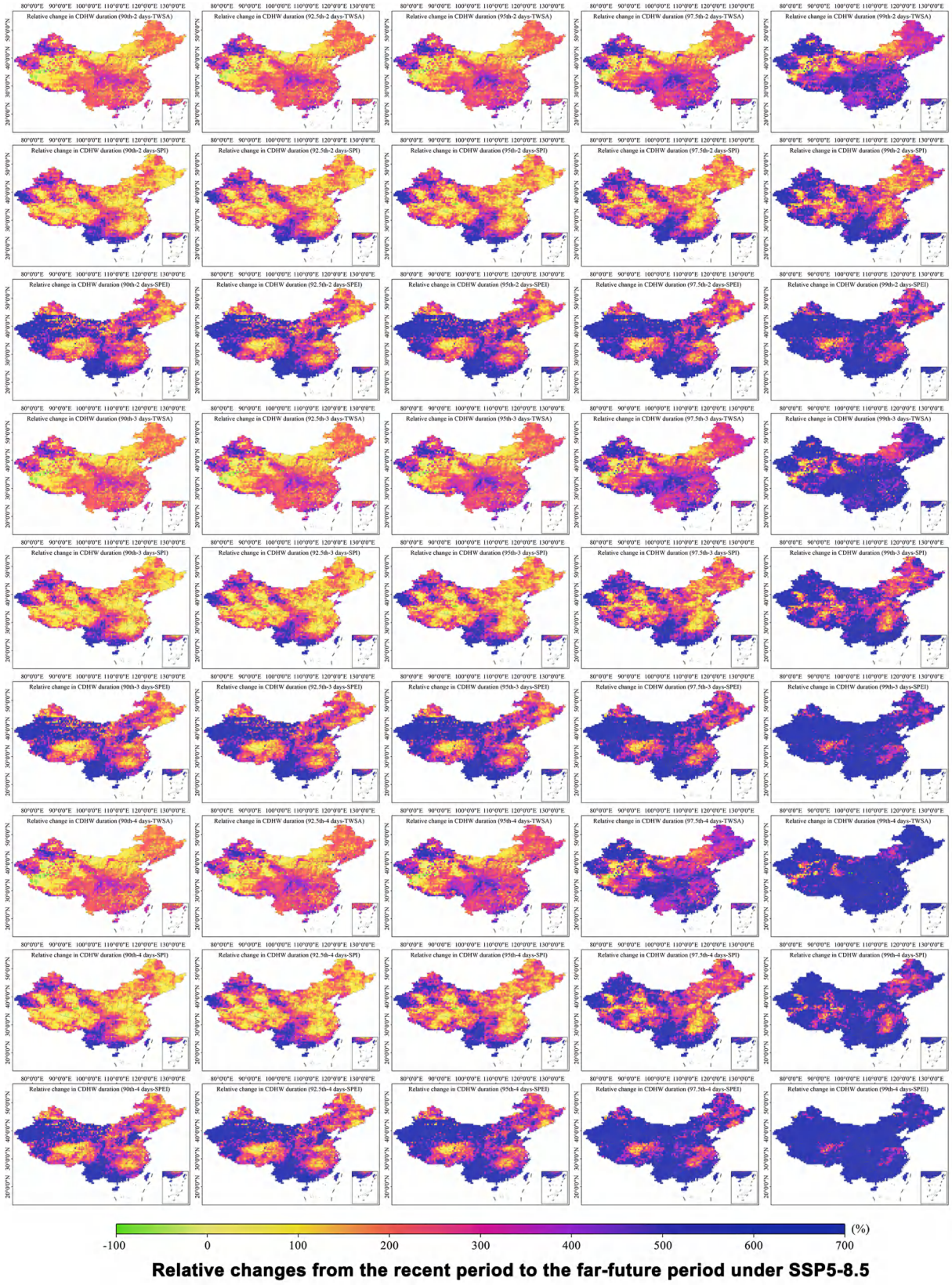


**Fig. S7.** | **The changes in the duration of CDHWs under different definitions.** Spatial patterns of relative changes in duration of CDHWs under different definitions between recent (1981 to 2014) and far-future (2058 to 2100) periods under SSP-5.85 scenarios.

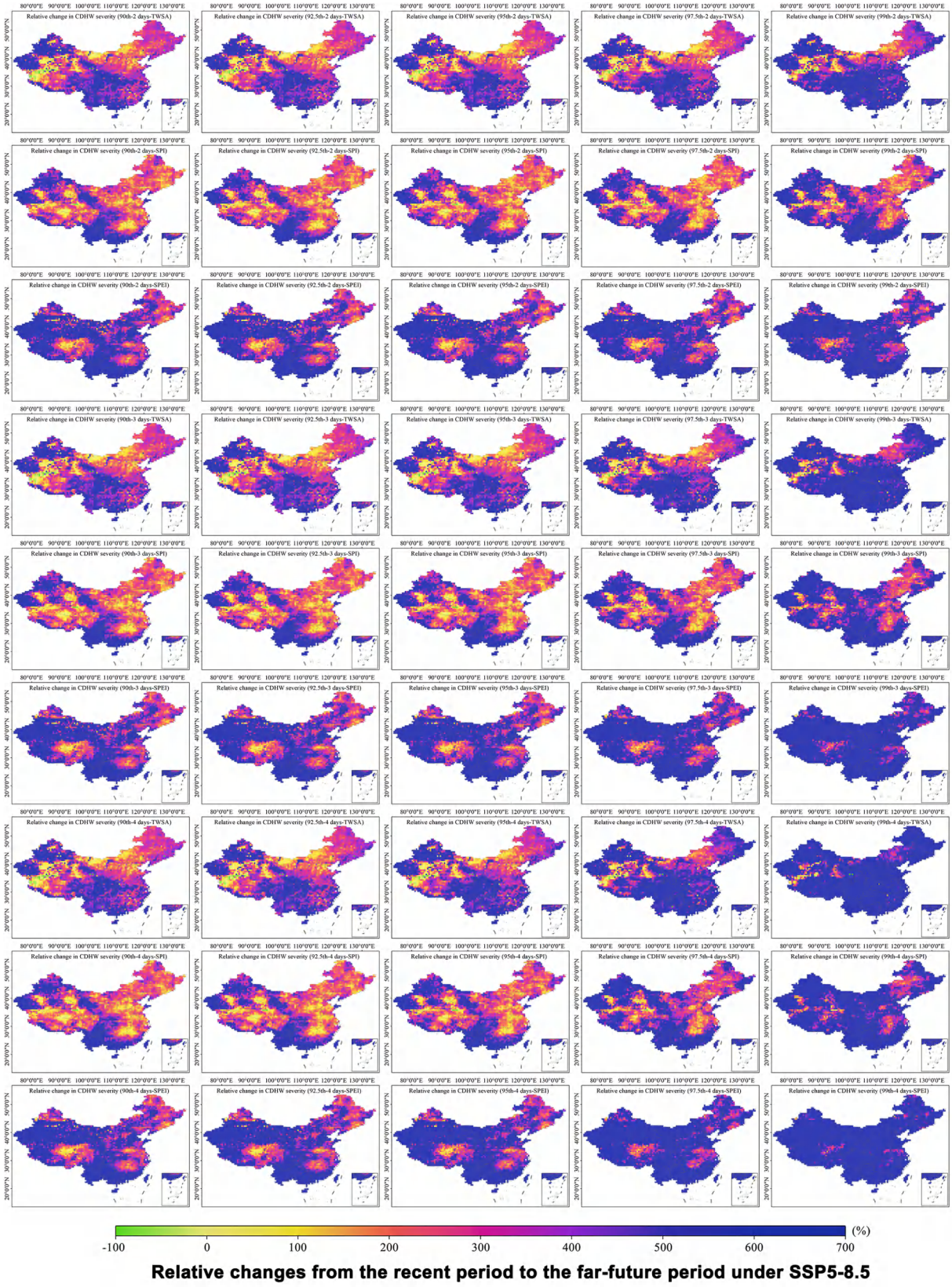


**Fig. S8.** | **The changes in the severity of CDHWs under different definitions.** Spatial patterns of relative changes in severity of CDHWs under different definitions between recent (1981 to 2014) and far-future (2058 to 2100) periods under SSP-5.85 scenarios.

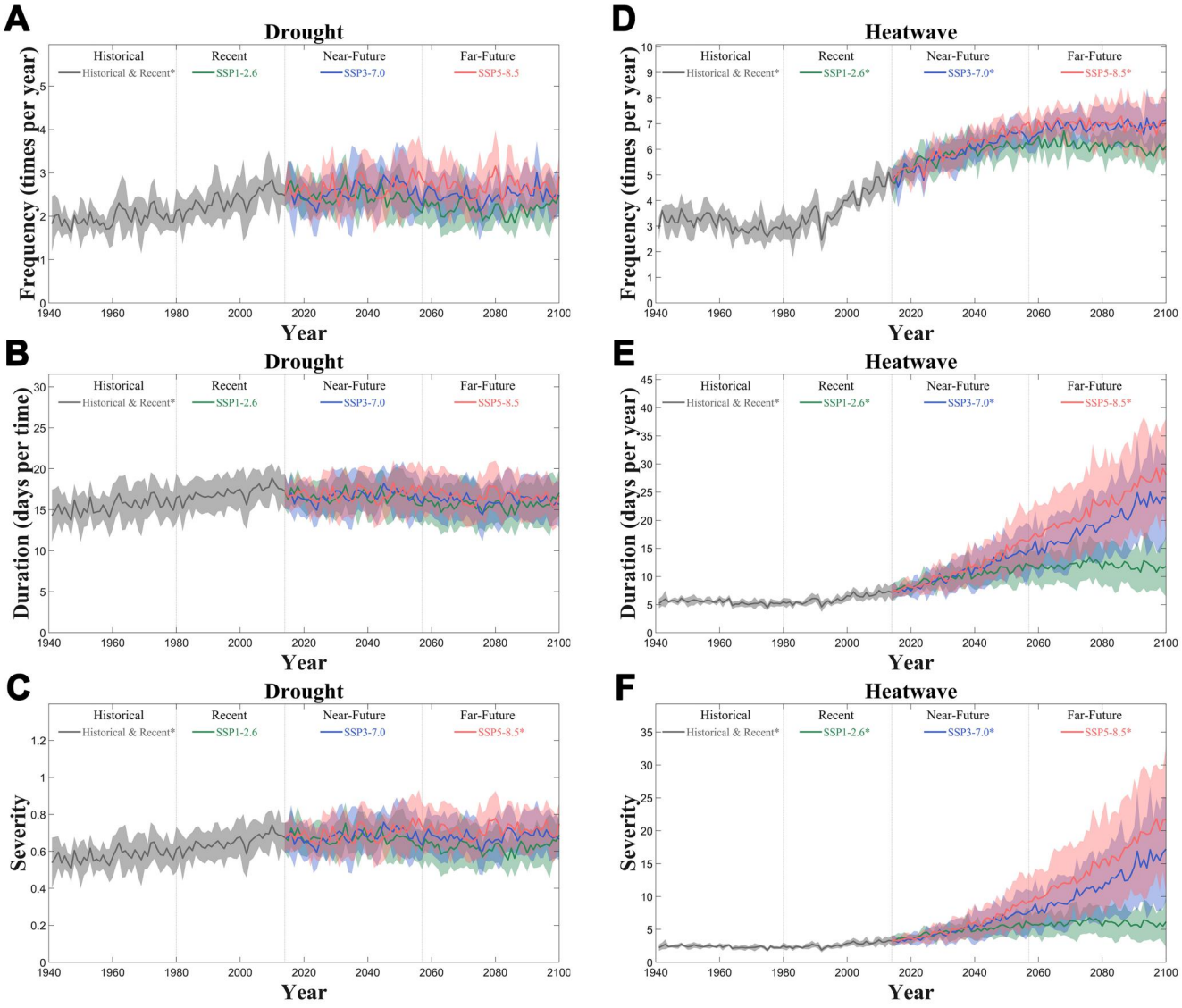


**Fig. S9.** | **Historical and projected changes in drought and heatwave characteristics.** **A**-**C**, Variation in GCM-GHM-based MME mean projections of drought characteristics—(**A**) frequency, (**B**) duration, and (**C**) severity—spatially averaged over China for historical (1941 to 1980), recent (1981 to 2014) and future periods (2015 to 2100) based on the selected future climate scenarios (SSP1-2.6, SSP3-7.0, and SSP5-8.5). **D**-**F**, Variation in GCM-based MME mean projections of heatwave characteristics. The asterisks indicate that the change is significant ($p<0.05$), which is detected by Mann-Kendall trend test. The shading represents the 95% CIs. The droughts in **A**-**C** are all identified based TWS-DSI, and the heatwaves in **D**-**E** are all identified based on the 92.5th percentile temperature threshold and 3-day duration threshold.

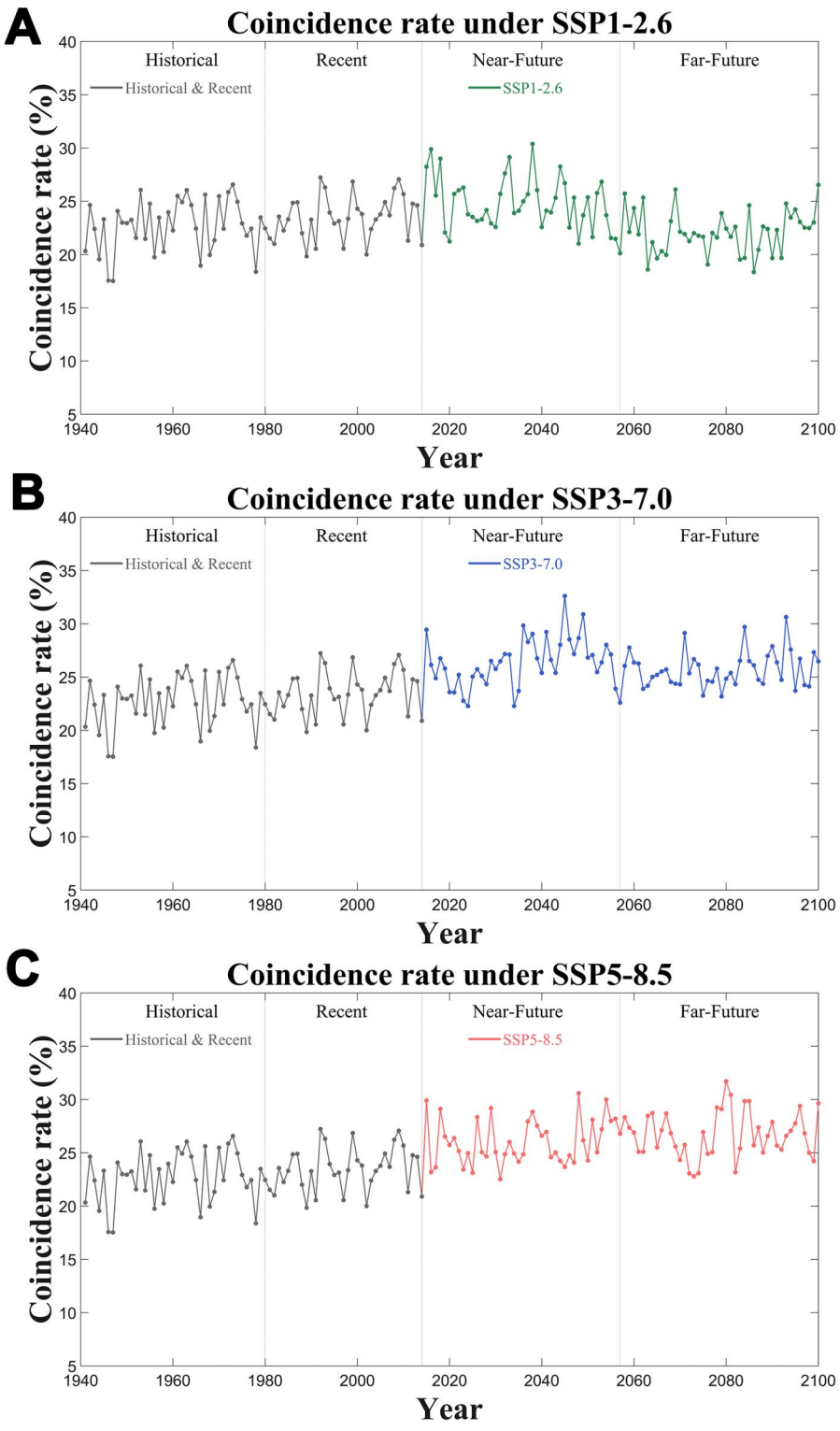


**Fig. S10.** | **Historical and projected changes in coincidence rate under different scenarios.** Variation in GCM-GHM-based MME mean projections of coincidence rate—spatially averaged over China for historical (1941 to 1980), recent (1981 to 2014) and future period (2015 to 2100) based on the selected future climate scenarios ((**A**) SSP1-2.6, (**B**) SSP3-7.0, and (**C**) SSP5-8.5). The asterisks indicate that the change is significant ($p<0.05$) as detected by the Mann-Kendall trend tests. The CDHWs in **A**-**C** are all identified based on the 92.5th percentile temperature threshold, 3-day duration threshold, and TWS-DSI as the drought index.

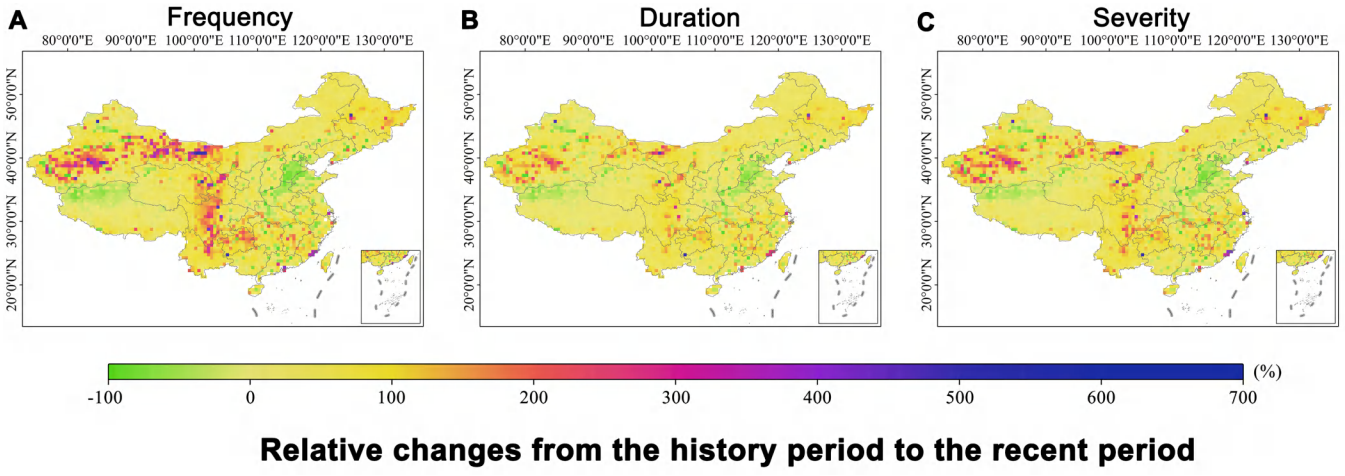


**Fig. S11.** | **The changes in the characteristics of CDHWs under model simulations.** Spatial patterns of relative changes in (**A**) frequency, (**B**) duration and (**C**) severity of CDHWs between two periods (i.e. historical: 1941 to 1980, and recent: 1981 to 2014). The CDHWs in **A**-**C** are all identified based on the 92.5th percentile temperature threshold, 3-day duration threshold, and TWS-DSI as the drought index.

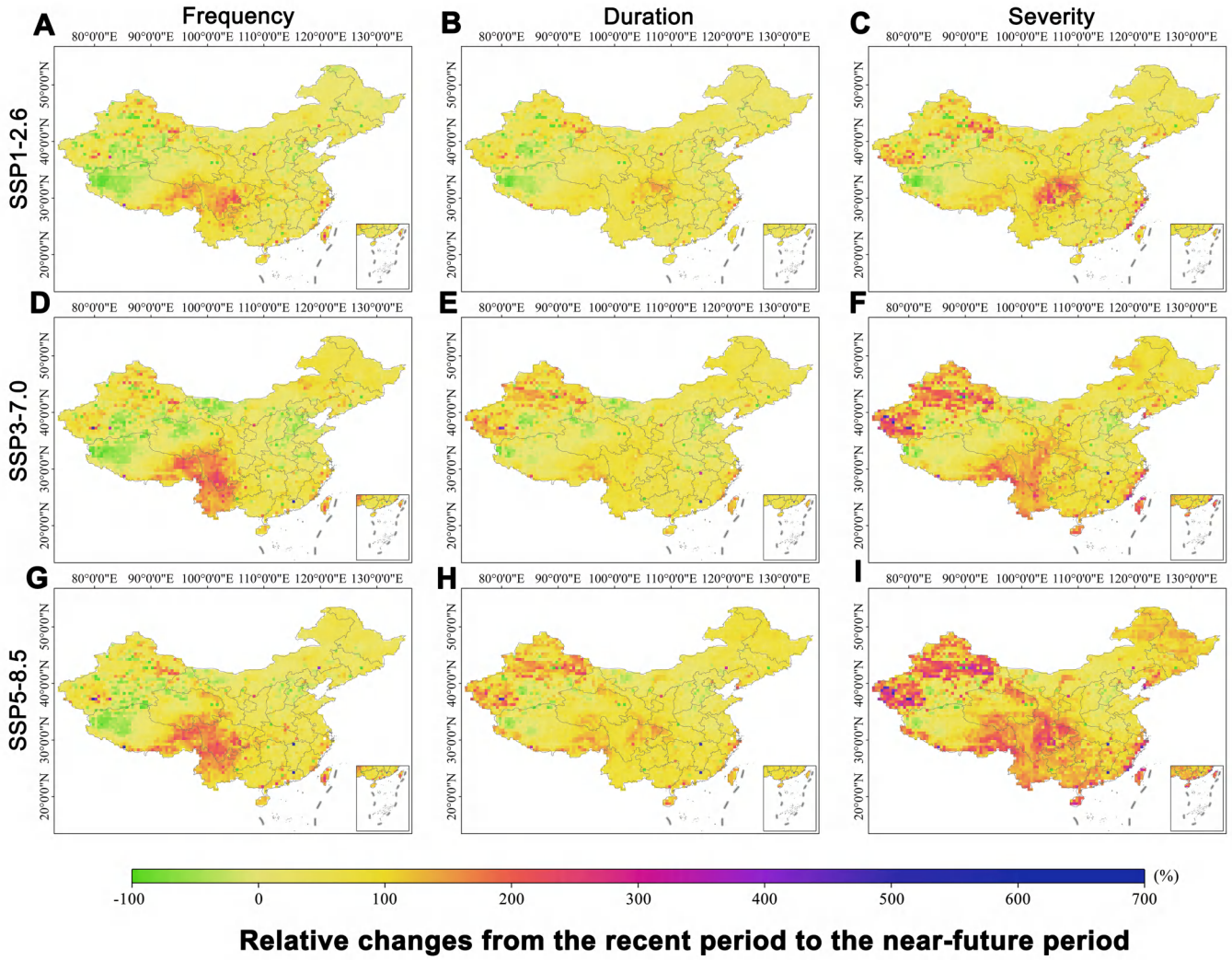


**Fig. S12.** | **The changes in CDHW characteristics under model simulations.** Spatial patterns of relative changes in CDHW frequency, duration and severity between recent (1981 to 2014) and near-future (2015 to 2057) periods under different SSP-RCP scenarios. The CDHWs in **A**-**I** are all identified based on the 92.5th percentile temperature threshold, 3-day duration threshold, and TWS-DSI as the drought index.

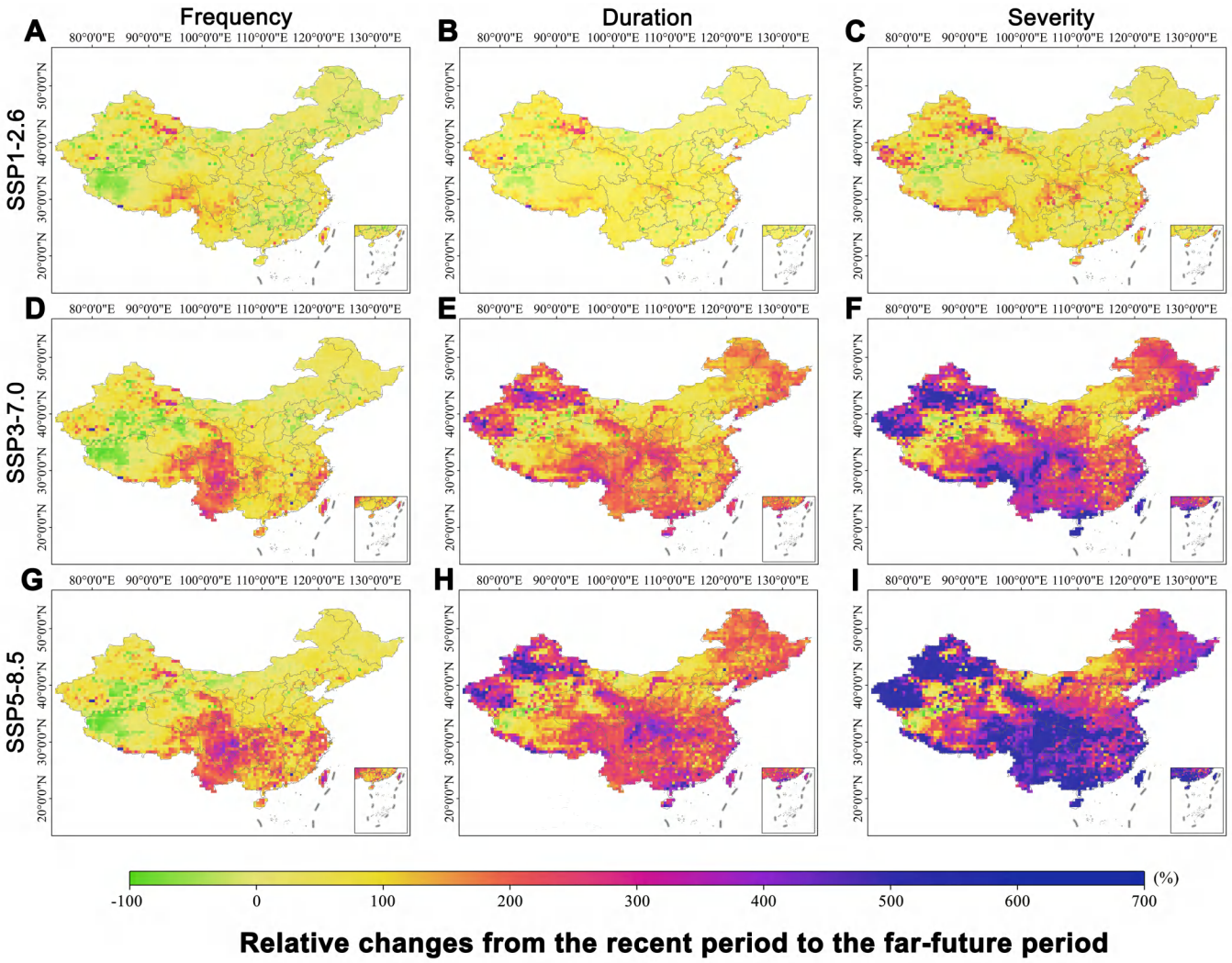


**Fig. S13.** | **The changes in CDHW characteristics under model simulations.** Spatial patterns of relative changes in CDHW frequency, duration and severity between recent and far-future (2058 to 2100) periods under different SSP-RCP scenarios. The CDHWs in **A**-**I** are all identified based on the 92.5th percentile temperature threshold, 3-day duration threshold, and TWS-DSI as the drought index.

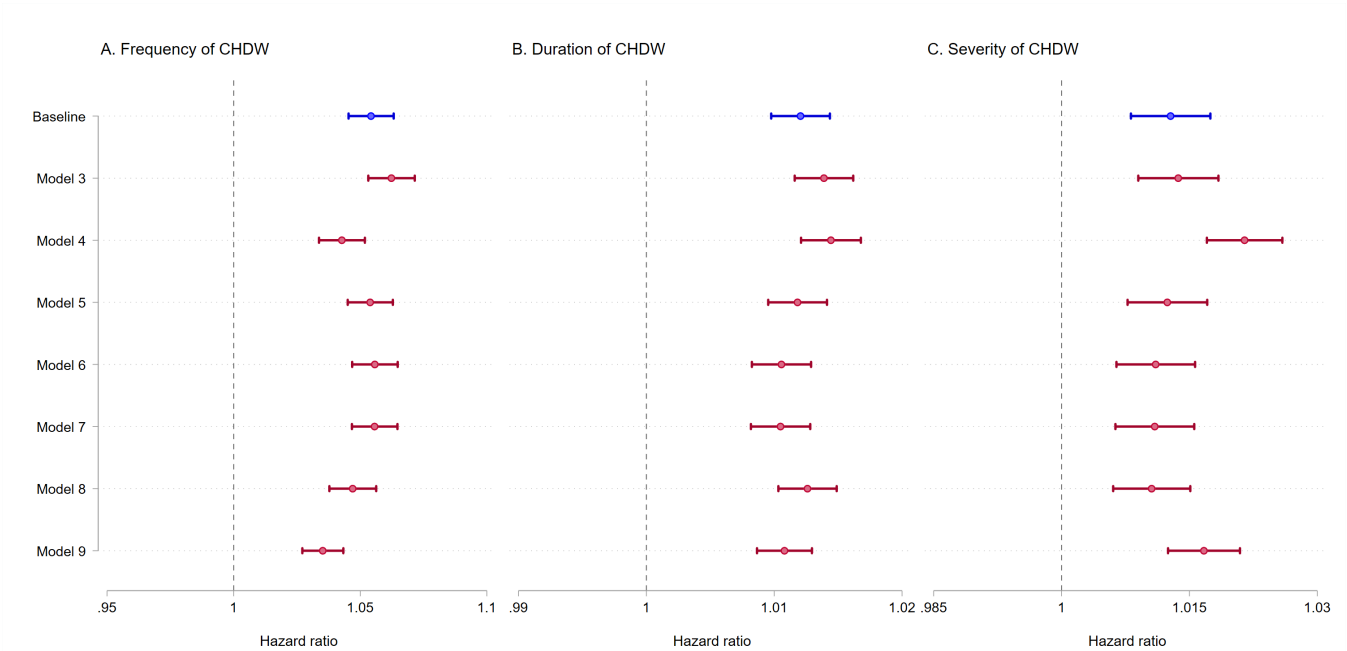


**Fig. S14.** | **Robustness tests for the baseline regression.** The robustness tests for the baseline of **A**, frequency, **B**, duration and **C**, severity of CDHWs. The first row describes the baseline estimates. The second row excludes older adult samples from Guangxi province which has the highest number of deaths. The third row excludes older adult samples from the year with the highest number of deaths in 2006. The fourth row adds urban-rural residences as an additional control variable. The fifth row adds counties of the older adults as an additional control variable. The sixth row adds urban-rural residences and counties of the older adults as additional control variables. The seventh row adds diseases of the older adults as additional control variables. The eighth row only controls for age and sex. Points and lines represent HR estimates and their corresponding 95% CIs, respectively (please see Supplementary Table 9 for more details).

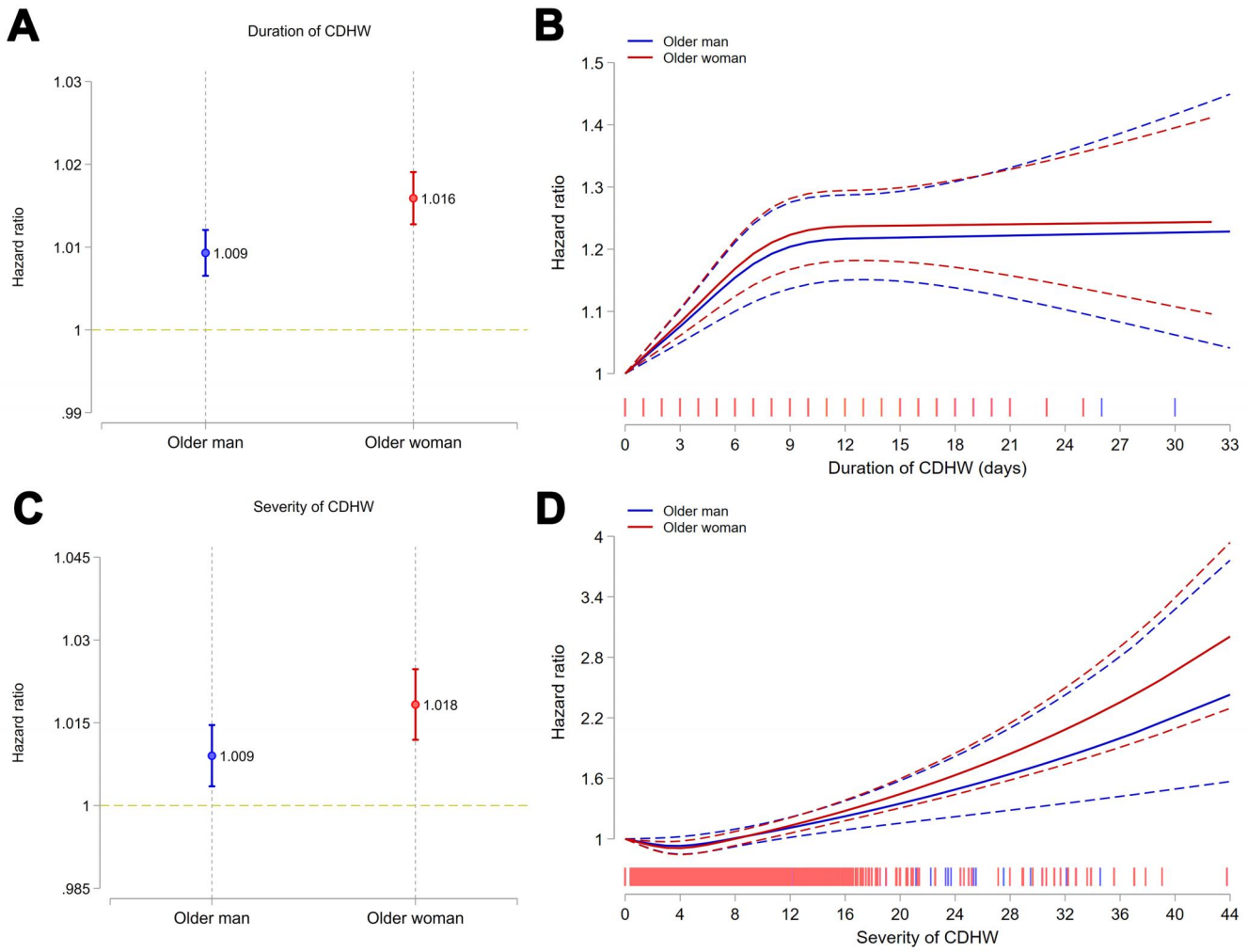


**Fig. S15.** | **HRs of deaths associated with 1-unit increase in duration and severity of CDHWs by sex subgroup. A**, HRs and 95% CIs for the association between all-cause mortality and duration of CDHW exposures by sex sub group for the baseline model. Points and lines represent HR estimates and their 95% CIs, respectively. **B**, HRs and 95% CIs for the association between all-cause mortality and severity of CDHW exposures by sex sub group for the baseline model. Points and lines represent HR estimates and their 95% CIs, respectively. **C**, Curve associations between all-cause mortality and 1-day increase in duration of CDHW by sex sub-group for Model 2. The reference duration is 0. **D**, Curve associations between all-cause mortality and 1-unit increase in severity of CDHW by sex sub-group for Model 2. The reference severity is 0.

## Supplemental Tables

**Table S1. | Summary of the model simulations under ISIMIP3b.**

| GHM | SSP-RCP scenario | Historical | SSP1-2.6 | SSP3-7.0 | SSP5-8.5 |
|---|---|---|---|---|---|
| | Simulation period / GCM | 1941-2014 | 2015-2100 | 2015-2100 | 2015-2100 |
| CWatM | GFDL-ESM4 | ✓ | ✓ | ✓ | ✓ |
| | IPSL-CM6A-LR | ✓ | ✓ | ✓ | ✓ |
| | MPI-ESM1-2-HR | ✓ | ✓ | ✓ | ✓ |
| | MRI-ESM2-0 | ✓ | ✓ | ✓ | ✓ |
| | UKESM1-0-LL | ✓ | ✓ | ✓ | ✓ |
| H08 | GFDL-ESM4 | ✓ | ✓ | ✓ | ✓ |
| | IPSL-CM6A-LR | ✓ | ✓ | ✓ | ✓ |
| | MPI-ESM1-2-HR | ✓ | ✓ | ✓ | ✓ |
| | MRI-ESM2-0 | ✓ | ✓ | ✓ | ✓ |
| | UKESM1-0-LL | ✓ | ✓ | ✓ | ✓ |

**Table S2.** | **Information of the used global hydrological models.**

| Model name | Evapotranspiration module | Snow module | Groundwater module | Runoff module (surface/subsurface runoff) | River routing module | Reservoir operation | Human water use | Reference |
|---|---|---|---|---|---|---|---|---|
| CWatM | Penman-Monteith formulation | Degree-day method | Explicit (single reservoir) | Saturation excess, baseflow | Kinematic water formulation | Yes | Irrigation, domestic, industry, livestock | Burek et al. (2020)(1) |
| H08 | Bulk formulation | Energy balance method | Explicit (renewable and non-renewable reservoirs) | Saturation excess, baseflow | Linear reservoir model | Yes | Irrigation | Hanasaki et al. (2018)(2) |

**Table S3. | Statistics of the survey data (Individuals=35,085; Records=86,305).**

| Variable | Observation | Mean | Std. Dev. | Min | Max | Missing Observation |
|---|---|---|---|---|---|---|
| Death | 86,305 | 0.247 | 0.431 | 0 | 1 | 0 |
| Age (years) | 86,305 | 88.105 | 11.253 | 65 | 120 | 0 |
| BMI | 82,599 | 23.259 | 5.353 | 11.718 | 38.205 | 3,706 |
| Education (years) | 85,858 | 1.941 | 3.352 | 0 | 25 | 447 |
| Household income (yuan) | 85,567 | 18575.35 | 27566.67 | 0 | 96752 | 738 |
| Sex | 86,305 | | | | | 0 |
| Woman | 36,600 (57.59%) | | | | | |
| Man | 49,705 (42.41%) | | | | | |
| Marital status | 85,924 | | | | | 381 |
| Currently married, living with spouse | 24,125 (28.08%) | | | | | |
| Separated | 1,409 (1.64%) | | | | | |
| Divorced | 324 (0.38%) | | | | | |
| Widowed | 59,193 (68.89%) | | | | | |
| Never married | 873 (1.02%) | | | | | |
| Smoking status | 85,826 | | | | | 479 |
| Never | 57,293 (66.75%) | | | | | |
| Currently | 1,307 (1.52%) | | | | | |
| Past | 13,328 (15.53%) | | | | | |
| Always | 13,898 (16.19%) | | | | | |
| Drinking status | 85,694 | | | | | 611 |
| Never | 58,803 (68.62%) | | | | | |
| Currently | 2,430 (2.84%) | | | | | |
| Past | 12,779 (14.91%) | | | | | |
| Always | 11,682 (13.63%) | | | | | |
| Physical activity | 85,522 | | | | | 783 |
| Never | 50,744 (59.33%) | | | | | |
| Currently | 7,913 (9.25%) | | | | | |
| Past | 11,174 (13.07%) | | | | | |
| Always | 15,691 (18.35%) | | | | | |
| Residence | 86,305 | | | | | 0 |
| Urban | 48,958 (56.73%) | | | | | |
| Rural | 37,347 (43.27%) | | | | | |
| Hypertension | 82,370 | 0.208 | 0.406 | 0 | 1 | 3,935 |
| Diabetes | 81,867 | 0.301 | 0.172 | 0 | 1 | 4,438 |
| Heart disease | 82,126 | 0.099 | 0.299 | 0 | 1 | 4,179 |
| Stroke and cerebrovascular disease | 82,283 | 0.067 | 0.251 | 0 | 1 | 4,022 |
| Bronchitis/emphysema/pneumonia and asthma | 82,554 | 0.124 | 0.331 | 0 | 1 | 3,751 |
| Tuberculosis | 82,253 | 0.008 | 0.088 | 0 | 1 | 4,052 |
| Cataracts | 82,185 | 0.127 | 0.333 | 0 | 1 | 4,120 |
| Glaucoma | 79,084 | 0.025 | 0.155 | 0 | 1 | 7,221 |
| Cancer | 81,399 | 0.006 | 0.078 | 0 | 1 | 4,906 |
| Gastrointestinal ulcers | 79,032 | 0.049 | 0.217 | 0 | 1 | 7,273 |
| Parkinson's disease | 80,184 | 0.006 | 0.078 | 0 | 1 | 6,121 |
| Pressure ulcers | 79,364 | 0.008 | 0.091 | 0 | 1 | 6,941 |
| Arthritis | 82,736 | 0.174 | 0.379 | 0 | 1 | 3,569 |
| Dementia | 82,880 | 0.034 | 0.182 | 0 | 1 | 3,425 |

## Table S4. | Testing for co-linearity among variables under different CDHW definitions.

| CDHW definition | | | VIF | | | | | | | | | | | | | | | |
|---|---|---|---|---|---|---|---|---|---|---|---|---|---|---|---|---|---|---|
| Temperature threshold | Duration threshold | Drought index | Frequency | Duration | Severity | Age | Sex | Smoking status | Drinking status | Exercising status | Household income | BMI | Marital status | Education status | Relative humidity | Ozone concentrations | PM1 concentrations | PM2.5 concentrations | PM10 concentrations |
| 90% | 2 | SPI | 1.56 | 18.81 | 17.23 | 1.42 | 1.65 | 1.45 | 1.26 | 1.1 | 1.04 | 1.07 | 1.47 | 1.34 | 2.12 | 1.14 | 11.85 | 40.84 | 38.18 |
| 90% | 3 | SPI | 1.74 | 19.61 | 17.48 | 1.42 | 1.65 | 1.45 | 1.26 | 1.1 | 1.04 | 1.07 | 1.47 | 1.34 | 2.13 | 1.14 | 11.85 | 40.8 | 38.21 |
| 90% | 4 | SPI | 1.85 | 19.94 | 17.65 | 1.42 | 1.65 | 1.45 | 1.26 | 1.1 | 1.04 | 1.07 | 1.47 | 1.34 | 2.12 | 1.14 | 11.85 | 40.76 | 38.15 |
| 90% | 2 | SPEI | 1.39 | 15.33 | 14.81 | 1.42 | 1.65 | 1.45 | 1.26 | 1.1 | 1.04 | 1.07 | 1.47 | 1.34 | 2.12 | 1.14 | 11.83 | 40.57 | 38.1 |
| 90% | 3 | SPEI | 1.53 | 14.89 | 13.87 | 1.42 | 1.65 | 1.45 | 1.26 | 1.1 | 1.04 | 1.07 | 1.47 | 1.34 | 2.12 | 1.14 | 11.83 | 40.51 | 38.07 |
| 90% | 4 | SPEI | 1.65 | 15.33 | 14.02 | 1.42 | 1.65 | 1.45 | 1.26 | 1.1 | 1.04 | 1.07 | 1.47 | 1.34 | 2.12 | 1.14 | 11.82 | 40.49 | 38.04 |
| 90% | 2 | TWSA | 1.26 | 5.82 | 5.59 | 1.42 | 1.65 | 1.45 | 1.26 | 1.11 | 1.05 | 1.07 | 1.47 | 1.34 | 2.13 | 1.17 | 11.86 | 41.25 | 38.77 |
| 90% | 3 | TWSA | 1.32 | 6.16 | 5.77 | 1.42 | 1.65 | 1.45 | 1.26 | 1.11 | 1.04 | 1.07 | 1.47 | 1.34 | 2.14 | 1.16 | 11.85 | 41.09 | 38.72 |
| 90% | 4 | TWSA | 1.42 | 6.39 | 5.85 | 1.42 | 1.65 | 1.45 | 1.26 | 1.11 | 1.04 | 1.07 | 1.47 | 1.34 | 2.14 | 1.16 | 11.84 | 41.11 | 38.73 |
| 92.50% | 2 | SPI | 1.64 | 20 | 18.06 | 1.42 | 1.65 | 1.45 | 1.26 | 1.1 | 1.04 | 1.07 | 1.47 | 1.33 | 2.13 | 1.14 | 11.85 | 40.83 | 38.14 |
| 92.50% | 3 | SPI | 1.78 | 20.7 | 18.34 | 1.42 | 1.65 | 1.45 | 1.26 | 1.1 | 1.04 | 1.07 | 1.47 | 1.33 | 2.12 | 1.14 | 11.87 | 40.9 | 38.17 |
| 92.50% | 4 | SPI | 1.76 | 18.55 | 16.59 | 1.42 | 1.65 | 1.45 | 1.26 | 1.1 | 1.04 | 1.07 | 1.47 | 1.33 | 2.12 | 1.14 | 11.87 | 40.9 | 38.15 |
| 92.50% | 2 | SPEI | 1.48 | 13.61 | 12.81 | 1.42 | 1.65 | 1.45 | 1.26 | 1.1 | 1.04 | 1.07 | 1.47 | 1.34 | 2.12 | 1.14 | 11.86 | 40.5 | 38.02 |
| 92.50% | 3 | SPEI | 1.58 | 14.3 | 13.16 | 1.42 | 1.65 | 1.45 | 1.26 | 1.1 | 1.04 | 1.07 | 1.47 | 1.33 | 2.12 | 1.14 | 11.85 | 40.55 | 38.04 |
| 92.50% | 4 | SPEI | 1.57 | 12.38 | 11.58 | 1.42 | 1.65 | 1.45 | 1.26 | 1.1 | 1.04 | 1.07 | 1.47 | 1.33 | 2.12 | 1.14 | 11.84 | 40.5 | 38.07 |
| 92.50% | 2 | TWSA | 1.34 | 6.64 | 6.14 | 1.42 | 1.65 | 1.45 | 1.26 | 1.11 | 1.04 | 1.07 | 1.47 | 1.34 | 2.13 | 1.16 | 11.84 | 41.15 | 38.74 |
| 92.50% | 3 | TWSA | 1.41 | 6.89 | 6.29 | 1.42 | 1.65 | 1.45 | 1.26 | 1.1 | 1.04 | 1.07 | 1.47 | 1.34 | 2.13 | 1.16 | 11.84 | 41.2 | 38.75 |
| 92.50% | 4 | TWSA | 1.48 | 6.7 | 6 | 1.42 | 1.65 | 1.45 | 1.26 | 1.1 | 1.04 | 1.07 | 1.47 | 1.34 | 2.13 | 1.15 | 11.84 | 41.11 | 38.7 |
| 95% | 2 | SPI | 1.62 | 23.25 | 21.05 | 1.42 | 1.65 | 1.45 | 1.26 | 1.1 | 1.04 | 1.07 | 1.47 | 1.33 | 2.12 | 1.14 | 11.93 | 41.07 | 38.15 |
| 95% | 3 | SPI | 1.8 | 22.82 | 20.18 | 1.42 | 1.65 | 1.45 | 1.26 | 1.1 | 1.04 | 1.07 | 1.47 | 1.33 | 2.12 | 1.14 | 11.96 | 41.12 | 38.13 |
| 95% | 4 | SPI | 2.09 | 23.52 | 20.14 | 1.42 | 1.65 | 1.45 | 1.26 | 1.1 | 1.04 | 1.07 | 1.47 | 1.33 | 2.12 | 1.14 | 11.91 | 40.91 | 38.08 |
| 95% | 2 | SPEI | 1.56 | 13.76 | 12.7 | 1.42 | 1.65 | 1.45 | 1.26 | 1.1 | 1.04 | 1.07 | 1.47 | 1.33 | 2.12 | 1.14 | 11.91 | 40.6 | 38 |
| 95% | 3 | SPEI | 1.72 | 14.18 | 12.7 | 1.42 | 1.65 | 1.45 | 1.26 | 1.1 | 1.04 | 1.07 | 1.47 | 1.33 | 2.12 | 1.14 | 11.89 | 40.67 | 37.99 |
| 95% | 4 | SPEI | 1.98 | 14.35 | 12.43 | 1.42 | 1.65 | 1.45 | 1.26 | 1.1 | 1.04 | 1.07 | 1.47 | 1.33 | 2.12 | 1.14 | 11.86 | 40.5 | 37.98 |
| 95% | 2 | TWSA | 1.39 | 7.01 | 6.42 | 1.42 | 1.65 | 1.45 | 1.26 | 1.1 | 1.04 | 1.07 | 1.47 | 1.34 | 2.13 | 1.15 | 11.86 | 41.17 | 38.69 |
| 95% | 3 | TWSA | 1.49 | 7.51 | 6.7 | 1.42 | 1.65 | 1.45 | 1.26 | 1.1 | 1.04 | 1.07 | 1.47 | 1.34 | 2.13 | 1.15 | 11.86 | 41.3 | 38.7 |
| 95% | 4 | TWSA | 1.6 | 7.73 | 6.71 | 1.42 | 1.65 | 1.45 | 1.26 | 1.1 | 1.04 | 1.07 | 1.47 | 1.34 | 2.14 | 1.14 | 11.86 | 41.13 | 38.66 |
| 97.50% | 2 | SPI | 1.77 | 25.95 | 23.42 | 1.42 | 1.65 | 1.45 | 1.26 | 1.1 | 1.04 | 1.07 | 1.47 | 1.33 | 2.13 | 1.14 | 11.89 | 40.88 | 38.13 |
| 97.50% | 3 | SPI | 2.08 | 25.89 | 23.07 | 1.42 | 1.65 | 1.45 | 1.26 | 1.1 | 1.04 | 1.07 | 1.47 | 1.33 | 2.13 | 1.14 | 11.9 | 40.98 | 38.06 |
| 97.50% | 4 | SPI | 2.45 | 25.35 | 22.33 | 1.42 | 1.65 | 1.45 | 1.26 | 1.1 | 1.04 | 1.07 | 1.47 | 1.33 | 2.13 | 1.15 | 11.89 | 40.81 | 37.99 |
| 97.50% | 2 | SPEI | 1.79 | 15.65 | 14.74 | 1.42 | 1.65 | 1.45 | 1.26 | 1.1 | 1.04 | 1.07 | 1.47 | 1.33 | 2.13 | 1.14 | 11.91 | 40.4 | 37.9 |
| 97.50% | 3 | SPEI | 2.05 | 15.36 | 14.67 | 1.42 | 1.65 | 1.45 | 1.26 | 1.1 | 1.04 | 1.07 | 1.47 | 1.33 | 2.13 | 1.14 | 11.9 | 40.48 | 37.94 |
| 97.50% | 4 | SPEI | 2.45 | 15.83 | 14.58 | 1.42 | 1.65 | 1.45 | 1.26 | 1.1 | 1.04 | 1.06 | 1.47 | 1.33 | 2.12 | 1.15 | 11.89 | 40.41 | 37.91 |
| 97.50% | 2 | TWSA | 1.42 | 7.32 | 6.71 | 1.42 | 1.65 | 1.45 | 1.26 | 1.1 | 1.04 | 1.07 | 1.47 | 1.34 | 2.13 | 1.15 | 11.86 | 41.15 | 38.59 |
| 97.50% | 3 | TWSA | 1.61 | 7.71 | 6.81 | 1.42 | 1.65 | 1.45 | 1.26 | 1.1 | 1.05 | 1.07 | 1.47 | 1.33 | 2.13 | 1.15 | 11.85 | 41.14 | 38.5 |
| 97.50% | 4 | TWSA | 1.85 | 8.14 | 6.95 | 1.42 | 1.65 | 1.45 | 1.26 | 1.1 | 1.05 | 1.07 | 1.47 | 1.33 | 2.13 | 1.15 | 11.84 | 41.03 | 38.36 |
| 99% | 2 | SPI | 1.84 | 34.94 | 32.25 | 1.42 | 1.65 | 1.45 | 1.26 | 1.1 | 1.04 | 1.07 | 1.47 | 1.33 | 2.12 | 1.15 | 11.91 | 40.71 | 37.96 |
| 99% | 3 | SPI | 2.25 | 31.42 | 29.25 | 1.42 | 1.65 | 1.45 | 1.26 | 1.1 | 1.04 | 1.07 | 1.47 | 1.33 | 2.12 | 1.15 | 11.99 | 40.85 | 37.94 |
| 99% | 4 | SPI | 3.49 | 32.55 | 29.38 | 1.42 | 1.65 | 1.45 | 1.26 | 1.1 | 1.04 | 1.07 | 1.47 | 1.33 | 2.12 | 1.15 | 11.96 | 40.81 | 37.97 |
| 99% | 2 | SPEI | 2.09 | 19.09 | 16.9 | 1.42 | 1.65 | 1.45 | 1.26 | 1.1 | 1.04 | 1.06 | 1.47 | 1.33 | 2.12 | 1.15 | 11.88 | 40.4 | 37.93 |
| 99% | 3 | SPEI | 2.39 | 18.18 | 16.36 | 1.42 | 1.65 | 1.45 | 1.26 | 1.1 | 1.04 | 1.06 | 1.47 | 1.33 | 2.11 | 1.15 | 11.93 | 40.45 | 37.88 |
| 99% | 4 | SPEI | 3.75 | 20.47 | 16.92 | 1.42 | 1.65 | 1.45 | 1.26 | 1.1 | 1.04 | 1.06 | 1.47 | 1.33 | 2.11 | 1.15 | 11.91 | 40.48 | 37.93 |
| 99% | 2 | TWSA | 1.67 | 9.9 | 8.55 | 1.42 | 1.65 | 1.45 | 1.26 | 1.1 | 1.05 | 1.07 | 1.47 | 1.33 | 2.13 | 1.15 | 11.84 | 40.82 | 38.24 |
| 99% | 3 | TWSA | 2.12 | 10.41 | 8.39 | 1.42 | 1.65 | 1.45 | 1.26 | 1.1 | 1.05 | 1.07 | 1.47 | 1.33 | 2.13 | 1.15 | 11.84 | 40.79 | 38.15 |
| 99% | 4 | TWSA | 2.99 | 11.73 | 8.71 | 1.42 | 1.65 | 1.45 | 1.26 | 1.1 | 1.05 | 1.07 | 1.47 | 1.33 | 2.13 | 1.16 | 11.83 | 40.8 | 38.16 |

Notes: VIF stands for Variance Inflation Factor, and if VIF is less than 10, it indicates that there is no co-linearity among the variables.

**Table S5. | The Akaike Information Criterion (AIC) and Bayesian Information Criterion (BIC) for baseline regressions under different CDHW definitions.**

| CDHW definition | | | AIC | BIC |
|---|---|---|---|---|
| Temperature threshold | Duration threshold | Drought index | | |
| 90% | 2 | SPI | 36871.8 | 36885.8 |
| 90% | 3 | SPI | 36821.6 | 36835.6 |
| 90% | 4 | SPI | 36808.7 | 36822.6 |
| 90% | 2 | SPEI | 36943.3 | 36957.3 |
| 90% | 3 | SPEI | 36893.9 | 36907.9 |
| 90% | 4 | SPEI | 36915.8 | 36929.7 |
| 90% | 2 | TWSA | 36775.2 | 36789.2 |
| 90% | 3 | TWSA | 36711 | 36725 |
| 90% | 4 | TWSA | 36778.2 | 36792.2 |
| 92.50% | 2 | SPI | 36868.7 | 36882.6 |
| 92.50% | 3 | SPI | 36819.8 | 36833.7 |
| 92.50% | 4 | SPI | 36854.3 | 36868.2 |
| 92.50% | 2 | SPEI | 36888.2 | 36902.2 |
| 92.50% | 3 | SPEI | 36891.4 | 36905.4 |
| 92.50% | 4 | SPEI | 36866.7 | 36880.6 |
| 92.50% | 2 | TWSA | 36762.8 | 36776.7 |
| 92.50% | 3 | TWSA | 36708.3 | 36722.3 |
| 92.50% | 4 | TWSA | 36819.8 | 36833.8 |
| 95% | 2 | SPI | 36812.4 | 36826.3 |
| 95% | 3 | SPI | 36815 | 36829 |
| 95% | 4 | SPI | 36763.9 | 36777.8 |
| 95% | 2 | SPEI | 36895 | 36908.9 |
| 95% | 3 | SPEI | 36910.5 | 36924.5 |
| 95% | 4 | SPEI | 36887.4 | 36901.3 |
| 95% | 2 | TWSA | 36781.9 | 36795.8 |
| 95% | 3 | TWSA | 36825.1 | 36839.1 |
| 95% | 4 | TWSA | 36845.9 | 36859.9 |
| 97.50% | 2 | SPI | 36719.4 | 36733.4 |
| 97.50% | 3 | SPI | 36759.7 | 36773.6 |
| 97.50% | 4 | SPI | 36820.7 | 36834.7 |
| 97.50% | 2 | SPEI | 36948.4 | 36962.3 |
| 97.50% | 3 | SPEI | 36926.9 | 36940.8 |
| 97.50% | 4 | SPEI | 36900.6 | 36914.5 |
| 97.50% | 2 | TWSA | 36749.7 | 36763.7 |
| 97.50% | 3 | TWSA | 36968.5 | 36982.5 |
| 97.50% | 4 | TWSA | 36995.2 | 37009.2 |
| 99% | 2 | SPI | 36770.6 | 36784.6 |
| 99% | 3 | SPI | 36898.2 | 36912.2 |
| 99% | 4 | SPI | 36928 | 36941.9 |
| 99% | 2 | SPEI | 37027.8 | 37041.7 |
| 99% | 3 | SPEI | 36966 | 36979.9 |
| 99% | 4 | SPEI | 36993.5 | 37007.4 |
| 99% | 2 | TWSA | 36850.2 | 36864.2 |
| 99% | 3 | TWSA | 36951.7 | 36965.6 |
| 99% | 4 | TWSA | 36950.1 | 36964 |

Notes: Each row in the table represents a separate regression using cox proportional hazards model. Among them, the combination with the lowest AIC and BIC is highlighted in red font.

**Table S6. | Testing for co-linearity among variables of baseline regression model.**

| Variables | VIF |
|---|---|
| Frequency of CDHW | 1.4 |
| Duration of CDHW | 6.87 |
| Severity of CDHW | 6.23 |
| Age | 1.42 |
| Sex | 1.65 |
| Smoking status | 1.45 |
| Drinking status | 1.26 |
| Exercising status | 1.1 |
| Household income | 1.04 |
| BMI | 1.05 |
| Marital status | 1.47 |
| Education status | 1.34 |
| Relative humidity | 1.48 |
| Ozone concentrations | 1.08 |
| PM2.5 concentrations | 1.4 |

Notes: VIF stands for Variance Inflation Factor, and if VIF is less than 10, it indicates that there is no co-linearity among the variables.

**Table S7. | HRs of the baseline Cox proportional hazards model.**

| Variables | Hazard ratio |
|---|---|
| Frequency of CDHWs | 1.05424*** |
| | [0.00455] |
| Duration of CDHWs | 1.01206*** |
| | [0.00117] |
| Severity of CDHWs | 1.01279*** |
| | [0.00238] |
| Age | 1.04797*** |
| | [0.00089] |
| 1.Sex | 1.15485*** |
| | [0.02115] |
| 2.Smoking status | 1.05114 |
| | [0.05687] |
| 3.Smoking status | 1.05880** |
| | [0.02434] |
| 4.Smoking status | 1.20344*** |
| | [0.02485] |
| 2.Drinking status | 1.00567 |
| | [0.03912] |
| 3.Drinking status | 1.04840** |
| | [0.02233] |
| 4.Drinking status | 1.19327*** |
| | [0.02414] |
| 2.Physical activity | 0.80025*** |
| | [0.01980] |
| 3.Physical activity | 1.29252*** |
| | [0.02364] |
| 4.Physical activity | 0.98454 |
| | [0.01940] |
| Household income | 0.88843*** |
| | [0.00294] |
| BMI | 1.00874*** |
| | [0.00176] |
| 2.Marital status | 1.29201*** |
| | [0.07410] |
| 3.Marital status | 1.71694*** |
| | [0.19096] |
| 4.Marital status | 1.36043*** |
| | [0.02865] |
| 5.Marital status | 1.35770*** |
| | [0.10075] |
| Education | 0.99169*** |
| | [0.00276] |
| Relative humidity | 1.00822*** |
| | [0.00125] |
| Ozone concentration | 0.99847 |
| | [0.00102] |
| PM2.5 concentration | 1.00508*** |
| | [0.00103] |
| No. of subjects | 33,971 |
| No. of failures | 19,662 |
| Time at risk | 236,247 |
| Observations | 83,295 |

Notes: Each column represents a separate regression using the Cox proportional hazards model. The numbers show the HR of each measure on mortality risk of older adults. Standard errors are shown in parentheses. *p<0.1, **p<0.05, ***p<0.01.

**Table S8.** | **Schoenfeld residual test for proportional hazards assumption of baseline Cox proportional hazards model.**

| Variables | rho | chi2 | df | Prob>chi2 |
|---|---|---|---|---|
| Frequency of CDHWs | -0.00626 | 0.97 | 1 | 0.3239 |
| Duration of CDHWs | 0.00732 | 1.33 | 1 | 0.2487 |
| Severity of CDHWs | 0.00801 | 1.59 | 1 | 0.2069 |
| Age | -0.00571 | 0.81 | 1 | 0.3682 |
| Sex | 0.00447 | 0.5 | 1 | 0.4812 |
| Smoking status | -0.00199 | 0.1 | 1 | 0.7538 |
| Drinking status | -0.00190 | 0.06 | 1 | 0.8005 |
| Exercising status | -0.00212 | 0.11 | 1 | 0.7383 |
| Household income | 0.00168 | 0.07 | 1 | 0.7912 |
| BMI | -0.00237 | 0.14 | 1 | 0.7088 |
| Marital status | -0.00259 | 0.17 | 1 | 0.6832 |
| Education status | -0.00177 | 0.08 | 1 | 0.7803 |
| Relative humidity | -0.00899 | 2.01 | 1 | 0.1566 |
| Ozone concentrations | -0.00189 | 0.09 | 1 | 0.7658 |
| PM2.5 concentrations | 0.01098 | 2.99 | 1 | 0.0836 |

**Table S9. | Robustness checks of the baseline Cox proportional hazards model.**

| Variables | Hazard ratio | | | | | | | |
|---|---|---|---|---|---|---|---|---|
| Frequency of CDHWs | 1.05424*** | 1.06230*** | 1.04272*** | 1.05391*** | 1.05574*** | 1.05565*** | 1.04700*** | 1.03519*** |
| | [0.00455] | [0.00468] | [0.00463] | [0.00455] | [0.00459] | [0.00458] | [0.00472] | [0.00414] |
| Duration of CDHWs | 1.01206*** | 1.01389*** | 1.01444*** | 1.01183*** | 1.01057*** | 1.01049*** | 1.01260*** | 1.01080*** |
| | [0.00117] | [0.00117] | [0.00119] | [0.00117] | [0.00118] | [0.00118] | [0.00116] | [0.00110] |
| Severity of CDHWs | 1.01279*** | 1.01369*** | 1.02147*** | 1.01241*** | 1.01104*** | 1.01093*** | 1.01057*** | 1.01670*** |
| | [0.00238] | [0.00240] | [0.00226] | [0.00238] | [0.00235] | [0.00236] | [0.00231] | [0.00215] |
| Age | 1.04797*** | 1.04769*** | 1.04902*** | 1.04791*** | 1.04758*** | 1.04756*** | 1.04516*** | 1.05300*** |
| | [0.00089] | [0.00091] | [0.00094] | [0.00089] | [0.00090] | [0.00090] | [0.00095] | [0.00074] |
| 1.Sex | 1.15485*** | 1.14401*** | 1.17338*** | 1.15788*** | 1.15163*** | 1.15261*** | 1.15006*** | 1.15818*** |
| | [0.02115] | [0.02140] | [0.02257] | [0.02119] | [0.02115] | [0.02118] | [0.02233] | [0.01640] |
| 2.Smoking status | 1.05114 | 1.05949 | 1.00671 | 1.05022 | 1.05136 | 1.05108 | 0.99250 | |
| | [0.05687] | [0.05825] | [0.05886] | [0.05682] | [0.05700] | [0.05698] | [0.05875] | |
| 3.Smoking status | 1.05880** | 1.07456*** | 1.04808* | 1.05946** | 1.06999*** | 1.07018*** | 1.03440 | |
| | [0.02434] | [0.02534] | [0.02536] | [0.02434] | [0.02460] | [0.02460] | [0.02560] | |
| 4.Smoking status | 1.20344*** | 1.21657*** | 1.20038*** | 1.20086*** | 1.19452*** | 1.19378*** | 1.17064*** | |
| | [0.02485] | [0.02558] | [0.02619] | [0.02481] | [0.02487] | [0.02487] | [0.02596] | |
| 2.Drinking status | 1.00567 | 1.01339 | 0.98954 | 1.00483 | 1.00129 | 1.00106 | 0.95646 | |
| | [0.03912] | [0.04003] | [0.04109] | [0.03910] | [0.03903] | [0.03902] | [0.04050] | |
| 3.Drinking status | 1.04840** | 1.05243** | 1.03188 | 1.04961** | 1.04760** | 1.04804** | 1.04265* | |
| | [0.02233] | [0.02278] | [0.02330] | [0.02234] | [0.02253] | [0.02253] | [0.02374] | |
| 4.Drinking status | 1.19327*** | 1.19573*** | 1.19440*** | 1.19120*** | 1.19908*** | 1.19840*** | 1.15384*** | |
| | [0.02414] | [0.02470] | [0.02545] | [0.02409] | [0.02458] | [0.02457] | [0.02504] | |
| 2.Physical activity | 0.80025*** | 0.80502*** | 0.77613*** | 0.79573*** | 0.80865*** | 0.80717*** | 0.73750*** | |
| | [0.01980] | [0.02031] | [0.02043] | [0.01971] | [0.02011] | [0.02008] | [0.01957] | |
| 3.Physical activity | 1.29252*** | 1.29251*** | 1.28035*** | 1.28247*** | 1.28157*** | 1.27834*** | 1.20583*** | |
| | [0.02364] | [0.02405] | [0.02492] | [0.02361] | [0.02375] | [0.02384] | [0.02367] | |
| 4.Physical activity | 0.98454 | 0.99517 | 0.96313* | 0.97641 | 0.98393 | 0.98131 | 0.96579* | |
| | [0.01940] | [0.02022] | [0.02008] | [0.01939] | [0.01949] | [0.01958] | [0.02038] | |
| Household income | 0.88843*** | 0.88200*** | 0.89370*** | 0.88719*** | 0.88310*** | 0.88272*** | 0.88618*** | |
| | [0.00294] | [0.00318] | [0.00301] | [0.00299] | [0.00302] | [0.00306] | [0.00315] | |
| BMI | 1.00874*** | 1.00864*** | 1.01023*** | 1.00870*** | 1.00885*** | 1.00884*** | 1.00863*** | |
| | [0.00176] | [0.00176] | [0.00179] | [0.00176] | [0.00176] | [0.00176] | [0.00178] | |
| 2.Marital status | 1.29201*** | 1.29147*** | 1.26711*** | 1.29372*** | 1.31066*** | 1.31109*** | 1.31143*** | |
| | [0.07410] | [0.07726] | [0.07688] | [0.07423] | [0.07632] | [0.07635] | [0.08284] | |
| 3.Marital status | 1.71694*** | 1.74783*** | 1.72556*** | 1.71316*** | 1.71474*** | 1.71356*** | 1.54970*** | |
| | [0.19096] | [0.19915] | [0.20495] | [0.19025] | [0.19550] | [0.19515] | [0.18918] | |
| 4.Marital status | 1.36043*** | 1.35609*** | 1.36978*** | 1.36108*** | 1.36343*** | 1.36359*** | 1.36032*** | |
| | [0.02865] | [0.02920] | [0.03032] | [0.02865] | [0.02897] | [0.02896] | [0.03021] | |
| 5.Marital status | 1.35770*** | 1.35062*** | 1.34698*** | 1.35020*** | 1.36934*** | 1.36677*** | 1.35773*** | |
| | [0.10075] | [0.10579] | [0.10676] | [0.10010] | [0.10125] | [0.10104] | [0.10551] | |
| Education | 0.99169*** | 0.99161*** | 0.99058*** | 0.99084*** | 0.98939*** | 0.98912*** | 0.99103*** | |
| | [0.00276] | [0.00283] | [0.00292] | [0.00276] | [0.00277] | [0.00278] | [0.00289] | |
| Relative humidity | 1.00822*** | 1.00803*** | 1.00756*** | 1.00862*** | 1.02677*** | 1.02680*** | 1.01497*** | |
| | [0.00125] | [0.00126] | [0.00133] | [0.00126] | [0.00164] | [0.00164] | [0.00135] | |
| Ozone concentration | 0.99847 | 0.99828* | 0.99650*** | 0.99837 | 0.99115*** | 0.99116*** | 1.00034 | |
| | [0.00102] | [0.00103] | [0.00106] | [0.00101] | [0.00106] | [0.00106] | [0.00108] | |
| PM2.5 concentration | 1.00508*** | 1.00605*** | 1.00281*** | 1.00525*** | 1.01184*** | 1.01185*** | 1.00380*** | |
| | [0.00103] | [0.00105] | [0.00109] | [0.00104] | [0.00110] | [0.00110] | [0.00110] | |
| Model | 1 | 3 | 4 | 5 | 6 | 7 | 8 | 9 |
| No. of subjects | 33,971 | 30,134 | 33,971 | 33,971 | 33,971 | 33,971 | 31,331 | 35,128 |
| No. of failures | 19,662 | 16,754 | 17,734 | 19,662 | 19,662 | 19,662 | 16,855 | 21,341 |
| Time at risk | 236,247 | 207,186 | 234,034 | 236,247 | 236,247 | 236,247 | 196,210 | 255,901 |
| Observations | 83,295 | 79,336 | 81,517 | 83,295 | 83,295 | 83,295 | 71,302 | 89,231 |

Notes: Each column represents a separate regression using the Cox proportional hazards model. The numbers show the HR of each measure on mortality risk of older adults. Standard errors are shown in parentheses. *p<0.1, **p<0.05, ***p<0.01.

**Table S10. | The heterogeneous impacts of CDHW characteristics on mortality risk of older adults in the age subgroup.**

| Variables | Hazard ratio | | |
|---|---|---|---|
| Frequency of CDHWs | 1.12641 | 1.05486*** | 1.05396*** |
| | [0.08207] | [0.00472] | [0.00456] |
| Frequency of CDHWs*age_group[65-69] | 1.00000 | | |
| | [0.00000] | | |
| Frequency of CDHWs*age_group[70-74] | 0.97626 | | |
| | [0.07654] | | |
| Frequency of CDHWs*age_group[75-79] | 0.93529 | | |
| | [0.07015] | | |
| Frequency of CDHWs*age_group[80-84] | 0.92134 | | |
| | [0.06854] | | |
| Frequency of CDHWs*age_group[85-89] | 0.93540 | | |
| | [0.06901] | | |
| Frequency of CDHWs*age_group[90-95] | 0.92256 | | |
| | [0.06772] | | |
| Frequency of CDHWs*age_group[95-99] | 0.93443 | | |
| | [0.06848] | | |
| Duration of CDHWs | 1.01196*** | 1.03494 | 1.01204*** |
| | [0.00112] | [0.02357] | [0.00116] |
| Duration of CDHWs*age_group[65-69] | | 1.00000 | |
| | | [0.00000] | |
| Duration of CDHWs*age_group[70-74] | | 0.98450 | |
| | | [0.02398] | |
| Duration of CDHWs*age_group[75-79] | | 0.98950 | |
| | | [0.02319] | |
| Duration of CDHWs*age_group[80-84] | | 0.98587 | |
| | | [0.02301] | |
| Duration of CDHWs*age_group[85-89] | | 0.97663 | |
| | | [0.02252] | |
| Duration of CDHWs*age_group[90-95] | | 0.97745 | |
| | | [0.02241] | |
| Duration of CDHWs*age_group[95-99] | | 0.97461 | |
| | | [0.02230] | |
| Severity of CDHWs | 1.01184*** | 1.01133*** | 1.04447 |
| | [0.00237] | [0.00212] | [0.03953] |
| Severity of CDHWs*age_group[65-69] | | | 1.00000 |
| | | | [0.00000] |
| Severity of CDHWs*age_group[70-74] | | | 0.98006 |
| | | | [0.04130] |
| Severity of CDHWs*age_group[75-79] | | | 1.00120 |
| | | | [0.03936] |
| Severity of CDHWs*age_group[80-84] | | | 0.98686 |
| | | | [0.03866] |
| Severity of CDHWs*age_group[85-89] | | | 0.97020 |
| | | | [0.03741] |
| Severity of CDHWs*age_group[90-95] | | | 0.96941 |
| | | | [0.03701] |
| Severity of CDHWs*age_group[95-99] | | | 0.96509 |
| | | | [0.03674] |
| Control variables | ✓ | ✓ | ✓ |
| No. of subjects | 33,971 | 33,971 | 33,971 |
| No. of failures | 19,662 | 19,662 | 19,662 |
| Time at risk | 236,247 | 236,247 | 236,247 |
| Observations | 83,295 | 83,295 | 83,295 |

Notes: Each column represents a separate regression using Cox proportional hazards model. The numbers show the HR of each measure on mortality risk of older adults. Standard errors are shown in parentheses. *p<0.1, **p<0.05, ***p<0.01.

**Table S11. | The heterogeneous impacts of CDHW characteristics on mortality risk of older adults in the sex subgroup.**

| Variables | Hazard ratio | | |
|---|---|---|---|
| Frequency of CDHWs | 1.05595*** | 1.05512*** | 1.05419*** |
| | [0.00569] | [0.00508] | [0.00455] |
| Frequency of CDHWs*sex_group | 0.99615 | | |
| | [0.00778] | | |
| Duration of CDHWs | 1.01178*** | 1.00930*** | 1.01203*** |
| | [0.00102] | [0.00141] | [0.00114] |
| Duration of CDHWs*sex_group | | 1.00654*** | |
| | | [0.00188] | |
| Severity of CDHWs | 1.01278*** | 1.01285*** | 1.00902*** |
| | [0.00238] | [0.00243] | [0.00283] |
| Severity of CDHWs*sex_group | | | 1.00919** |
| | | | [0.00373] |
| 1.Sex | 1.16220*** | 1.16247*** | 1.16189*** |
| | [0.02542] | [0.02549] | [0.02511] |
| Age | 1.04798*** | 1.04783*** | 1.04777*** |
| | [0.00089] | [0.00089] | [0.00089] |
| 2.Smoking status | 1.05114 | 1.08440 | 1.08355 |
| | [0.05685] | [0.05870] | [0.05843] |
| 3.Smoking status | 1.05896** | 1.10554*** | 1.10690*** |
| | [0.02434] | [0.02461] | [0.02467] |
| 4.Smoking status | 1.20352*** | 1.24583*** | 1.25057*** |
| | [0.02485] | [0.02507] | [0.02512] |
| 2.Drinking status | 1.00569 | 1.00248 | 1.01150 |
| | [0.03911] | [0.03904] | [0.03949] |
| 3.Drinking status | 1.04812** | 1.06051*** | 1.07257*** |
| | [0.02234] | [0.02242] | [0.02268] |
| 4.Drinking status | 1.19331*** | 1.21697*** | 1.21925*** |
| | [0.02414] | [0.02446] | [0.02451] |
| 2.Physical activity | 0.80022*** | 0.80918*** | 0.80327*** |
| | [0.01980] | [0.01993] | [0.01988] |
| 3.Physical activity | 1.29248*** | 1.30419*** | 1.29232*** |
| | [0.02364] | [0.02382] | [0.02368] |
| 4.Physical activity | 0.98459 | 0.99666 | 0.98815 |
| | [0.01940] | [0.01960] | [0.01949] |
| Household income | 0.88844*** | 0.88955*** | 0.88819*** |
| | [0.00294] | [0.00295] | [0.00295] |
| BMI | 1.00874*** | 1.00854*** | 1.00859*** |
| | [0.00176] | [0.00177] | [0.00177] |
| 2.Marital status | 1.29217*** | 1.29578*** | 1.28817*** |
| | [0.07407] | [0.07415] | [0.07384] |
| 3.Marital status | 1.71661*** | 1.71944*** | 1.71484*** |
| | [0.19080] | [0.18673] | [0.18804] |
| 4.Marital status | 1.36012*** | 1.32661*** | 1.32349*** |
| | [0.02864] | [0.02770] | [0.02766] |
| 5.Marital status | 1.35803*** | 1.39321*** | 1.37659*** |
| | [0.10069] | [0.10285] | [0.10216] |
| Education | 0.99170*** | 0.99658 | 0.99696 |
| | [0.00276] | [0.00268] | [0.00266] |
| Relative humidity | 1.00822*** | 1.00841*** | 1.00803*** |
| | [0.00125] | [0.00123] | [0.00125] |
| Ozone concentration | 0.99847 | 0.99676*** | 0.99852 |
| | [0.00102] | [0.00101] | [0.00102] |
| PM2.5 concentration | 1.00509*** | 1.00349*** | 1.00484*** |
| | [0.00103] | [0.00102] | [0.00103] |
| No. of subjects | 33,971 | 33,971 | 33,971 |
| No. of failures | 19,662 | 19,662 | 19,662 |
| Time at risk | 236,247 | 236,247 | 236,247 |
| Observations | 83,295 | 83,295 | 83,295 |

Notes: Each column represents a separate regression using Cox proportional hazards model. The numbers show the HR of each measure on mortality risk of older adults. Standard errors are shown in parentheses. *p<0.1, **p<0.05, ***p<0.01.

**Table S12. | The baseline mortality rates in China (deaths per thousand older adults).**

| Year | Sex | Age | GBD 2019 Central Value | GBD 2019 Lower bound | GBD 2019 Upper bound | Our estimates based on IF |
|---|---|---|---|---|---|---|
| 2017 | woman | 65 - 69 | 58.3479 | 67.5663 | 49.6646 | 60.7113 |
| | | 70 - 74 | 106.8721 | 122.2522 | 91.9779 | 111.5928 |
| | | 75 - 79 | 179.2183 | 202.4823 | 156.2598 | 171.4418 |
| | | 80 - 84 | 317.6486 | 349.5825 | 284.7623 | 330.366 |
| | | 85 - 89 | 472.4616 | 512.4582 | 429.84 | 502.2881 |
| | | 90 - 94 | 647.5205 | 683.9867 | 608.2065 | 644.6004 |
| | | 95 - 99 | 795.9281 | 823.211 | 765.9193 | 852.2263 |
| | man | 65 - 69 | 103.4956 | 121.6697 | 86.2603 | 106.0596 |
| | | 70 - 74 | 175.9385 | 203.395 | 149.1542 | 167.8389 |
| | | 75 - 79 | 279.5364 | 315.6121 | 243.0195 | 263.252 |
| | | 80 - 84 | 451.9994 | 493.2856 | 407.5921 | 475.0367 |
| | | 85 - 89 | 746.7031 | 772.6532 | 715.7196 | 766.542 |
| | | 90 - 94 | 845.423 | 865.3247 | 820.1493 | 852.4227 |
| | | 95 - 99 | 880.4467 | 893.9098 | 863.0156 | 918.9933 |
| 2018 | woman | 65 - 69 | 57.7524 | 68.296 | 48.5671 | 58.9293 |
| | | 70 - 74 | 105.6169 | 123.1005 | 89.8699 | 108.8311 |
| | | 75 - 79 | 177.5168 | 203.7137 | 153.1191 | 166.9682 |
| | | 80 - 84 | 314.5934 | 350.3723 | 279.5667 | 321.1248 |
| | | 85 - 89 | 468.6575 | 513.3569 | 423.1024 | 487.7575 |
| | | 90 - 94 | 644.0954 | 685.084 | 601.8894 | 625.1923 |
| | | 95 - 99 | 793.641 | 824.7964 | 760.7382 | 825.9211 |
| | man | 65 - 69 | 100.4842 | 119.8498 | 83.1126 | 103.1057 |
| | | 70 - 74 | 174.3305 | 204.0454 | 146.8407 | 163.7361 |
| | | 75 - 79 | 275.0956 | 314.1055 | 237.6298 | 256.4717 |
| | | 80 - 84 | 448.7861 | 493.5928 | 402.7613 | 462.1858 |
| | | 85 - 89 | 724.1838 | 754.5988 | 690.0785 | 744.8801 |
| | | 90 - 94 | 831.5318 | 854.3596 | 803.6104 | 827.1911 |
| | | 95 - 99 | 871.2803 | 886.7218 | 849.487 | 891.0227 |
| 2019 | woman | 65 - 69 | 57.2218 | 69.2373 | 47.1469 | 57.2174 |
| | | 70 - 74 | 104.4596 | 124.3968 | 87.1877 | 106.1088 |
| | | 75 - 79 | 176.0077 | 205.7967 | 149.1856 | 162.5258 |
| | | 80 - 84 | 311.8367 | 352.1387 | 273.2601 | 311.8335 |
| | | 85 - 89 | 465.1583 | 515.1252 | 414.5054 | 473.128 |
| | | 90 - 94 | 640.8695 | 686.3889 | 593.3419 | 605.7266 |
| | | 95 - 99 | 791.4119 | 825.101 | 753.9602 | 799.6004 |
| | man | 65 - 69 | 99.3482 | 121.2582 | 80.0551 | 100.2731 |
| | | 70 - 74 | 172.2942 | 205.6588 | 141.7371 | 159.7495 |
| | | 75 - 79 | 272.7037 | 316.5297 | 230.8328 | 249.8816 |
| | | 80 - 84 | 445.0924 | 495.3482 | 393.3546 | 449.5387 |
| | | 85 - 89 | 719.873 | 754.3504 | 681.0377 | 723.6052 |
| | | 90 - 94 | 829.2142 | 854.797 | 798.1843 | 802.5168 |
| | | 95 - 99 | 868.3118 | 884.7486 | 847.0889 | 863.753 |

**Table S13. | Summary of socio-demographic projections consistent with SSPs.**

| Year | Sex | Age | Population | | | Baseline mortality rates | | |
|---|---|---|---|---|---|---|---|---|
| | | | SSP1-2.6 | SSP3-7.0 | SSP5-8.5 | SSP1-2.6 | SSP3-7.0 | SSP5-8.5 |
| 2050 | woman | 65-69 | 46.1133013 | 43.06942158 | 46.13794768 | 22.7978017 | 32.93084156 | 22.54188165 |
| | | 70-74 | 40.3763234 | 36.10414001 | 40.39537365 | 48.99963949 | 68.04519248 | 49.66547162 |
| | | 75-79 | 47.70098134 | 39.39677599 | 47.69887374 | 71.55446415 | 102.0812858 | 71.80978784 |
| | | 80-84 | 40.71244618 | 29.61665537 | 40.70849797 | 131.9367722 | 190.9464954 | 131.9162895 |
| | | 85-89 | 23.37165229 | 14.0242306 | 23.37176125 | 200.2511111 | 291.0168548 | 199.4798814 |
| | | 90-94 | 11.40263106 | 5.181423302 | 11.40279665 | 257.6657446 | 376.0359813 | 256.0784846 |
| | | 95-99 | 4.444153712 | 1.412687345 | 4.444043123 | 334.475535 | 491.3896024 | 331.6077639 |
| | man | 65-69 | 46.28930254 | 41.48871701 | 46.29537372 | 45.05650846 | 64.15079277 | 44.5646174 |
| | | 70-74 | 38.7316722 | 32.60175137 | 38.74121703 | 82.28642736 | 109.1877196 | 84.23564642 |
| | | 75-79 | 42.78677326 | 32.41376002 | 42.77991392 | 123.7930193 | 167.722982 | 125.7332485 |
| | | 80-84 | 33.9912629 | 21.97292482 | 33.98513621 | 214.3374005 | 296.0308234 | 216.2352028 |
| | | 85-89 | 17.25268978 | 8.894866741 | 17.25175124 | 334.5098163 | 470.2267377 | 335.1117715 |
| | | 90-94 | 7.399314709 | 2.804994522 | 7.399092731 | 359.3611346 | 513.5923284 | 357.5870099 |
| | | 95-99 | 2.311261601 | 0.606140286 | 2.311142388 | 378.9850752 | 546.5827689 | 375.9032369 |
| 2100 | woman | 65-69 | 18.31410978 | 28.31890455 | 18.34120341 | 7.742812139 | 17.00638001 | 7.350729486 |
| | | 70-74 | 20.27507935 | 27.85616321 | 20.31045671 | 19.01358912 | 39.60766901 | 19.55894203 |
| | | 75-79 | 23.15662667 | 25.46644602 | 23.20267578 | 28.52396794 | 60.11393377 | 29.21300373 |
| | | 80-84 | 25.91857383 | 21.27475873 | 25.97365752 | 54.10869775 | 116.2657805 | 54.59069438 |
| | | 85-89 | 26.92591626 | 14.59543869 | 26.99383163 | 84.78500571 | 183.0813626 | 85.0462021 |
| | | 90-94 | 28.62034158 | 8.611135716 | 28.66836036 | 112.1805626 | 242.2494816 | 112.0832789 |
| | | 95-99 | 22.76233853 | 3.322324484 | 22.79397214 | 145.3305325 | 316.4354499 | 144.6073195 |
| | moman | 65-69 | 20.52232908 | 29.90303274 | 20.53313996 | 16.35609072 | 36.86830448 | 15.57156012 |
| | | 70-74 | 22.8039897 | 28.42177601 | 22.81888322 | 34.65388684 | 67.40945779 | 36.13256193 |
| | | 75-79 | 26.02354532 | 24.55498745 | 26.04391886 | 51.95192424 | 104.0495478 | 53.38261058 |
| | | 80-84 | 28.87099494 | 18.83437085 | 28.89366536 | 89.71363392 | 184.608421 | 90.79463366 |
| | | 85-89 | 29.56840036 | 11.54482415 | 29.59554526 | 140.122011 | 295.1297167 | 141.2116441 |
| | | 90-94 | 30.24555027 | 5.850640011 | 30.24924365 | 152.2981587 | 322.4117007 | 151.9413353 |
| | | 95-99 | 22.24445345 | 1.863520566 | 22.24227326 | 160.1987004 | 342.1414154 | 158.8586875 |

Notes: Population data are sourced from the IIASA SSP population datasets (3), measured in millions. And baseline mortality rates are predicted using the International Futures (IFs) model v7.89 (4), measured in deaths per thousand older adults.

## Supplemental Notes

**Supplemental Note 1: SSP-RCP scenario framework.** The SSP-RCP scenario framework is designed to explore plausible futures of human activities, emissions, and the changing climate, making it an important tool in climate change research and climate model predictions. It consists of two main components: SSPs (Shared Socioeconomic Pathways) and RCPs (Representative Concentration Pathways). The SSPs narrate possible alternative trends in socioeconomic and environmental development (5). The SSPs are divided into five scenarios as follows: (1) SSP1: Sustainable Development, emphasizing social equity and environmental sustainability, with a focus on renewable energy use. (2) SSP2: Continued Development, maintaining existing trends. (3) SSP3: Regional Rivalry, emphasizing regional competition and social inequality. (4) SSP4: Inequality but High Adaptability, focusing on climate change adaptation. (5) SSP5: Fossil-fueled Development, emphasizing economic growth and technological innovation. The distinct differences across the SSPs are driven by the basic SSP elements which are population, urbanization, and GDP (3). In addition, each RCP represents the warming targets for the emission pathways of energy systems and land use, as measured as certain radiative forcing levels (in $W/m^2$) by the end of the century (6). The IPCC AR5 report presents four distinct RCPs (7), including: (1) RCP2.6: A low-emission scenario (8). (2) RCP4.5: A stabilization scenario (9). (3) RCP6.0: A scenario with climate policy interventions (10). (4) RCP8.5: A scenario without mitigation efforts (11). These RCPs outline various pathways for understanding and assessing future climate change scenarios. The integration of SSPs and RCPs is built upon the framework of Shared Climate Policy Assumptions, including the vital details like the evolution of international climate policies and the overarching goals for long-term climate mitigation. The common SSP-RCP combinations include SSP1-1.9, SSP1-2.6, SSP2-4.5, SSP3-7.0, and SSP5-8.5. The aim of this unified scenario framework is to encompass the fundamental traits of global climate policies that extend until the end of the century (12).

The SSP-RCP scenario framework has been widely adopted across research communities in scientific assessments such as CMIP6 (13) and the IPCC AR6 report (14). This study selects three SSP-RCP scenarios (SSP1-2.6, SSP3-7.0, and SSP5-8.5), which are consistent with the emission scenarios in the IPCC AR6 report (14). The end-of-century warming levels for these scenarios range from a lower limit of 2.6 $W/m^2$ (approximately 2°C) to an upper limit of 8.5 $W/m^2$ (close to 5°C).

**Supplemental Note 2: Validations of the GCM-GHM coupling model simulations.** We validate the $T_{max}$, daily mean air temperature, and daily precipitation simulations from five GCMs and the TWS simulations from ten GCM-GHM coupling models, as well as the results from the MME means, using $T_{max}$, daily mean air temperature, and daily precipitation data from Chinese temperature stations for the period 1942-2014 and TWS data from Gravity Recovery and Climate Experiment (GRACE)-constrained reconstruction and reanalysis data during 2002-2014. We construct the multi-model ensemble (MME) mean using two ways. The first way takes the simple arithmetic average of the results from the ten GCM-GHM coupling models. The second way uses Pearson correlation coefficients between each GCM-GHM coupling model and the validation data as weights to calculate a weighted average.

We obtain daily $T_{max}$, daily mean air temperature, and daily precipitation data by processing 3-hourly temperature and precipitation records from the ground stations in the Chinese region, captured from the National Climatic Data Center (NCDC) of the United States. Due to the extended time span of the data and inconsistent data gaps at different stations, it is a challenge to maintain a complete time series spanning from 1942 to 2014. Consequently, we take the data in each station as an individual time series for each year. We then conduct Pearson correlation analyses between the data in this station and the simulated data for the corresponding grid, aiming to validate the accuracy of the simulated data.

For the validation of the GCM-GHM coupling models TWS, we utilize the surface water anomaly data from the GRACE satellite, which provides complete time series data with a resolution of $1°\times1°$ spanning from 2002 to 2014. We perform a bilinear interpolation of the GCM-GHM coupling models TWS to match the $1°\times1°$ resolution and compute the Pearson correlation coefficient between the interpolated data and the corresponding grid cells of the GRACE satellite data for validation purposes.

The average of Pearson correlation coefficients between $T_{max}$ simulated by individual models and the validation data are around 0.8 (Supplementary Fig. S2a), and around 0.9 for daily mean air temperature (Supplementary Fig. S2b), and around 0.6 for daily precipitation (Supplementary Fig. S2c). and around 0.6 for TWS (Supplementary Fig. S2b). The Pearson correlation coefficients between the MME mean and the validation data indicate a significant improvement compared to the simulations by individual models (Supplementary Fig. S2a-d).

**Supplemental Note 3: Adjust administrative codes of the counties.** To protect the privacy of the older adults in CLHLS, their exact geographic coordinates are obscured, and we can only match each older adult sample with the CDHW characteristics of their counties of residence. However, between 2005 and 2014, 109 county administrative codes were changed for various reasons. To address this, we reassigned new administrative codes to the older adult samples whose codes changed. Specifically, there are four types:

Firstly, there are 16 counties that have been merged with neighboring counties to form new counties due to the county consolidation policy, and their real geographic locations do not change. For example, in July 2010, the Chinese State Council approved the revocation of Xicheng District (110102) and Xuanwu District (110104) in Beijing, and established a new Xicheng District (110102). We replace the older administrative codes with the new ones of the merged counties.

Secondly, there are 85 counties that have formed new counties due to policies such as "abolishing counties and establishing districts", "abolishing cities and establishing districts", "abolishing districts and establishing counties", "abolishing districts and establishing cities", and "adjusting administrative regions". The administrative regions of these counties do not change significantly or at all. For example, in April 2015, the Chinese State Council approved the abolishment of Xushui County (130625) and the establishment of Xushui District (110102). We replace the original administrative codes of these counties with the new ones after the adjustment.

Thirdly, there are 7 counties where administrative codes were recorded incorrectly during the survey, leading to the inability to match CDHW characteristics. We have corrected the erroneous county codes, such as recording Hetang District (430202) as Hetang District (430220).

Fourthly, there is one county that has been split into multiple counties. For example, the Daxing'anling area (232700) was split into Mohe City (232701), Tahe County, and Huma County. We replaced the original county code with the code of the county with the largest area after the split.

**Supplemental Note 4: Control variables.** In the baseline Cox proportional hazards model, we include 9 survey indicators as control variables to enhance the description of the model and reduce the interference of confounders. These indicators are comprised of sex, age, smoking status, drinking status, physical activity, body-mass index (BMI), household income, marital status, and education. Among them, sex is a binary categorical variable, where 0 represents females and 1 represents males. Age is a continuous variable obtained by subtracting the older adults' birth date from their survey or death date. Smoking status, drinking status, and physical activity are individually divided into four levels from low to high, namely, "1: never smoked, drank and exercised", "2: currently smoke, drink and exercise", "3: smoked, drank and exercised in the past", "4: always smoke, drink and exercise". BMI is calculated using height and weight. Weight is a continuous variable, and samples with weights below 20 kg or above 200 kg are excluded due to possible data errors. Height is a continuous variable similar to weight, and samples with height below 55 cm or above 200 cm are excluded. Household income is household per capita annual income, which is a continuous variable that reflects the economic status of the older adult family. Marital status includes "1-currently married, living with spouse", "2-separated", "3-divorced", "4-widowed" and "5-never married". Education is the years of education of the older adult samples.

In the robustness tests, we also include other control variables containing urban-rural residence, counties of the older adults, and the diseases suffered from CLHLS older adult samples. Among them, the urban-rural attribute is a binary categorical variable, i.e. 0 indicating living in rural areas and 1 indicating living in urban areas. The diseases include hypertension, diabetes, heart disease, stroke and cerebrovascular disease, bronchitis/emphysema/pneumonia and asthma, tuberculosis, cataracts, glaucoma, cancer, gastrointestinal ulcers, Parkinson's disease, pressure ulcers, arthritis, and dementia. All of the above diseases are binary variables, i.e. 0 indicating the absence of the disease, and 1 indicating the presence of the disease.

**Supplemental Note 5: Droughts indices.** We use three different drought indices in this study: (1) the terrestrial water storage-based drought severity index (TWS-DSI) to identify terrestrial terrestrial water storage deficits (15), (2) the standardized precipitation index (SPI) to identify precipitation deficits (16), and (3) the standardized precipitation-evapotranspiration index (SPEI) to capture the combined effects of precipitation and evaporative demand on regional water availability (17).

TWS-DSI can capture changes in vertically integrated water storage and is used to identify terrestrial drought conditions (15). A negative TWS-DSI means that the TWS is lower than the average level during the study period. It is used to represent the drought magnitude. The TWS-DSI is calculated by using Eq. [1].

$$\mathrm{TWS-DSI}_{i,j} = (\mathrm{TWS}_{i,j} - \overline{\mathrm{TWS}_j})/\sigma_j \quad [1]$$

where $\mathrm{TWS}_{i,j}$ refers to the TWS anomalies at year $i$ and month $j$. and denote the mean value and standard deviation of TWS anomalies at month $j$. For the GCM-GHM TWS outputs, we determine the same time-mean baseline as the GRACE data, and thus obtain monthly TWS anomalies during 1941-2100 by subtracting the mean value of TWS for 2004–2009. In calculating the mean and standard deviation of TWS for any specified period, we use a common reference period (that is, 1941–2014) to ensure robust comparison of drought events across time periods.

To calculate the 6-month SPI, we fit a gamma distribution to the 6-month cumulative precipitation time series over the 1941-2014 calibration period for each spatial grid cell. Subsequently, the cumulative precipitation value for each month is assigned a probability of occurrence based on the gamma distribution specific to that grid cell. These probabilities are then transformed onto the standard normal distribution (with zero mean and unit variance) to derive SPI values (i.e., z-scores). For SPEI, we estimate potential evapotranspiration using the Thornthwaite equation (18), and repeat this process using precipitation minus potential evapotranspiration to compute SPEI. Similar to TWS-DSI, future SPI/SPEI values (2015-2100) are also calculated using the historical (1941-2014) gamma distributions. The calculations of SPI/SPEI were conducted using the Python climate indices module (19), modified by Deeksha Rastogi et al. (20), enabling SPI/SPEI calculations for future periods based on historical calibration.

**Supplemental Note 6: Decomposing the drivers of CDHW-attributable deaths.** We dissect the contributions of driving factors including: (1) effect of population size, (2) effect of change in age structure (that is, population ageing), (3) effect of changes in CDHW exposures, and (4) effect of mortality rates independent of exposure to CDHWs (that is, the change in the baseline mortality rate due to changes in access to healthcare, treatment and other risk factors), to the change in attributable deaths to CDHWs using the decomposition method (21). Population and age structure data are sourced from the IIASA SSP population datasets (3), baseline mortality rates are predicted using the International Futures (IFs) model v7.89 (4), and CDHW characteristics are derived from the predictions of the GCM-GHM coupling model used in this study.

This approach estimate the contribution of different factors by sequentially introducing each factor into the AN equation. The difference between each consecutive step provided an estimate of the relative contribution of each factor. For example:

$$AN_{t0} = \sum_{a=65}^{99} P_{t0} \times Age_{t0,a} \times y^{0}_{t0,a} \times AF_{t0} \quad [2]$$

$$A_{t} = \sum_{a=65}^{99} P_{t} \times Age_{t0,a} \times y^{0}_{t0,a} \times AF_{t0} \quad [3]$$

$$B_{t} = \sum_{a=65}^{99} P_{t} \times Age_{t,a} \times y^{0}_{t0,a} \times AF_{t0} \quad [4]$$

$$C_{t} = \sum_{a=65}^{99} P_{t} \times Age_{t,a} \times y^{0}_{t,a} \times AF_{t0} \quad [5]$$

$$D_{t} = \sum_{a=65}^{99} P_{t} \times Age_{t,a} \times y^{0}_{t,a} \times AF_{t} \quad [6]$$

where $AN_{t0}$ is the attributable deaths in the baseline period t0, which are calculated based on the factors in the baseline period. $A_t$, $B_t$ and $C_t$ are the intermediate variables, which consider the changes in population, age structure, and baseline mortality rate incrementally from the baseline period to target period. $D_t$ is the attributable deaths in the target period, which consider all the changes in four factors. Using Eqs. [2]-[6], we calculate the percent contribution of each factor as follows.

1)Population size effect (%) = $(A_t\text{-}AN_{t0})/AN_{t0}$.

2)Population ageing effect (%) = $(B_t\text{-}A_t)/AN_{t0}$.

3)Baseline mortality rate change effect (%) = $(C_t\text{-}B_t)/AN_{t0}$.

4)Exposure change effect (%) = $(D_t\text{-}C_t)/AN_{t0}$.

5)Total change (%) = $(D_t\text{-}AN_{t0})/AN_{t0}$.

Notably, the order in which each factor is included can influence the results. That is to say, if the sequence of adding factors is not considered, a large bias may occur. Thus, we estimate the results under all sequence permutations (a total of 24 possible sequences) of the four factors. The final estimation of contributions from different factors is the average of the results for all sequences.

## Supplemental references


1. Burek, P., Satoh, Y., Kahil, T., Tang, T., Greve, P., Smilovic, M., ... and Wada, Y. (2020). Development of the Community Water Model (CWatM v1. 04)–a high-resolution hydrological model for global and regional assessment of integrated water resources management. Geoscientific Model Development, 13(7), 3267-3298. 10.5194/gmd-13-3267-2020.
2. Hanasaki, N., Yoshikawa, S., Pokhrel, Y., and Kanae, S. (2018). A global hydrological simulation to specify the sources of water used by humans. Hydrology and Earth System Sciences, 22(1), 789-817. 10.5194/hess-22-789-2018.
3. Riahi, K., Van Vuuren, D. P., Kriegler, E., Edmonds, J., O'neill, B. C., Fujimori, S., ... and Tavoni, M. (2017). The Shared Socioeconomic Pathways and their energy, land use, and greenhouse gas emissions implications: An overview. Global environmental change, 42, 153-168. 10.1016/j.gloenvcha.2016.05.009.
4. International Futures, F.S.P.C.: International Futures (IFs) Modeling System, v. 7. 89, Josef Korbel School of International Studies, University of Denver (2022). https://pardee.du.edu/access-ifs.
5. O'Neill, B. C., Kriegler, E., Riahi, K., Ebi, K. L., Hallegatte, S., Carter, T. R., ... and Van Vuuren, D. P. (2014). A new scenario framework for climate change research: the concept of shared socioeconomic pathways. Climatic change, 122, 387-400. 10.1007/s10584-013-0905-2.
6. Van Vuuren, D. P., Edmonds, J., Kainuma, M., Riahi, K., Thomson, A., Hibbard, K., ... and Rose, S. K. (2011). The representative concentration pathways: an overview. Climatic change, 109, 5-31. 10.1007/s10584-011-0148-z.
7. Stocker, T. (Ed.). (2014). Climate change 2013: the physical science basis: Working Group I contribution to the Fifth assessment report of the Intergovernmental Panel on Climate Change. Cambridge university press.
8. Van Vuuren, D. P., Stehfest, E., den Elzen, M. G., Kram, T., van Vliet, J., Deetman, S., ... and van Ruijven, B. (2011). RCP2. 6: exploring the possibility to keep global mean temperature increase below 2 C. Climatic change, 109, 95-116. 10.1007/s10584-011-0152-3.
9. Thomson, A. M., Calvin, K. V., Smith, S. J., Kyle, G. P., Volke, A., Patel, P., ... and Edmonds, J. A. (2011). RCP4. 5: a pathway for stabilization of radiative forcing by 2100. Climatic change, 109, 77-94. 10.1007/s10584-011-0151-4.
10. Masui, T., Matsumoto, K., Hijioka, Y., Kinoshita, T., Nozawa, T., Ishiwatari, S., ... and Kainuma, M. (2011). An emission pathway for stabilization at 6 Wm−2 radiative forcing. Climatic change, 109, 59-76. 10.1007/s10584-011-0150-5.
11. Riahi, K., Rao, S., Krey, V., Cho, C., Chirkov, V., Fischer, G., ... and Rafaj, P. (2011). RCP 8.5—A scenario of comparatively high greenhouse gas emissions. Climatic change, 109, 33-57. 10.1007/s10584-011-0149-y.
12. Kriegler, E., Edmonds, J., Hallegatte, S., Ebi, K. L., Kram, T., Riahi, K., ... and Van Vuuren, D. P. (2014). A new scenario framework for climate change research: the concept of shared climate policy assumptions. Climatic Change, 122, 401-414. 10.1007/s10584-013-0971-5.
13. Eyring, V., Bony, S., Meehl, G. A., Senior, C. A., Stevens, B., Stouffer, R. J., and Taylor, K. E. (2016). Overview of the Coupled Model Intercomparison Project Phase 6 (CMIP6) experimental design and organization. Geoscientific Model Development, 9(5), 1937-1958. 10.5194/gmd-9-1937-2016.
14. Masson-Delmotte, V., Zhai, P., Pirani, A., Connors, S. L., Péan, C., Berger, S., ... and Zhou, B. (2021). Climate change 2021: the physical science basis. Contribution of working group I to the sixth assessment report of the intergovernmental panel on climate change, 2(1), 2391.
15. Zhao, M., Zhang, J., Velicogna, I., Liang, C., and Li, Z. (2021). Ecological restoration impact on total terrestrial water storage. Nature Sustainability, 4(1), 56-62. 10.1038/s41893-020-00600-7.
16. McKee, T. B., Doesken, N. J., and Kleist, J. (1993, January). The relationship of drought frequency and duration to time scales. In Proceedings of the 8th Conference on Applied Climatology (Vol. 17, No. 22, pp. 179-183).
17. Vicente-Serrano, S. M., Beguería, S., and López-Moreno, J. I. (2010). A multiscalar drought index sensitive to global warming: the standardized precipitation evapotranspiration index. Journal of climate, 23(7), 1696-1718. 10.1175/2009JCLI2909.1.
18. Thornthwaite, C. W. (1948). An approach toward a rational classification of climate.Geographical review, 38(1), 55-94. 10.2307/210739.
19. Adams, J. (2017). climate_indices, an open source Python library providing reference implementations of commonly used climate indices. Climate indices in Python. https://github.com/monocongo/climate_indices.
20. Rastogi, D., Trok, J., Depsky, N., Monier, E., and Jones, A. (2023). Historical evaluation and future projections of compound heatwave and drought extremes over the conterminous United States in CMIP6. Environmental Research Letters, 19(1), 014039. 10.1088/1748-9326/ad0efe.
21. Stanaway, J. D., Afshin, A., Gakidou, E., Lim, S. S., Abate, D., Abate, K. H., ... and Borschmann, R. D. (2019). Erratum: Global, regional, and national comparative risk assessment of 84 behavioural, environmental and occupational, and metabolic risks or clusters of risks for 195 countries and territories, 1990–2017: a systematic analysis for the Global Burden of Disease Study 2017. The Lancet. 10.1016/S0140-6736(19)31429-1.